UNIVERSITÀ
DEGLI STUDI
DI PADOVA

Sede Amministrativa: Università degli Studi di Padova

Dipartimento di: GEOSCIENZE

CORSO DI DOTTORATO DI RICERCA IN: SCIENZE DELLA TERRA
CURRICOLO: UNICO
CICLO: 29

DIFFERENTIAL RADAR INTERFEROMETRY APPLIED TO THE DETECTION AND MONITORING OF GEOLOGICAL HAZARDS

Tesi redatta con il contributo finanziario dell'Istituto Nazionale Previdenza Sociale (INPS) - Gestione dipendenti pubblici - Direzione Regionale Veneto.

Coordinatore: Ch.mo Prof. Fabrizio Nestola
Supervisore: Ch.mo Dr. Mario Floris
Co-Supervisore: Ch.mo Prof. Claudia Meisina

Dottorando: Simone Fiaschi

CONTENTS

ABSTRACT

We live in a constantly changing environment, characterized by climate changes, extreme weather events and the occurrence of more frequent geological hazards that have a strong negative impact on the territory and society, interrupting services, damaging buildings and infrastructure and jeopardizing the life of millions of people worldwide. For this reason, there is the need to build a society resilient to natural-hazards, which can understand how the natural system behaves and responds to natural and human-induced modifications and can adapt to these changes. The monitoring of the territory is necessary to comprehend the triggering factors and the mechanisms of geological hazards and to plan the most suitable actions to prevent and mitigate the risk. The monitoring of geological hazards with conventional ground-based techniques such as Global Positioning System (GPS) and levelling is usually expensive and time consuming, which limits the number of measured points and the overall duration of the surveys. One of the best way to overcome to these problems is to use remote-sensing techniques to monitor large portion of territory reducing operating costs and time. Advanced Differential Synthetic Aperture Radar Interferometry (A-DInSAR) is one of the best tool to monitor and study ground displacements over very large portions of territory in a cost-effective way. In this Doctoral Thesis, we applied A-DInSAR to the monitoring of the geological instabilities occurring in different areas characterized by unique geological and environmental features. The selected areas include different environments such as vegetate territories, low and steep topography, coastal areas, salty deserts, urbanized land, each of them affected by hazards of natural and anthropic origin such as landslides, subsidence and karstic activity. In each case study, the monitoring activity presented its own challenges that were overcome adopting specific technical solutions in the data processing and management. The aim of this work is to give an overview of the potential of A-DInSAR techniques when applied to the study of geological hazards in different environments. This can be useful to show to local Authorities that A-DInSAR can be fully integrated as part of the activities carried out to manage the territory and to prevent and mitigate the risk related to geological hazards.

RIASSUNTO

Viviamo in un mondo in costante evoluzione, caratterizzato da cambiamenti climatici, eventi naturali estremi e dal verificarsi di sempre più frequenti catastrofi di natura geologica che hanno forte ripercussione sul territorio e sulla società, con l'interruzione di servizi, danni alle strutture e infrastrutture mettendo a rischio la vita di milioni di persone in tutto il mondo. Per questo c'è la necessità di costruire una società resiliente al rischio geologico e che sia in grado di capire in che modo la natura reagisce e si adatta ai cambiamenti sia naturali che causati dalle attività umane. Il monitoraggio del territorio è essenziale per riuscire a comprendere i meccanismi che portano al verificarsi di un evento e in questo modo riuscire a prevenire e mitigare il rischio con azioni ed opere adatte. Il monitoraggio e lo studio di eventi geologici quali subsidenze e frane attraverso tecniche geodetiche da terra come per esempio Global Positioning System (GPS) e livellazione è solitamente molto dispendioso sia in termini di tempo che di denaro, fattore che limita notevolmente il numero di misurazioni che si possono effettuare e la durata complessiva delle attività di monitoraggio. Uno dei metodi migliori per ovviare a questi problemi è l'utilizzo di tecniche di remote-sensing che permettono di investigare aree molto vaste con tempi e costi molto ridotti. Le tecniche Avanzate di Interferometria Radar Differenziale ad Apertura Sintetica (A-DInSAR) sono uno dei migliori strumenti per poter studiare i movimenti della superficie terrestre sia a scala regionale che locale con misurazioni ad elevata accuratezza e precisione in maniera economicamente vantaggiosa. In questa Tesi di Dottorato, le tecniche A-DInSAR sono applicate allo studio fenomeni geologici in diverse aree di studio. Le aree scelte comprendono zone densamente vegetate, pianeggianti e montuose, aree costiere e deserti salati, ognuna delle quali soggetta a instabilità sia naturali che antropiche come frane, subsidenze e fenomeni derivanti da attività carsica. L'applicazione di queste tecniche nei diversi contesti ha presentato difficoltà e sfide che sono state superate adottando specifiche soluzioni durante l'elaborazione dei dati satellitari. Lo scopo principali di questo lavoro è quello di mostrare le potenzialità delle tecniche A-DInSAR applicate in diversi contesti geologici e mostrare quali informazioni possono essere ottenute dall'utilizzo di dati SAR e quale contributo tali informazioni possono portare nell'ambito della pianificazione ambientale e territoriale. Questo può essere molto utile per dimostrare alle Autorità come l'integrazione di monitoraggi basati su tecniche A-DInSAR all'interno delle opere di prevenzione e mitigazione del rischio idrogeologico sia necessario per uno sviluppo sostenibile del territorio.

INTRODUCTION

Climate change is nowadays one of the most controversial and complex subject discussed by the scientific community that arouses increasing interest among the governments, media and public opinion (Konisky et al., 2016). The impact of climate changes on the environment and the territory as consequence of the human activities is becoming more evident every year as it effects in different ways the daily life of hundreds of millions of people worldwide. The present-day increase of the oceanic water level, or sea level rise (SLR), is probably one of the major indicator of climate change. The melting of glaciers and ice-caps, the increase of the water temperature and the change in ocean circulations are the main factors contributing to the global-scale acceleration of SLR (Church et al., 2013). The areas that are expected to become more vulnerable to flooding and land loss because of SLR are clearly the coastal communities (FitzGerald et al., 2008; Cazenave et al., 2014) where the 10% of the world population lives (McGranahan et al., 2007). Examples of low-lying coastal cities highly vulnerable to SLR are Miami (Wdowinski et al., 2016), New York (Rosenzweig and Solecki, 2013), New Orleans (Dixon et al., 2006), and Mumbai (Ranger et al., 2011) that were identified as the world's most vulnerable cities to flooding (Hallegatte and Corfee-Molot, 2013). Coastal areas are also important ecosystems very sensitive to SLR, which preservation is crucial for biodiversity and habitat conservation (Crossland et al., 2005). Moreover, the occurrence of more frequent and severe extreme weather events, which relationship with climate changes is still under debate by the scientific community (Jankovich and Schultz, 2016), exposes people and property to great risk of damage. The impact of environmental hazards and disasters such as floods and landslides is greater in developing countries, often because the not adequate economic, social, political and cultural conditions act as factors of high vulnerability to natural disasters (Alcántara-Ayala, 2002).

These events can be considered as *natural*, by means that human activity does not have direct control on them and their occurrence is very hardly predictable. On the other hand, human-induced hazards are easily predictable and are directly attributable to specific activities. Nevertheless, these hazards are generally localized but omnipresent, with very negative effects on territory and society, as each one of us can probably tell from his first-hand experience. Among the different anthropogenic hazards, one of the most frequent and evident is land subsidence, which occurrence is often related to underground water extraction activities, mining, and oil and gas production (Johnson ed., 1991; Donaldson et al., 1995; Galloway and Burbey, 2011). Also the over-exploitation and poor management of superficial water resources may lead to strong negative environmental, territorial, economical, and social impact as happened, for example, in these three major cases: the Dead Sea (Shwarz et al., 2016), the Aral Sea (Micklin, 2016) and the Urmia lake (Alizadeh-Choobari 2016). The interaction and coexistence between natural and anthropogenic phenomena affects the territory with damage to buildings, interruption of services and loss of human lives. Since we live in a changing environment, there is the need to understand the response of natural systems to both human and natural modifications, and build a societal resilience to natural disasters (Djalante, 2012). We have now the instruments and knowledge necessary to monitor the territory and understand how it evolves and reacts to human activities, which is one of key points for risk assessment and reduction. In fact,

assessing the evolution of the temporal and spatial distribution of the ground movements is essential to delineate the most affected areas and to understand the mechanisms involved (Yerro et al., 2014). In this way, it is possible to mitigate these events, to prevent damage and to plan more sustainable urban and territorial development.

The monitoring of the territory can be carried out through ground-based geodetic techniques such as levelling, Global Positioning System (GPS) and total stations that are intensively used to perform very accurate measurements of ground displacements such as plate tectonic motion, volcanic activity, landslides and subsidence in several different scenarios. However, one of the main limit of these techniques is that the measurements are limited to individual points and cannot be carried out in adverse territory conditions or in inaccessible areas. Furthermore, the field campaigns are very time consuming and expensive, limiting the number of points that can be measured on each survey. This strongly reduces the extension of the area to be monitored, the survey frequency and the total duration of the monitoring activity.

A big step ahead in the Earth surface monitoring systems has been brought in the 1970s by the idea of radar interferometry for topographic mapping (Graham, 1974) that potentially overcame to all the operational limits of the ground-based techniques. In 1978, the National Aeronautics and Space Administration (NASA) launched the SEASAT satellite equipped with the first Synthetic Aperture Radar (SAR) sensor (Allan, 1983; Elachi, 1991; Raney, 1982). Only after, Gabriel et al. (1989) described the capabilities of repeated acquisition SAR Interferometry (InSAR) to detect changes in the ground surface and provided the first description of Differential InSAR (DInSAR). This technique was successfully applied for the first time by Massonnet et al. (1993) to measure the movements produced by the 1992 earthquake in Landers, California. Since then, to maximize the potential of InSAR and permit time series analysis, different Advanced DInSAR (A-DInSAR) algorithms were developed such as Permanent Scatteres (PS) (Ferretti et al., 2001), Small BAseline Subset (SBAS) (Berardino et al., 2002), Interferometric Point Target Analysis (IPTA) (Werner et al., 2003), Stanford Method for Persistent Scatterers (StaMPS) (Hooper et al., 2004), Coherent Pixel technique (CPT) (Blanco-Sanchez et al., 2008), SqueeSAR™ (Ferretti et al., 2011). A-DInSAR is nowadays a well-documented technique for the characterisation of ground motions over large spatial areas capable of detecting movements with metric resolution and millimetric accuracy. This technique can be applied to monitor and study earthquakes, volcanic activity, ice-sheet motion, landslides, land subsidence, sinkholes, and other geological hazards. An extensive review of InSAR, the different techniques developed, their applications and limits can be found in Ouchi (2013), Crosetto et al. (2016), Osmanoglu et al. (2016), and reference therein.

In the past few years, the growing need to monitor the Earth surface to study and mitigate natural and human induced hazards lead to increasing investments in the space segment and in particular in the SAR technology. In 1991, the European Space Agency (ESA) started the first SAR mission entirely designed for Earth Observation (EO) with the launch of the ERS-1 satellite. Since then, several research and commercial SAR satellites were sent in orbit by the main space agencies, the Italian Space Agency (ASI), the Canadian Space Agency (CSA), ESA, the German Aerospace Center (DLR), and the Japan Aerospace Exploration Agency (JAXA). Each SAR satellite is unique in terms of equipped instruments (radar band, ground resolution, acquisition mode, look angle, etc.) and technical characteristics (orbital tube, acquisition frequency, etc.), providing data potentially suitable for every EO necessity and, at the same time, creating new opportunities and making possible new

applications. Today, the latest and most advanced SAR mission is represented by the two satellites Sentinel-1 constellation. The Sentinel-1A, the first of the twin satellites, was launched in April 2014 by ESA, and was equipped with instrument designed specifically for EO purposes: C-band sensor, image swath of 250 km with the Interferometric Wide Swath (IWS) acquisition mode, spatial resolution of 5 m in Range and 20 in Azimuth, and repeat time of 12 days. Since April 2016, the launch of the twin satellite Sentinel-1B permitted to reduce this revisit time to 6 days, enhancing the Earth monitoring activities in terms of temporal frequency and overall quality of the achievable results. Despite the incredible potential of A-DInSAR techniques has been widely demonstrated and documented with hundreds of high quality scientific papers and publications, there is always the room for further improvements regarding the processing algorithms (e.g. phase unwrapping, degree of automation, processing speed), data validation and management, and applicability. For these reasons, the use of A-DInSAR as principal instrument to investigate areas characterized by peculiar geological and environmental conditions represents an important way to further test the potential and capabilities of this technique, highlighting its advantages and drawbacks and making possible the development of new applications.

The research carried out in this Thesis addresses to give, through my practical experience, an overview of possible applications of A-DInSAR to geosciences, demonstrating in which way the information extracted from the exploitation of SAR images can support a sustainable territorial development and which are the benefits that these techniques can provide to local and regional geological and geomorphological studies, to the detection and monitoring of geological hazards and to the hydrogeological risk assessment and mitigation. The range of the presented applications is wide and regards five main case studies characterized by completely different environmental and territorial features and affected by different ground displacements of natural and anthropic origin, such as land subsidence, landslides and karstic activity. For each case study, all the available SAR images provided by different satellites including the new Sentinel-1A have been processed. The products and potential of Sentinel-1A are still not well known by the scientific community, so the use of this sensor in the different case studies can also provide an overview about the applicability of this new satellite. The use of different datasets allowed us to carry out monitoring activity that, in most cases, covered 25 years, from 1992 to 2016. This gave us a unique opportunity to know and understand how the studied displacements evolve and behave, which is one of the key information necessary to properly carry out geo-hazards risk mitigation activities. Furthermore, the combination of results obtained from images acquired with different bands (X, C and L) is described, showing how the use of different radar wavelengths can sometimes be useful to better characterize the studied territory. The processing of the SAR images has been carried out through both the PS and the SBAS techniques using the SARscape© modules of ENVI. The performance of the two approaches depends on several factors among which the characteristics of the territory (vegetation coverage, scatterers quality and distribution) and of the displacement (velocity, spatial extent) under investigation. SBAS was used more frequently because it performs better over very wide areas characterized by distributed scatterers, while PS works well when subtle deformations must be detected and only small and isolated reflectors are available. Each case study presented challenges that were faced case by case, adapting the processing parameters and managing the results differently accordingly to our necessities. Further details about the adopted approaches are described in the corresponding Chapters.

The terms DInSAR and Advanced DInSAR (A-DInSAR) are used interchangeably throughout the Thesis, referring to the same class of multi-temporal DInSAR techniques.

Part of the work was carried out during two main research periods spent at the Sarmap S.A. Company (Switzerland) and at the Rosenstiel School of Marine and Atmospheric Science (RSMAS), University of Miami, Florida (USA).

The Thesis is structured as follows:

In Chapter 1, the results obtained from the monitoring of the land subsidence affecting the territory of Ravenna (Italy) are presented. Four different SAR datasets, covering a period of 25 years, are exploited thought the SBAS technique. Different statistical analyses are applied to the obtained velocity and displacement maps in order to better comprehend the relationship between the high rates of subsidence detected and the main mechanisms that have influence on the subsidence in the area. A novel methodology is also applied to analyse in a systematic way all the measured points and fully exploit their informative content. The paper titled "From ERS-1/2 to Sentinel-1: two decades of subsidence monitored through A-DInSAR techniques in the Ravenna area (Italy)" was published in *GISscience & Remote Sensing* (Fiaschi et al., 2016).

In Chapter 2, the potential of the new ESA's Sentinel-1A satellite is tested in the monitoring of a landslide-prone territory located in the Italian Pre-Alps. The PS technique applied to the Sentinel-1A images acquired in descending and ascending orbits, allowed us to detect several shallow landslides in the study area. To assess the capabilities of this new SAR sensor in densely vegetated territories, we compared the obtained results with the available PSI results obtained from ERS-1/2 and ENVISAT images processed by Tele-Rilevamento Europa (T.R.E.) in the framework of the Territorial Italian Plan promoted by the Italian Environment Ministry. The location and extension of the landslides detected with the PS analysis are also overlapped with the available landslides inventory, showing areas affected by movement not mapped before. The work demonstrates the benefits of using the Sentinel-1A images for the continuous monitoring of the territory providing information useful for the landslides detection and characterization. The paper titled "Testing the potential of Sentinel-1 TOPS interferometry for the detection and monitoring of landslides at local scale" was submitted to *Environmental Earth Sciences*.

In Chapter 3, is described a very interesting case study where for the first time the SBAS technique is applied to monitor 25 years of displacements in the Lisan Peninsula area, Dead Sea, Jordan. A very complete SAR dataset made of images acquired by different satellites in X, C and L-bands was processed in order to produce the velocity and displacement maps of the entire study area. The results reveal the complexity of the displacement dynamics in the area, affected by very high rate of subsidence up to 200 mm/yr along the coastline, uplift in the northern section of the peninsula and differential movements in its southern section. The exploitation of X, C and L-band images, helped in better characterize the movements in the Lisan Peninsula, obtaining information over areas that are not possible to observe using only one sensor because of spatial decorrelation and/or complete loss of information where the movements are too fast to be detected by short wavelengths. The paper titled

"The monotonous rising of the Lisan diapir revealed by 25 years of DInSAR observations. Dead Sea, Jordan" was submitted to *ISPRS Journal of Photogrammetry and Remote Sensing*.

In Chapter 4, we want to assess the contribution of land subsidence to the increasing coastal flooding hazard in the US Atlantic regions. DInSAR is applied to monitor land subsidence affecting Miami Beach (Florida) and Norfolk (Virginia) using PS and SBAS techniques. The analyses show several areas affected by moderate subsidence in both cities confirming the importance of considering also the localized subsidence as one of the main parameters in the flooding hazard assessment.

In the Conclusions, a summary of the outcomes of this Thesis is finally presented.

In the Appendix, a study concerning the negative impact of land subsidence on the territory and its relation with human development is presented. The Dead Sea area is taken as a model because it clearly shows what effects the human induced land subsidence has on the environment and on the development of a territory. The role played by remote sensing techniques (both visible and radar) in monitoring geomorphologic environmental degradation is empathized showing how a clear identification of geomorphic features is necessary to preserve the major assets at risk. My contribution to this work concerned the processing of all the available SAR datasets with the SBAS technique, the post processing management of the results and the extraction of the subsidence values presented in the Results section. The paper "Sustainable development and anthropogenic induced geomorphic hazards in subsiding areas" was published in *Earth Surface Processes and Landforms* (Abou Karaki et al., 2016).

References

Alcantara-Ayala, I. 2002. "Geomorphology, natural hazards, vulnerability and prevention of natural disasters in developing countries". *Geomorphology* 47: 107–124.

Alizadeh-Choobari, O., F. Ahmadi-Givi, N. Mirzaei and E. Owlad. 2016. "Climate change and anthropogenic impacts on the rapid shrinkage of Lake Urmia". *International Journal of Climatol*ogy. doi:10.1002/joc.4630.

Allan, T.D. 1983. "Satellite Microwave Remote Sensing". Ellis Horwood Series in *Marine Science*. 526 pp.

Berardino, P., G. Fornaro, R. Lanari and E. Sansosti. 2002. "A new algorithm for surface deformation monitoring based on small baseline differential SAR interferograms". *IEEE Transactions on Geoscience and Remote Sensing* 40 (11): 2375–2383.

Blanco-Sanchez, P., J.J. Mallorquí, S. Duque and D. Monells. 2008. "The coherent pixels technique (CPT): an advanced DInSAR technique for nonlinear deformation monitoring". *Pure and Applied Geophys*ics 165 (6): 1167–1193.

Cazenave, A., H.-B. Dieng, B. Meyssignac, K. von Schuckmann, B. Decharme and E. Berthier. 2014. "The rate of sea-level rise". *Nature Climate Change* 4: 358–361. doi:10.1038/nclimate2159.

Church, J.A., P.U. Clark, A. Cazenave, J.M. Gregory, S. Jevrejeva, A. Levermann, M. Merrifield, G. Milne, R. Nerem, and P. Nunn. 2013. "Sea Level Change". PM Cambridge University Press.

Colombo, D. 2014. “Ground deformation monitoring with satellite radar sensors”. EE Publishers. Available online: http://www.ee.co.za/article/ground-deformation-monitoring-satellite-radar-sensors.html. Accessed on 14 Oct. 2016.

Crosetto, M., O. Monserrat, M. Cuevas-González, N. Devanthéry and B. Crippa. 2016. “Persistent Scatterer Interferometry: A review”. *ISPRS Journal of Photogrammetry and Remote Sensing* 115: 78–89.

Crossland, C.J., H.H. Kremer, H.J. Lindeboom, J.I. Marshall Crossland and M.D.A. Le Tissier, eds. 2005. “Coastal Fluxes in the Anthropocene”. Springer-Verlag, Berlin, Germany, 252 pp.

Dixon, T.H., F. Amelung, A. Ferretti, F. Novali, F. Rocca, R. Dokka, G. Sella, S-W. Kim, S. Wdowinski and D. Whitman. 2013. “Space geodesy: Subsidence and flooding in New Orleans”. *Nature* 441: 587-588. doi:10.1038/441587a.

Djalante, R. 2012. “Adaptive governance and resilience: the role of multi-stakeholder platforms in disaster risk reduction”. *Natural Hazards and Earth System Sciences* 12: 2923–2942.

Donaldson, E.C., G.V. Chilingarian and T.F. Yen. 1995. “Subsidence due to Fluid Withdrawal”. Elsevier. 497 pp.

Elachi, C. 1988. “Spaceborne Radar Remote Sensing: Applications and Techniques”. IEEE press, New York.

Ferretti, A., C. Prati and F. Rocca. 2001. “Permanent scatterers in SAR interferometry”. *IEEE Transactions on Geoscience and Remote Sensing* 39 (1): 8–20.

Ferretti, A., A. Fumagalli, F. Novali, C. Prati, F. Rocca and A. Rucci. 2011. “A new algorithm for processing interferometric data-stacks: SqueeSAR”. *IEEE Transactions on Geoscience and Remote Sensing* 49 (9): 3460–3470.

FitzGerald, D.M., M.S. Fenster, B.A. Argow and I.V. Buynevich. 2008. “Coastal Impacts Due to Sea-Level Rise”. Annual Review of Earth and Planetary Sciences 36: 601–647.

Gabriel, K., R.M. Goldstein, and H.A. Zebker. 1989. “Mapping small elevation changes over large areas: differential interferometry”. *Journal of Geophysical Research* 94.

Galloway, D.L. and T.J. Burbey. 2011. “Review: Regional land subsidence accompanying groundwater extraction”. *Hydrogeology Journal* 19 (8): 1459-1486. doi:10.1007/s10040-011-0775-5.

Graham, L.C. 1974. “Synthetic interferometer radar for topographic mapping”. *Proceedings of the IEEE* 62: 763-768.

Hallegatte, S. and J. Corfee-Morlot. 2013. “Future flood losses in major coastal cities”. *Nature Climate Change*. doi: 10.1038/nclimate1979.

Hooper, A., H. Zebker, P. Segall, and B. Kampes. 2004. “A new method for measuring deformation on volcanoes and other natural terrains using InSAR persistent scatterers”. *Geophysical Research Letters* 31 (23): 5 pp.

Janković, V., and D. M. Schultz. 2016. “Atmosfear: Communicating the Effects of Climate Change on Extreme Weather”. *Weather, Climate, and Society.* doi: 10.1175/WCAS-D-16-0030.1.

Johnson, A.I. ed. 1991. *Land subsidence*. International Association of Hydrological Sciences.

Konisky, D.M., L. Hughes, C.H. Kaylor. 2016. “Extreme weather events and climate change concern”. *Climatic Change* 134: 533–547. doi:10.1007/s10584-015-1555-3.

Massonnet, D., M. Rossi, C. Carmona, F. Ardagna, G. Peltzer, K. Feigl, and T. Rabaute. 1993. “The displacement field of the Landers earthquake mapped by radar interferometry”. *Nature 364*: 138–142. doi:10.1038/364138a0.

McGranahan, G., D. Balk, B. Anderson. 2007. “The rising tide: assessing the risks of climate change and human settlements in low elevation coastal zones”. *Environment and Urbanization* 19: 17-37.

Micklin, P. 2016. “The future Aral Sea: hope and despair”. *Environmental Earth Sciences* 75 (9). doi:10.1007/s12665-016-5614-5.

Osmanoglu, B., F. Sunar, S. Wdowinski and E. Cabral-Cano. 2016. “Time series analysis of InSAR data: Methods and trends”. *ISPRS Journal of Photogrammetry and Remote Sensing* 115: 90–102.

Ouchi, K. 2013. “Recent Trend and Advance of Synthetic Aperture Radar with Selected Topics”. *Remote Sensing* 5: 716-807. doi: 10.3390/rs5020716.

Raney, R.K. 1982. “Review of spaceborne and airborne SAR systems”. Agard Lecture Series. 182 (11): 1–20.

Ranger, N., S. Hallegatte, S. Bhattacharya, M. Bachu, S. Priya, K. Dhore, F. Rafique, P. Mathur, N. Naville, F. Henriet, C. Herweijer, S. Pohit, J. Corfee-Morlot. 2011. “An assessment of the potential impact of climate change on flood risk in Mumbai”. *Climatic Change* 104: 139-167. doi:10.1007/s10584-010-9979-2.

Rosenzweig, C. and W. Solecki (Editors). New York City Panel on Climate Change, 2013: Climate Risk Information 2013: Observations, Climate Change Projections, and Maps. NPCC2. Prepared for use by the City of New York Special Initiative on Rebuilding and Resiliancy, New York, New York.

Schwarz, J., J. Bear. and G. Dagan. 2016. “Groundwater Development in Israel”. *Groundwater* 54: 143–148. doi:10.1111/gwat.12384.

Werner, C., U. Wegmuller, T. Strozzi, and A. Wiesmann. 2003. “Interferometric point target analysis for deformation mapping”. In: Geoscience and Remote Sensing Symposium Proceedings. IEEE International. 7: 4362–4364.

Yerro, A., J. Corominas, D. Monells and J.J. Mallorquì. 2014. “Analysis of the evolution of ground movements in a low densely urban area by means of DInSAR technique”. *Engineering Geology* 170: 52-65.

CHAPTER 1

From ERS-1/2 to Sentinel-1: two decades of subsidence monitored through A-DInSAR techniques in the Ravenna area (Italy).

Simone Fiaschi [1], Serena Tessitore [2], Roberta Bonì [3], Diego Di Martire [2], Vladimiro Achilli [4], Sven Borgstrom [5], Ahmed Ibrahim [2,6], Mario Floris [1], Claudia Meisina [3], Massimo Ramondini [7] and Domenico Calcaterra [2]

[1] Department of Geosciences, University of Padua, Padua, Italy.
[2] Department of Earth, Environment and Resources Sciences, Federico II University of Naples, Naples, Italy.
[3] Department of Earth and Environmental Science, University of Pavia, Pavia, Italy.
[4] Department of Civil, Environmental and Architectural Engineering, University of Padua, Padua, Italy.
[5] INGV, Osservatorio Vesuviano, Naples, Italy.
[6] Geology Department, Faculty of Science, South Valley University, Qena, Egypt.
[7] Department of Civil, Architectural and Environmental Engineering, Federico II University of Naples, Italy.

Abstract

Land subsidence due to underground resources exploitation is a well-known problem that affects many cities in the world, especially the ones located along the coastal areas where the combined effect of subsidence and sea level rise increases the flooding risk. In this study, 25 years of land subsidence affecting the Municipality of Ravenna (Italy) are monitored using Advanced Differential Interferometric Synthetic Aperture Radar (A-DInSAR) techniques. In particular, the exploitation of the new Sentinel-1A SAR data, allowed us to extend the monitoring period till 2016, giving a better understanding of the temporal evolution of the phenomenon in the area. Two statistical approaches are applied to fully exploit the informative potential of the A-DInSAR results in a fast and systematic way. Thanks to the applied analyses, we described the behaviour of the subsidence during the monitored period along with the relationship between the occurrence of the displacement and its main driving factors.

1. Introduction

Differential Synthetic Aperture Radar Interferometry (DInSAR) is a very powerful remote sensing tool able to measure the displacements on the Earth surface with millimetric accuracy. The first description of DInSAR was given by Gabriel et al. (1989), and it was successfully applied for

the first time as a ground motion detection technique in the early '90s with the study of the Landers earthquake in California and the Mount Etna volcano in Italy (Massonnet et al., 1993, 1995). This method uses the phase shift between two radar acquisitions (SAR images) made over the same place at different times to generate an interferogram and calculate the ground deformation. The interferometric phase ($\Delta\varphi$) is made by different contributions:

$$\Delta\varphi = \Delta\varphi_{topo} + \Delta\varphi_{def} + \Delta\varphi_{orb} + \Delta\varphi_{atm} + \Delta\varphi_{noise}$$

where $\Delta\varphi_{topo}$ is the contribution given by the topography, $\Delta\varphi_{def}$ is the contribution given by the deformation, $\Delta\varphi_{orb}$ is the phase given by uncompensated difference in the satellite's orbits, $\Delta\varphi_{atm}$ is the phase component given by atmospheric effects, and $\Delta\varphi_{noise}$ is the systematic noise. One of the main advantages of the DInSAR approach, is that the topographic component of the phase ($\Delta\varphi_{topo}$) is reduced using an external Digital Elevation Model (DEM) providing (qualitative) information on deformations, even with a reduced SAR data availability (Cascini et al., 2010). On the other hand, the main drawback is that analysing just one interferogram is not possible to remove the strong atmospheric disturbance that inevitably lead to inaccuracies in the detected movements, limiting its operational capability (Cascini et al., 2010). Furthermore, since DInSAR can only measure the total displacement between two points in time, it cannot distinguish between linear and non-linear motion. Hence, in order to cope with these limitations, a new class of DInSAR techniques called Persistent Scatterers Interferometry (PSI) was developed. In this work, we refer to PSI with the term Advanced DInSAR (A-DInSAR). There are two main A-DInSAR techniques: the Permanent Scatterers (PS) (Ferretti et al., 2000, 2001) and the Small BAseline Subset (Berardino et al., 2002). These techniques, exploit the information of multiple SAR acquisitions made over the same area to estimate and reduce the effects given by decorrelation phenomena and atmospheric phase shifts obtaining very accurate deformation measures over time. The PS technique analyses at full resolution dominant point scatterers (PS) that maintain phase stability over long periods. Any phase disturbance such as atmospheric artefacts and topographic inaccuracies are estimated and compensated retrieving the precise displacement of the PS. Since PS density is generally higher in urban environments, this technique is more suitable for ground deformation analysis in metropolitan areas (Soergel, 2010). The SBAS technique relies on the combination of interferometric pairs with small temporal and perpendicular baselines to measure the deformation of distributed scatterers. To enhance phase stability, a multi-look factor in Range and Azimuth is generally adopted but this leads to a reduced spatial resolution. The application of SBAS is more suited over large areas, where the absence of a high number of stable reflectors limits the applicability of the PS approach. For this reason, SBAS is widely used for Earth Observation purposes in several scenarios, such as low vegetated land, sparsely urbanized territory, and coastal areas. A-DInSAR has proven to be one of the most reliable tool for the detection and monitoring of different geological hazards such as earthquakes (Chini et al., 2016), landslides (Di Martire et al., 2016), subsidence (Tessitore at al., 2016) and volcanic activity (Meyer et al., 2015), and is nowadays widely used to map ground deformations due to natural and anthropogenic processes in different environments. Furthermore, one of the main advantages is the possibility to reconstruct the past behaviour of the displacement using archive data and perform time series analyses. This is useful in particular in the framework of geological hazard risk assessment and territory management; in fact, thanks to the analysis of the ground instability evolution it is possible to understand its cause-effect mechanism and to evaluate the most feasible corrective measures

(Tomás et al., 2005). While the monitoring of geological hazards with conventional ground-based techniques (e.g. inclinometers, levelling, GPS, etc.) is usually expensive and time consuming, A-DInSAR techniques permit to reduce operating costs and working time especially when used for large-scale surveys. Despite the great benefits brought by the application of radar interferometry to the geological hazard monitoring, the exploitation of very large SAR datasets can produce huge amounts of data that are often difficult to properly manage and interpret. Statistical methods can be applied to analyse the A-DInSAR processing results to fully exploit their informative content. In this work, we present the outcomes in monitoring the land subsidence affecting the Municipality of Ravenna with 25 years of SAR data, starting from 1992 with the ERS-1/2 and ending with the 2016 Sentinel-1A images. The obtained results are then cross-validated comparing two different A-DInSAR approaches, the SBAS and the Coherent Pixel Technique (CPT) (Mora et al., 2003; Iglesias et al., 2014). Furthermore, we show the application of a new methodology based on statistical analyses to manage in a systematic way the obtained results and better describe the behaviour of the subsidence during the monitoring period along with the relationship between the occurrence of the displacement and its main driving factors.

The main aims of this work are: i) to monitor the land subsidence affecting the territory of Ravenna using A-DInSAR techniques and extend the observed period to 2016 with the new Sentinel-1A satellite; ii) to understand the subsidence trends over the 25 years period and determine which are the main controlling factors through the application of statistical analyses; iii) to compare and cross-validate the results obtained through two different A-DinSAR approaches and demonstrate the reliability of the measured subsidence rates; iv) to assess the capabilities of the Sentinel-1A sensor in the monitoring of sparsely urbanized areas.

2. Study Area

The city of Ravenna is located in the Emilia Romagna Region (northeast of Italy), where land subsidence of natural and anthropogenic origin occurs since the last century (Teatini et al., 2005). One of the main causes of the subsidence in the area is the over-exploitation of the methane-gas and water reservoirs that started in the ‘40s along with the industrial growth and gradually reduced around the ‘80s (Gambolati et al., 1999). Concerned by the very high values of subsidence registered, the Municipality of Ravenna started in the late ‘70s the construction of a new public aqueduct to exploit the surface water that led to a reduced aquifer overdraft (Gambolati et al., 1999). Today, even if the ratio of the anthropogenic subsidence (< -20 mm/yr) lowered a lot in respect to the previous decades, it is still ten times higher than the natural one (-2 mm/yr) (Gambolati et al., 1991). This represents a serious threat in particular for the coastal areas where the subsidence effect added to the mean sea level rise increases the flooding risk (Carbognin and Tosi, 2002).

2.1. Geological settings

The territory of Ravenna (Figure 1a) lies over the south-eastern portion of the Po River plain, an area of about 38,000 km^2 bounded by the Alps in the north and the Apennines in the south (Teatini et al., 2005). The buried tectonic structures underlain around 2000 m of Quaternary sediments of Alpine and Apennines origin deposited under different environments, from continental to marine (Amorosi

et al., 1999; Carminati et al., 2003; Ghielmi et al., 2010). The pre-Quaternary basement is characterized by a complex structure of folds and faults that develop parallel to the main Apennine tectonic lines forming natural traps for the methane-gas (Gambolati et al., 1991). Several Pliocene and Pleistocene gas fields are located in thrusted anticlines, with depths ranging between 1000 m and 4500 m, simple drape structures and stratigraphic traps. The Quaternary sequence is made of normally consolidated layers of alternating silty-clay, sand and sandy silt (Figure 1c). A multi-layer aquifer system developed in the first 500 m of sediments accumulated since the Pleistocene. This system is characterized by sediments deposited during transgressive and regressive stages.

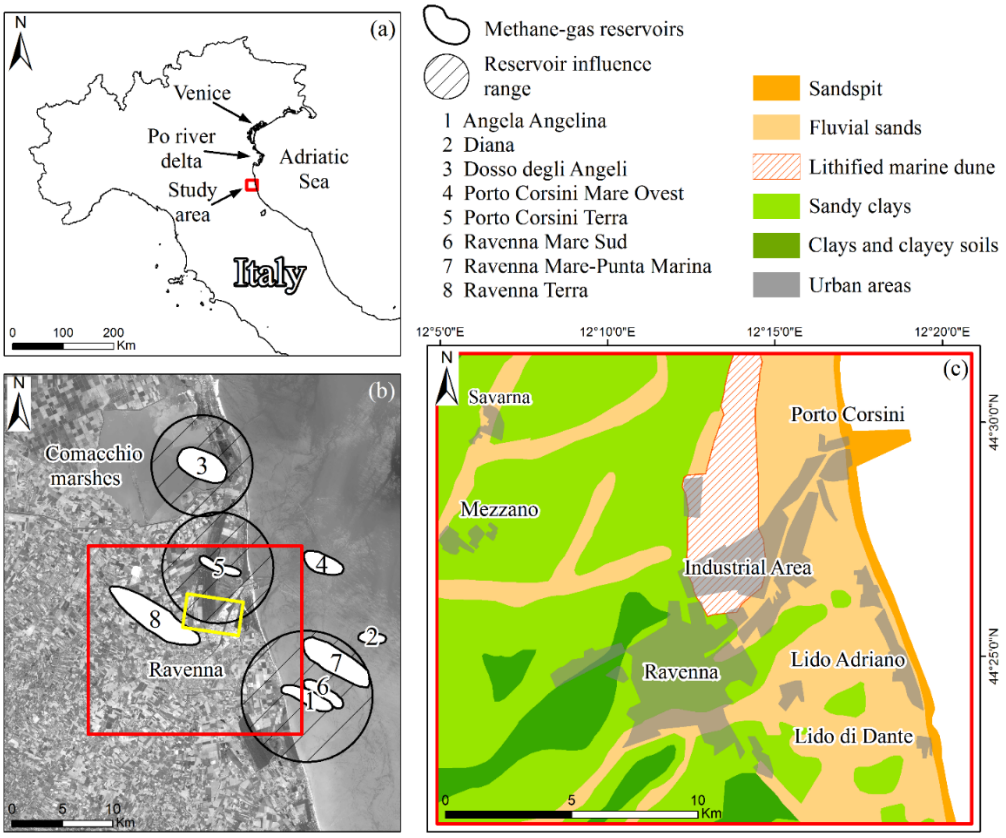

Figure 1. (a) Location of the study area; (b) Methane-gas reservoirs close to Ravenna. The yellow square is the area used for the cross-validation between the SBAS and CPT results. Basemap: 07/18/2016 Sentinel-2 image; (c) Geological map of the study area and main locations.

2.2. Mechanisms of the subsidence

The subsidence affecting the Adriatic Sea coastline in northern Italy can be related to different anthropic and natural factors that vary locally: tectonic, glacial isostatic adjustment, reclaimed peatland oxidation, groundwater withdrawal, gas extraction, natural sediments compaction. The Regional Agency for the Environmental Protection (ARPA) of Emilia-Romagna Region and the Emilia-Romagna Region (2010) estimate the overall contribution of the natural subsidence in -1.4 mm/yr at Ravenna, -2.5 mm/yr at Po river delta and -1 mm/yr at Venice. Gambolati et al. (1999), also modelled and calculated the natural subsidence due to sediments compaction with rates of -2.5 mm/yr at Ravenna, -4,-5 mm/yr in the Po river delta and 0.5 mm/yr at Venice. The present-day subsidence in the Po Plain is also given by the effects of the last deglaciation period that contributes with increasing values going from Venice (-1.1 mm/yr) to Ravenna (-3.5 mm/yr) (Carminati et al., 2003).

At regional scale, the main cause of the anthropogenic subsidence can be related to the combined effects of the extraction of underground water and methane-gas from on and off-shore reservoirs. At local scale, in particular along the coastline close to Ravenna, the high rates of subsidence are more related to the exploitation of the off-shore methane-gas fields closer to the shoreline (ENI and ARPA, 2003)

2.2.1. Subsidence due to methane-gas extraction

In the Ravenna area, there are eight main gas fields (Figure 1b), five of which are off-shore and three on-shore. The production that started in the '70s is still ongoing at the present-day for most of the fields: only two fields are inactive, Ravenna Terra and Porto Corsini Terra, which exploitation stopped in 1992 and 2014, respectively. The most productive fields are Dosso degli Angeli and Angela-Angelina, with average annual production from 1980 to 2016 of 450×10^6 Sm^3 and 600×10^6 Sm^3, respectively (http://unmig.mise.gov.it/).

Angela-Angelina gas field is one of the major reservoirs in Northern Adriatic. The production started in 1973 and is still active. Due to its proximity to the coastline (around 2 km), and the high productivity rates (Figure 2) the impact on the coastline produced by the depletion of the reservoirs can be much higher than the one of the other gas fields (Gambolati et al., 1999). Gambolati and Teatini (1998), simulated the subsidence caused by the reservoir compaction and estimated a maximum influence range of around 6.5 km (Figure 1b).

Dosso degli Angeli is an on-shore gas field located under the Comacchio Marshes, 20 km North of Ravenna. From the beginning of the production until 2004, the reservoir produced 30×10^9 Sm^3 of methane gas. The average annual production was constant until 1990 with more than 1×10^9 Sm^3. Afterwards, it slowly decreased till ending in 2004. In 2011 the production started again with an average annual production of 100×10^6 Sm^3. ARPA (2010), estimated in 5 km the influence range of the reservoir.

The Porto Corsini Terra gas field is located 6 km northeast of Ravenna. From 1980 until 2014, the average annual production was 20×10^6 Sm^3. Bertoni et al. (1995), estimated a maximum influence range of about 5.5 km (Figure 1b).

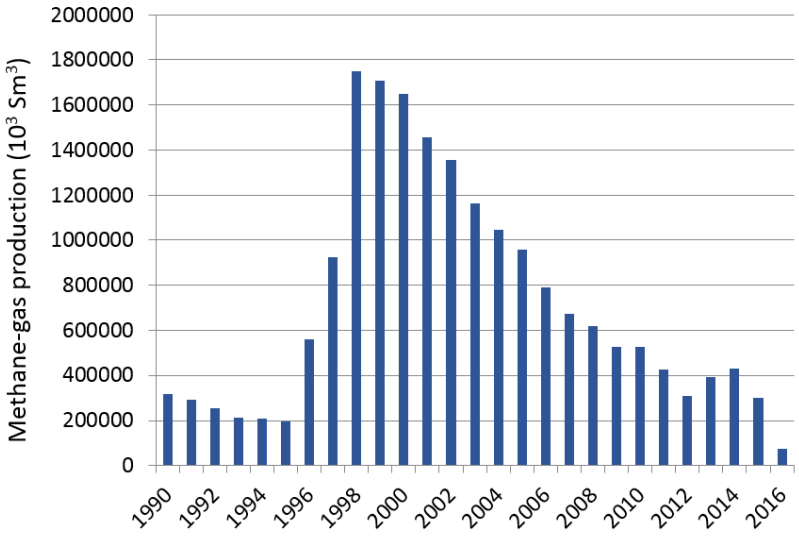

Figure 2. Production rate of the Angela-Angelina methane-gas field for the period 1990-2016.

2.2.2. Subsidence due to groundwater extraction

Another anthropogenic component of the subsidence affecting the study area is related to the water extraction activities. Since the water withdrawal rate is strongly dependent on different factors among which the number of used wells, the depth and geology of the exploited reservoirs, and the climate, the subsidence rates vary locally. The water use in the Region can be divided in four main categories: civil, industrial, agricultural and livestock. According to ARPA (2010), from 2002 to 2006 the simulated water withdrawals, in millions of m^3/yr, were: 32 for civil use, 10 for industrial use and 1 for livestock use (Figure 3). The water extraction rates for agricultural use are more variable because of its relationship with the climatic and seasonal conditions. The rates vary from 36×10^6 m^3/yr to 10×10^6 m^3/yr. Most of the withdrawals (1.72 m^3/s) for all the categories take place at depth ranging from -40 m to -100 m. Among these, the 54% of the extractions (0.94 m^3/s) are from -10 m to -40 m. Only the extractions for industrial use take place in the deeper reservoirs ranging from -200 m to -340 m of depth.

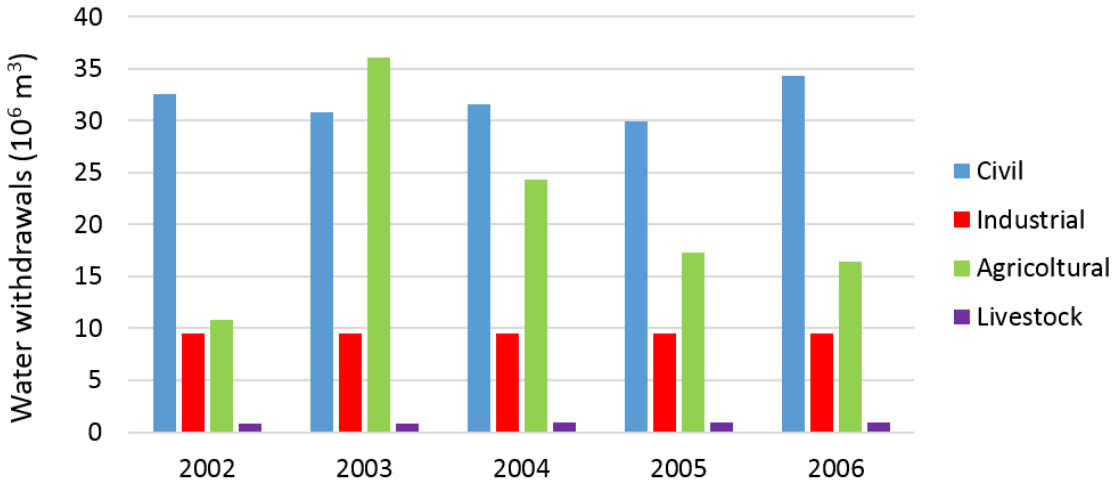

Figure 3. Groundwater withdrawals in millions of m^3 calculated for each type of well for the period 2002-2006, redrawn from ARPA (2010).

3. Methodology

3.1. A-DInSAR processing and available datasets

A-DInSAR techniques permit to obtain reliable deformation time series for the pixels that present good phase quality. The latter can be low due to geometrical and temporal decorrelation phenomena occurring in the interferograms. Therefore, a preliminary pixel selection is necessary to obtain trustworthy processing results. The pixel phase quality analysis can be carried out following three main criteria: (1) coherence stability (Berardino et al., 2002; Mora et al., 2003; Lanari et al., 2004); (2) amplitude dispersion index (Ferretti et al., 2001); (3) Temporal Sublook Spectral Coherence (Iglesias et al., 2014). In the first case (1), the pixels are chosen considering their mean coherence computed using all the multi-looked interferograms. Such pixel coherence is a function of the interferometric phase's standard deviation (Blanco et al., 2006). The displacement information is then calculated choosing a coherence threshold value, only for the pixels that present a high interferometric

quality. The amplitude dispersion index (2) permits to select pixels with a stable electromagnetic response (when their signal-to-noise ratio is high). The latter method (3), applies a point-like coherent scatterers selection, taking into account the temporal axis.

In the present work, A-DInSAR techniques have been used to get 25 years (1992-2016) of ground displacement monitoring in the Ravenna Municipality area exploiting four SAR datasets acquired by C- and X-band satellites. To this aim, the SBAS and CPT algorithms, respectively implemented in the SARscape® and SUBSOFT processor software packages have been used. Specifically, 57 ERS-1/2 (C-band), 60 ENVISAT (C-band), 53 TerraSAR-X StripMap (X-band) and 30 Sentinel-1A Interferometric Wide Swath (C-band) images acquired in descending geometry have been processed with SARscape®. The main features of each dataset and their temporal coverage have been reported in Table 1. The processing window adopted (study area) is 18 km × 21 km focusing the monitoring activity on the city of Ravenna and its shoreline (Figure 1b). The SUBSOFT processor has been used to process only the ENVISAT and TerraSAR-X datasets over a smaller area (6 km x 3 km) in the industrial area of Ravenna (Figure 1b), in order to perform the comparison analyses between the two different approaches and cross-validate the results.

Table 1. Details of the available SAR image datasets.

Satellite	**ERS-1/2**	**ENVISAT**	**TerraSAR-X**	**Sentinel-1A**
Period covered	05/10/1992-12/13/2000	04/02/2003-09/22/2010	02/25/2012-04/05/2014	10/12/2014-01/11/2016
Track No.	122	122	2	95
Number of images	57	60	53	30
Wavelength (cm)	5.6	5.6	3	5.6
Incidence angle (°)	23	23	29	39
Imaging mode	SAR	ASAR IM	StripMap	Wide Swath
Polarization	VV	VV	HH	VV

The SBAS processing workflow adopted in SARscape® consists of five main steps: (a) connection graph (CG) generation; (b) interferogram generation and unwrapping; (c) refinement and re-flattening; (d) first and second inversion; (e) geocoding. In the first step (a), the connection links between master and slaves image pairs are created based on the specified temporal and perpendicular baseline thresholds; (b) for each connection pairs the interferograms are generated and filtered using the Goldstein adaptive filter (Goldstein and Werner 1998). The phase is then unwrapped using the Delaunay Minimum Cost Flow (MFC) method (Costantini, 1998; Costantini and Rosen, 1999); (c) the constant and topographic phases are removed from the interferograms. Possible inaccuracies in the satellites' orbits are corrected and phase ramps, if present, are removed; (d) the residual heights and displacement velocities are derived and used to re-flatten the interferograms. Then, the atmospheric phase component is removed and the displacement velocities are calculated; (e) the final products are geocoded to the chosen cartographic projection.

In Table 2 are reported the main parameters adopted to process the four SAR datasets with the SARscape® approach. To remove the topographic component of the phase, the Shuttle Radar Topography Mission (SRTM) Digital Elevation Model (DEM) with a resolution of 1 arc second (30 m pixel size) was used. After the editing step in which the bad interferogram pairs are discarded for unwrapping and/or processing errors, a good amount of interferograms was still available. The edited CG plots for each dataset are reported in Figure 4.

Table 2. Main parameters and thresholds adopted in SARscape® for the SBAS processings.

Satellite	ERS-1/2	ENVISAT	TerraSAR-X	Sentinel-1A
Perpendicular thresh. (% of critical baseline)	50	45	35	45
Temporal thresh. (days)	900	730	190	150
Unwrapping thresh.	0.30	0.35	0.40	0.60
Multi-look Rg/Az	1/5	1/5	5/5	5/1
Resolution (m)	20	20	10	20
No. of generated interferograms	274	380	360	200

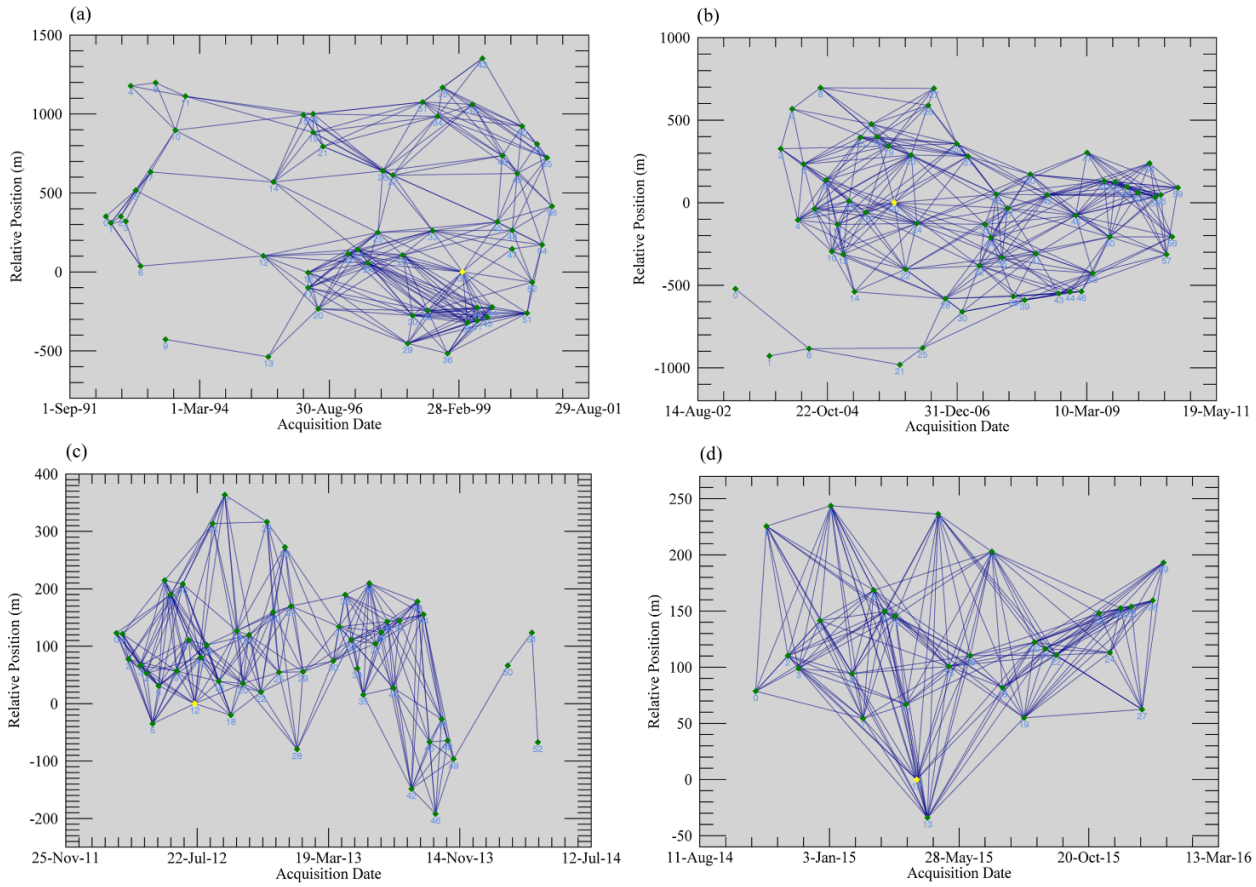

Figure 4. Interferogram pairs selected with SBAS after the editing session for (a) ERS-1/2, (b) ENVISAT, (c) TerraSAR-X, (d) Sentinel-1A**.**

The SUBSOFT processor, used to process the ENVISAT and TerraSAR-X data only, was implemented at the Remote Sensing Laboratory (RSLab) of the Universitat Politècnica de Catalunya (UPC) and is based on the algorithms proposed by Mora et al. (2003) and by Iglesias et al. (2014). The algorithm scheme is made of three main steps: (a) generation of the best interferogram set; (b) selection of the pixels with reliable phase within the interferogram set; (c) pixels phase analysis to calculate the deformation time series. For the pixel selection, the Temporal Sublook Spectral Coherence method, described previously, has been chosen. This method permits the selection of point-like scatterers by replacing the spatial average, which generates a degradation of the spatial resolution, with a temporal one. Specifically, the method is based on the analysis of their spectral properties along time. After the pixel selection, a Delaunay triangulation between the selected pixels is generated. Finally, the linear and non-linear deformations are computed through a model of coherence estimation.

With the SUBSOFT processor is not possible to generate Single Look Complex (SLC) (Level 1 product) images directly from the raw data (Level 0 product), and of the 60 ENVISAT images only 39 were provided by European Space Agency (ESA) as SLC. For this reason, only a smaller number of ENVISAT images covering the period 12/2005 - 09/2010 were processed to perform the cross-validation. For ENVISAT, the adopted processing parameters consist of a maximum spatial and temporal baseline respectively of 300 m and 246 days, a multi-look factor of 15 × 3 in Range and Azimuth, and an unwrapping threshold of 0.40. Considering these parameters, the obtained displacement standard deviation was 1.5 mm. In total, 80 interferograms were generated. The topographic component of the phase was removed using the 30 m resolution SRTM DEM.

For the TerraSAR-X data processing, a maximum spatial baseline of 125 m and a maximum temporal baseline of 125 days have been used. Considering the adopted spatial baseline threshold, 11 images not respecting the constrain have been dropped. From the remaining 42 images, 220 interferograms have been selected. The applied multi-look factor is 3 × 3 in Range and Azimuth, and the coherence threshold is 0.4, which implies a phase standard deviation of 15°: the corresponding displacement standard deviation is about 1 mm. The topographic component of the phase was removed using the 30 m resolution SRTM DEM.

3.2. Statistical analyses

Two statistical approaches were applied to the SBAS results in a Geographical Information System (GIS) in order to (a) identify the main areas affected by subsidence through the ground-motion areas detection and (b) comprehend the deformation mechanisms analysing their relationships with the main triggering factors.

The ground-motion areas detection method proposed by Bonì et al. (2016) is addressed to simplify the analysis of very large point datasets resulting from A-DInSAR processing, using a fast and systematic procedure. The methodology allows us to identify areas that present significant movements, the ground-motion areas, considering specific patterns in the time series of each measured point. This method can be very useful to highlight areas with peculiar ground deformation behavior that may require more deep analyses. The applied procedure consists of two main steps: (1) the time series accuracy assessment is performed applying the approach proposed by Notti et al.

(2015) in order to correct anomalous displacements affecting the time series in a certain date; (2) different statistical tests are applied to find the spatio-temporal pattern of the Principal Components (PC) of the movement and the kinematic model of the measured points. In particular, the Principal Component Analysis was performed implementing a matrix organization location versus time (T-mode) to detect the PC of ground-motion (Chaussard et al., 2014). The number of time-dependent components was detected for each dataset considering the change of slope in the Scree plot. Each component was represented by score maps as applied by others authors (Chaussard et al., 2014). More specifically, the PC scores obtained for each measured point represent the value of correlation with the trend of the PC in the whole dataset; the higher values correspond to higher correlation with the analyzed PC (Bonì et al., 2016). The software PSTime (Berti et al., 2013) was used to classify the time series into one of the three predefined target trends: uncorrelated, linear and non-linear (Berti et al., 2013). The approach is based on a sequence of statistical characterization tests that permit the automatic classification of each measured point. PSTime also detects the date (break-date) where an abrupt slope change in the non-linear time series is recorded. The evidence ratio of the breakpoint (BICW) index (Berti et al., 2013) is also assigned to the non-linear time series. The ground-motion areas were identified using a spatial cluster of the significant PC scores using a buffer zone of 50 m around each measured point. The PC score was used to find the spatial distribution of the ground-motion areas using the approach implemented by Meisina et al. (2008). The obtained kinematic model of the measured points was combined with the ground-motion areas to identify linear and non-linear processes: values of BICW higher than 1.2 were selected to distinguish non-linear time series from the linear ground-motion areas.

With the second statistical approach, the variance analysis is applied to the SBAS results, already imported in a GIS, to combine each measured point with the available ancillary data, evaluating the contribution to the subsidence of four main factors: geological setting, water extraction, gas extraction and land-use change. In particular, the analyses are carried out considering the relationship between the measured displacement values and the lithologies in the study area, the position of the water pumping wells, the distance from the methane-gas reservoirs and their production rates, the areas where land-use changes occurred. This method is based on the variances ratio and uses the distribution of Fisher-Snedecor (Fisher, 1942; Snedecor et al., 1967).

4. Results and Discussion

4.1. *A-DInSAR SBAS results*

The results obtained from the SBAS processing are reported as cumulated displacement maps projected to the vertical (Figure 5). In total, we detected 53,000 points with ERS-1/2, 71,200 with ENVISAT, 304,000 with TerraSAR-X and 100,000 with Sentinel-1A. The range of the detected velocities in the entire monitoring period (1992-2016) goes from -35 mm/yr to +5 mm/yr. Data coverage is good for all the datasets and is concentrated over the urbanized areas that present high coherence values. Strong subsidence mainly occurs along the coastal areas with higher values registered in the north and south. Most of the city centre is stable, with displacement values in the range of ±5 mm for the entire period.

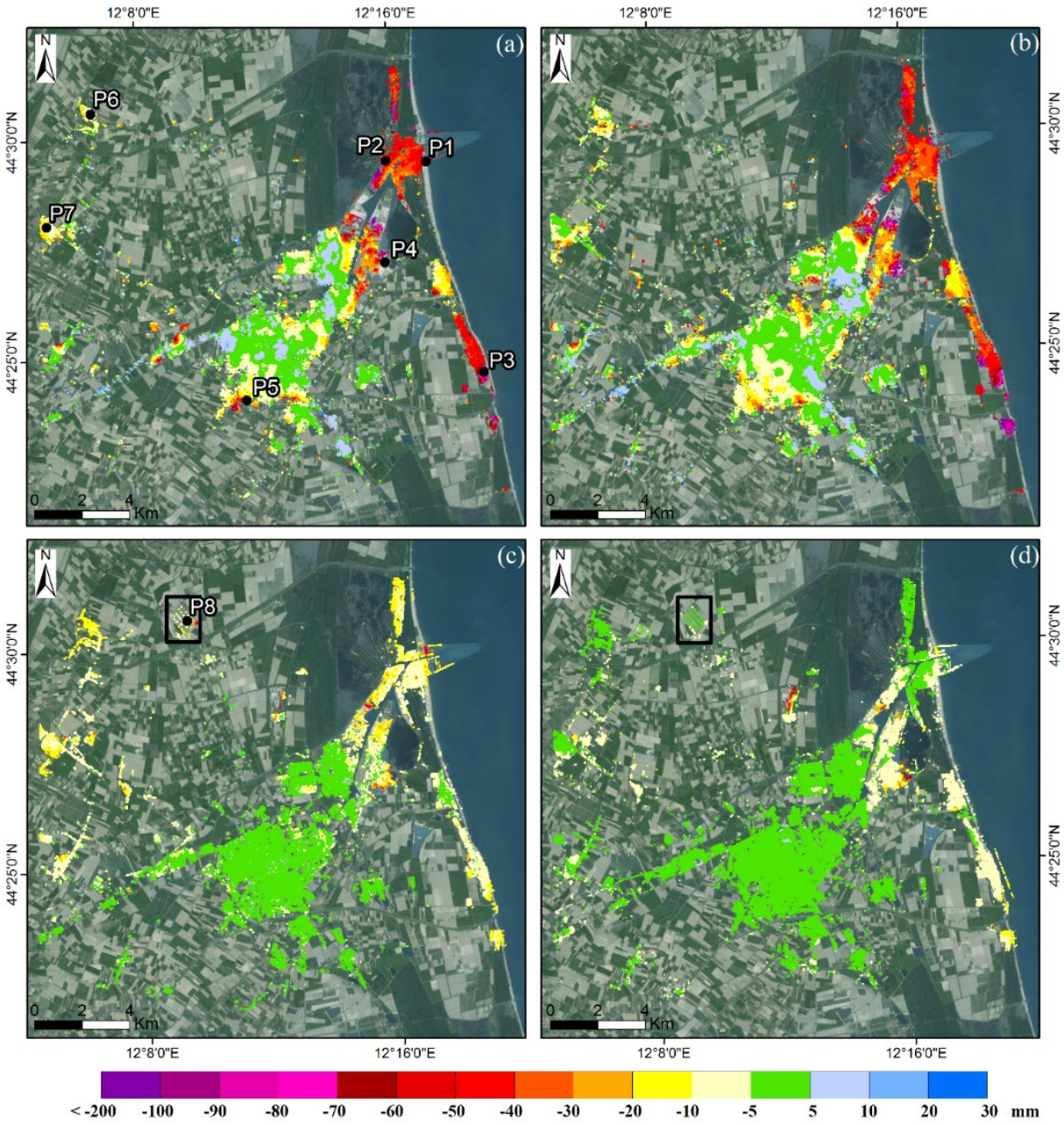

Figure 5. Vertical displacement maps obtained from the processing of (a) ERS-1/2 (1992-2000), (b) ENVISAT 2003-2010, (c) TerraSAR-X (2012-2014) and (d) Sentinel-1A (2014-2016) SAR images through SARscape®. The black dots, from P1 to P8, are the locations of the points considered for the time series analysis.

In Figure 5c and d, it is possible to notice a subsiding area detected in the north part of the study area (black square). This area is a solar panel field of recent construction that was completed in early 2011 and expanded with two new small adjacent solar fields in early 2012. This area is clearly visible with both TerraSAR-X and Sentinel-1A datasets showing the capabilities of the latter in the monitoring of ground displacement even at local scale. The subsidence affecting this area is probably caused by the load produced by the panels structure itself over rural land. Here, the maximum displacement registered reached -21 mm during 2012-2014 and -11 mm in 2014-2016.

To better understand the displacement patterns in the study area, the time series of seven control points (Figure 5a) have been analysed. The points were selected in the most critical areas, where the

resulted subsidence values are high, or in areas that present anomalous displacement in respect to the surroundings (e.g. localized subsidence in a generally stable area). The analysis takes into account the average displacement values of all the points that are within a distance of 100 m from the selected points in order to minimize the effect of outliers. For each point, the time series are generated (Figure 6) considering as constant the displacement velocity in the temporal gaps between the different datasets: 28 months between ERS-1/2 and ENVISAT, 17 months between ENVISAT and TerraSAR-X and 6 months between TerraSAR-X and Sentinel-1A.

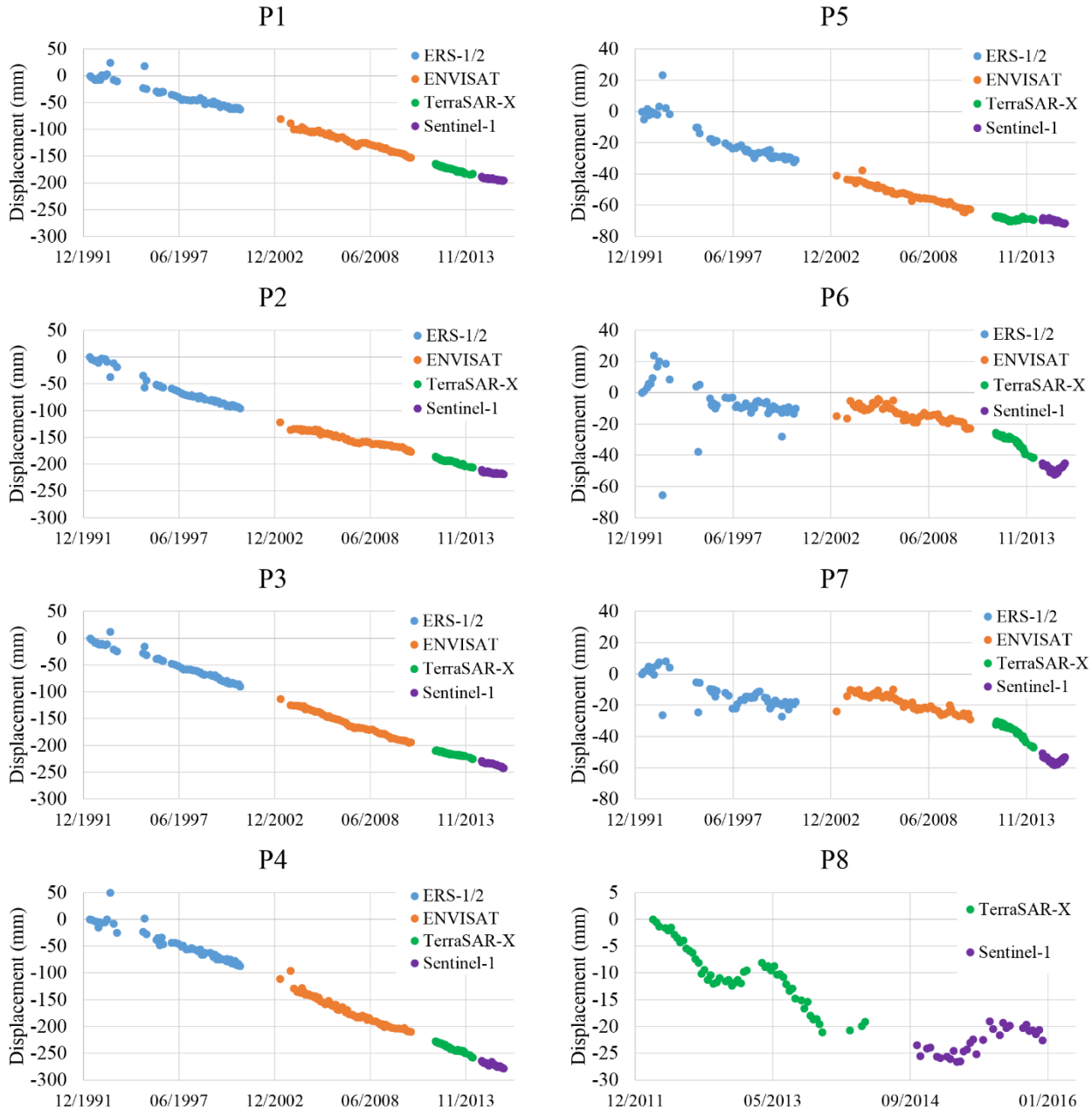

Figure 6. Cumulated displacement time series for the eight selected points reported in Figure 5a and c.

Considering the CG plot of Figure 4a, the 57 images available for ERS-1/2 are not well distributed in time and present from 1992 to 1995 a large time gap of around 700 days that separates 12 images (left side) from the main cluster (right side). Since we needed to analyse the subsidence

trends for the entire 1992–2000 period without losing any image, we adopted a temporal threshold of 900 days in order to connect all possible pairs. Unfortunately, the 700-day temporal baseline interferograms presented temporal decorrelation and consequent low coherence that reduced their quality. For this reason, during the 1992-1995 period some phase unwrapping errors occurred and generated the anomalous displacement values that are visible in the time series of Figure 6. Taking into account the entire 1992-2016 period, the time series of the points located close to the coastline show an almost linear trend of deformation with low variation in the slope of the linear regression line. These points present the highest displacement values that were calculated as -250 mm at Lido Adriano (P3) and as -280 mm in the industrial area (P4). The time series obtained for the latter, shows an almost constant velocity for the entire period. Along the coastline, the point P3 presents a linear subsidence trend until 2001 (-7 mm/yr); the trend starts to increase from 2003 until the end of 2015 (-11 mm/yr) and then it decreases again with values lower than the first period (-6 mm/yr). On the contrary, nine km to the north, the point located at Porto Corsini (P1) shows a constant increase of the displacement velocities from -7.8 mm/yr (1992-2000) to around -9.3 mm/yr (2014). The rates start to lower in 2014-16 with -5 mm/y. The points less affected by subsidence are the ones located at Ravenna (P5) with around -70 mm of cumulated displacement, and to the west of the study area in the towns of Savarna and Mezzano (points P6 and P7, respectively). Here the maximum displacement reached -60 mm in both locations. Even if the two towns are located at a distance of 5 km, there is a strong correspondence in the displacement trend that is not linear but presents fluctuations in the entire period. The slope of the linear fitting line remains constant during 1992-2010 with a velocity of around -2 mm/yr. The slope starts increasing from 2012 to 2013 and becomes steeper from April 2013 to June 2015, when the velocity reaches -9 mm/yr. The time series of P8, located over the solar panel field, presents a clear seasonal trend during the period 2012-2016, detected by both TerraSAR-X and Sentinel-1A satellites.

4.2. Cross-validation with the CPT technique

In order to assess the reliability of the results obtained with SBAS, the ENVISAT and TerraSAR-X datasets have been re-processed using the CPT technique and the outputs have been used for the cross-validation. The two approaches based on different phase quality estimation criteria can provide complementary information. In fact, the amplitude-based criterion generally provides high point density that can be used to carry out analyses at high resolution, such as for the monitoring of buildings (Tomás et al., 2014). On the other hand, to monitor subsidence or volcanic activity over larger areas the coherence-based processing is generally better suited. For this reason, a good match between the results obtained with the two techniques (cross-validation) can give a good indication of the processing quality and can be used as an effective validation method. As shown in other comparison experiments between A-DInSAR techniques (e.g. Herrera et al., 2009), in spite of their different pixel selection criterion based on the phase quality estimation, both approaches exhibit good performance in estimating deformations; their main difference consists of the operative resolution.

The ENVISAT and TerraSAR-X processing with CPT was carried out over a small area of 6 km x 3 km that covers the industrial area of Ravenna (Figure 1b), chosen because it is affected by very high rates of subsidence and presents high coherence values that permit to optimize the comparisons. The results, reported as vertical displacement map (Figure 7c and d), are in good agreement with the

SBAS results obtained over the same area (Figure 7a and b). The lower number of points obtained with the CPT in respect to SBAS (369 vs 5896 for ENVISAT and 16,500 vs 28,700 for TerraSAR-X) is due to the more restrictive thresholds and higher multi-look factor adopted in the processing steps as described in Section 3.1. The time series of the four points selected for each dataset for the comparisons (Figure 8) show a good correspondence between CPT and SBAS in terms of mean velocity and displacement trends. It is possible to notice a shift in the calculated displacement of about 2-3 mm/yr in each time series that is probably due to the different algorithm and methodology applied. This can be explained considering the different parameters adopted during the processing, such as unwrapping coherence threshold and multi-look factor (see Section 3.1) that imply different displacement standard deviations: for TerraSAR-X, the obtained standard deviation was 1.5 mm with SBAS and 1.0 mm with CPT, while for ENVISAT, it was 5.0 mm and 1.5 mm with SBAS and CPT, respectively. The comparison depicts the goodness of the results obtained with the SBAS technique.

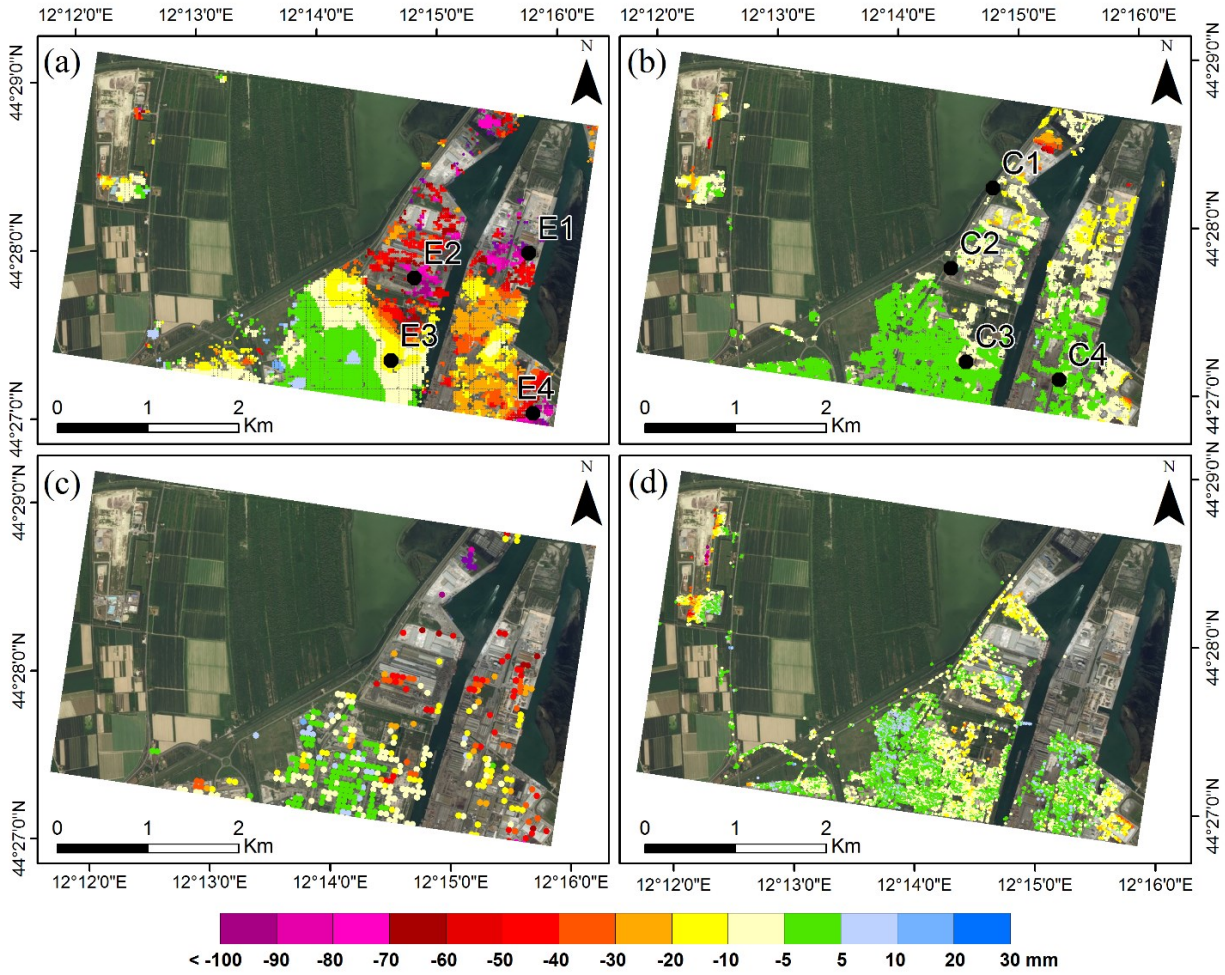

Figure 7. Cumulated displacement maps over the industrial area of Ravenna used to cross-validate the results: a) ENVISAT processed with SBAS. b) TerraSAR-X processed with SBAS. c) ENVISAT processed with CPT. d) TerraSAR-X processed with CPT. The black dots, from E1 to E4 and from C1 to C4, are the locations of the points selected to perform the comparison between the time series obtained respectively from ENVISAT and TerraSAR-X.

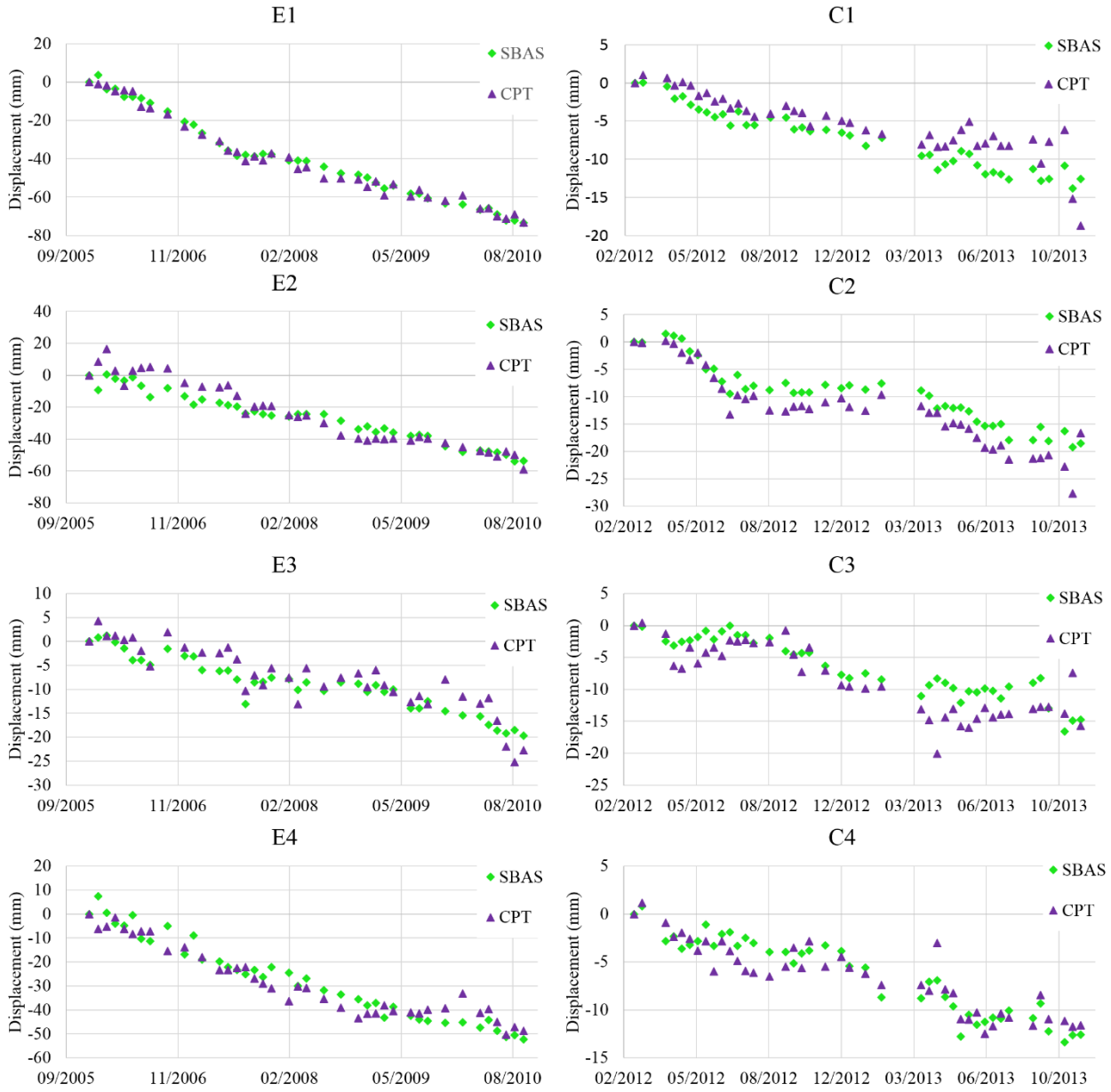

Figure 8. Comparison between the time series obtained with SBAS and CPT processing of the control points selected in the industrial area of Ravenna for ENVISAT (E1-E4) and TerraSAR-X (C1-C4).

4.3. Identification of ground-motion areas

The ground-motion detection methodology was applied to the A-DInSAR results considering three main components of motion: PC1, which describes a movement away from the satellite (i.e. subsidence); PC2, which describes a movement toward the satellite (i.e. uplift); PC3, which describes a seasonal component of motion. The results reveal that PC1 accounts for the 80-90% of the variance for all datasets while PC2 and PC3 explain the variance in a range from 1% to 10% of ENVISAT, TerraSAR-X and Sentinel-1A results. Considering that PC1 better describes most of the components of motion in all datasets, the analyses were performed using only PC1. Figure 9 shows the spatial distribution of the ground-motion areas detected using PC1 of the four datasets. According to the methodology, six main subsiding areas have been identified: Porto Corsini (A1), the industrial area

(A2), Lido Adriano (A3), Lido di Dante (A4), the Southwest area of Ravenna (A5), Savarna and Mezzano (A6).

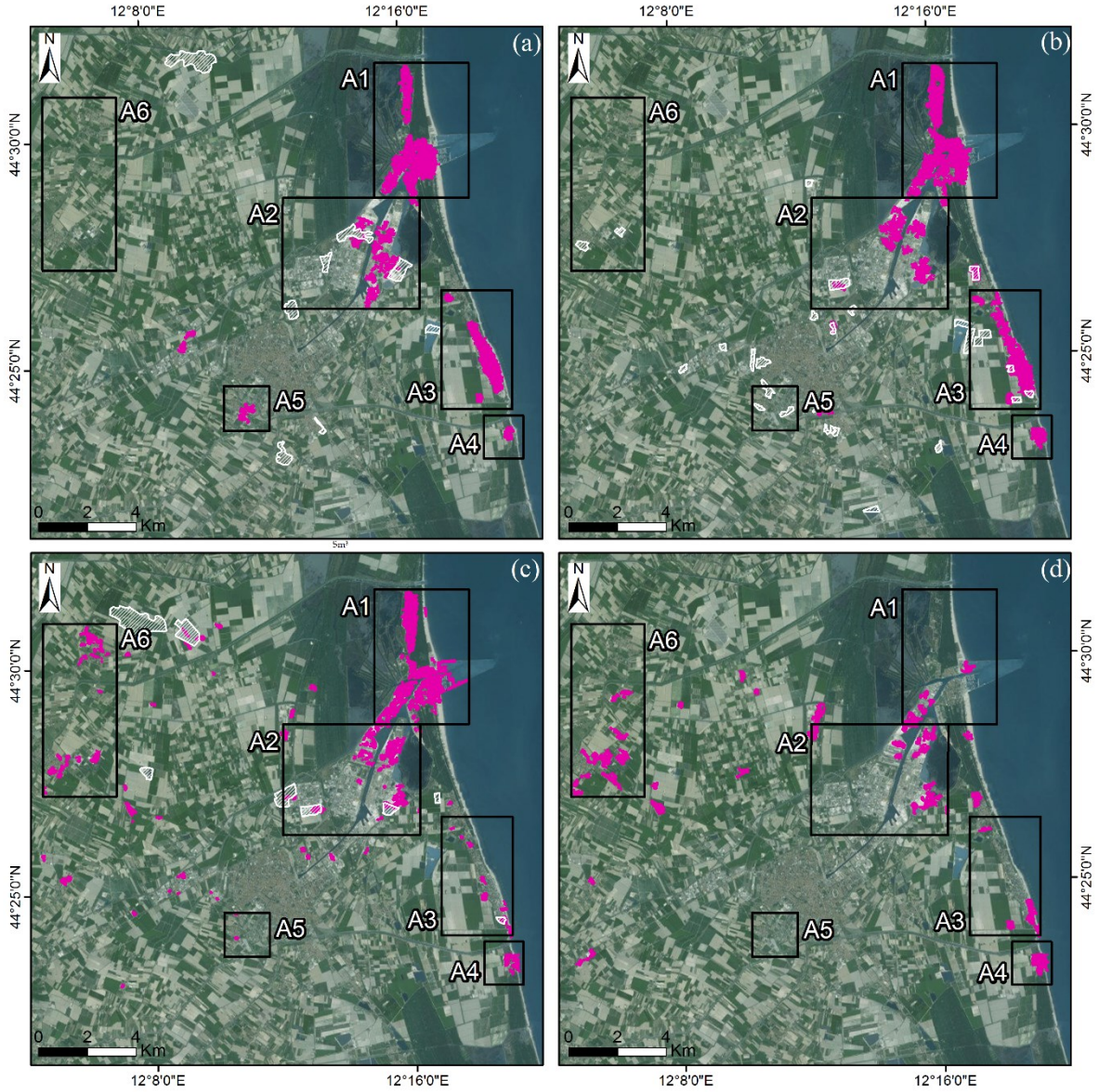

Figure 9. In pink, the six ground-motion areas delimited by squares (A1: Porto Corsini; A2: Industrial Area; A3: Lido Adriano; A4: Lido di Dante; A5: South-west of Ravenna; A6: Savarna and Mezzano) detected using the PC1 main component of motion for (a) ERS-1/2 (b) ENVISAT (c) TerraSAR-X and (d) Sentinel-1A datasets. The white striped areas are the Corine Land Cover changes described in Section 4.4.

After selecting the measured points localized in the six ground-motion areas affected by subsidence, the average velocity and the standard deviation for each dataset have been calculated (Table 3). Regarding the kinematic model, the results (Figure 10) highlight that 40-50% of the points measured using ERS-1/2 and ENVISAT datasets is characterized by a linear trend, 30-40% show a non-linear trend and 20-30% show an uncorrelated trend. Most of the measured points (around 43%) resulting from the TerraSAR-X data processing show a non-linear trend, while 30% is characterized by a linear trend and 27% by an uncorrelated trend. Unfortunately, the kinematic model analysis

cannot be performed with the Sentinel-1A results, because the automatic procedure can work only with time series longer than 22 months.

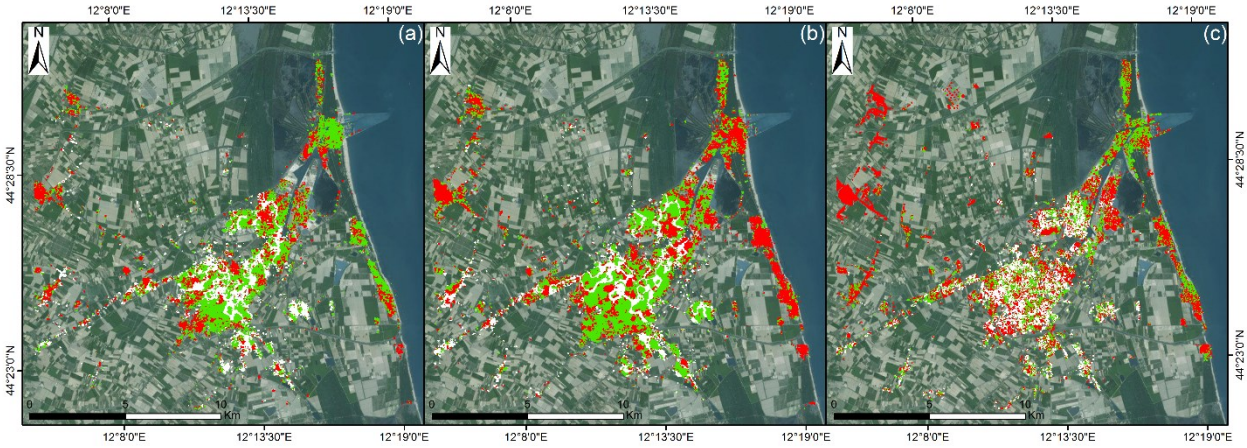

Figure 10. Points measured with (a) ERS-1/2 (b) ENVISAT and (c) TerraSAR-X, classified by their kinematic model: linear trend in green, non-linear trend in red and uncorrelated trend in white.

Table 3. Average vertical velocity (Vvert) and standard deviation (Std) calculated in the six different ground-motion areas for each dataset.

Period		10/05/1992-13/12/2000	02/04/2003-22/09/2010	25/02/2012-05/04/2014	12/10/2014-11/01/2016
Dataset		ERS-1/2	ENVISAT	TerraSAR-X	Sentinel-1A
A1 (Porto Corsini)	Vvert (mm/yr)	-7.23	-6.17	-7.91	-2.09
	Std (mm/yr)	2.34	1.31	0.85	0.85
A2 (Industrial area)	Vvert (mm/yr)	-6.37	-8.39	-10.05	-15.25
	Std (mm/yr)	2.17	3.35	4.49	9.46
A3 (Lido Adriano)	Vvert (mm/yr)	-6.83	-7.12	-7.07	-8.52
	Std (mm/yr)	1.24	2.07	1.27	0.90
A4 (Lido di Dante)	Vvert (mm/yr)	-7.94	-12.74	-7.45	-10.68
	Std (mm/yr)	0.92	1.47	0.94	1.12
A5 (Southwest of Ravenna)	Vvert (mm/yr)	-6.10	-5.23	-5.23	-2.72
	Std (mm/yr)	2.27	0.87	0.94	0.43
A6 (Savarna and Mezzano)	Vvert (mm/yr)	-3.70	-3.68	-10.11	-3.31
	Std (mm/yr)	0.78	0.69	0.72	1.76

4.4. Interpretation of ground motion areas

Statistical analyses were used to interpret which are the main factors influencing the detected ground motion areas. Unfortunately, the restricted availability of ancillary data limited the number of the possible factors to analyse. Anyway, the results obtained so far are in accordance with the main conclusions of the scientific literature (e.g. Teatini et al., 2005).

A first analysis was carried out to evaluate the influence that the geology has on the deformation values, associating the available geological information (Figure 1c) to each point measured with

SBAS. For all the four A-DInSAR processings, the test has shown a high influence of the geology on the measured deformation with values increasing towards the coastline. Specifically, bigger deformations occur over the fluvial sands lithology with an average value of -27.4±26.5 mm for 1992-2000, -26.5±27.8 mm for 2003-2010, -7.8±6.9 mm for 2012-2014, and -4.2±4.6 mm for 2014-2016. Small deformations are observed on the lithified marine dune with an average of -1.1±9.5 mm for 1992-2000, -3.2±12.4 mm for 2003-2010, -1.5±5.3 mm for 2012-2014, and -2.6±6.1 mm for 2014-2016.

A second analysis was applied to assess the relationship between the water wells, classified by type of use (agricultural, civil and livestock) and the subsidence velocity. Unfortunately, no data about the pumping rates for each well is available, so the analysis is based only on their location. A fishnet with cell size of 1 km × 1 km has been created and the average velocity for each cell has been computed (Figure 11).

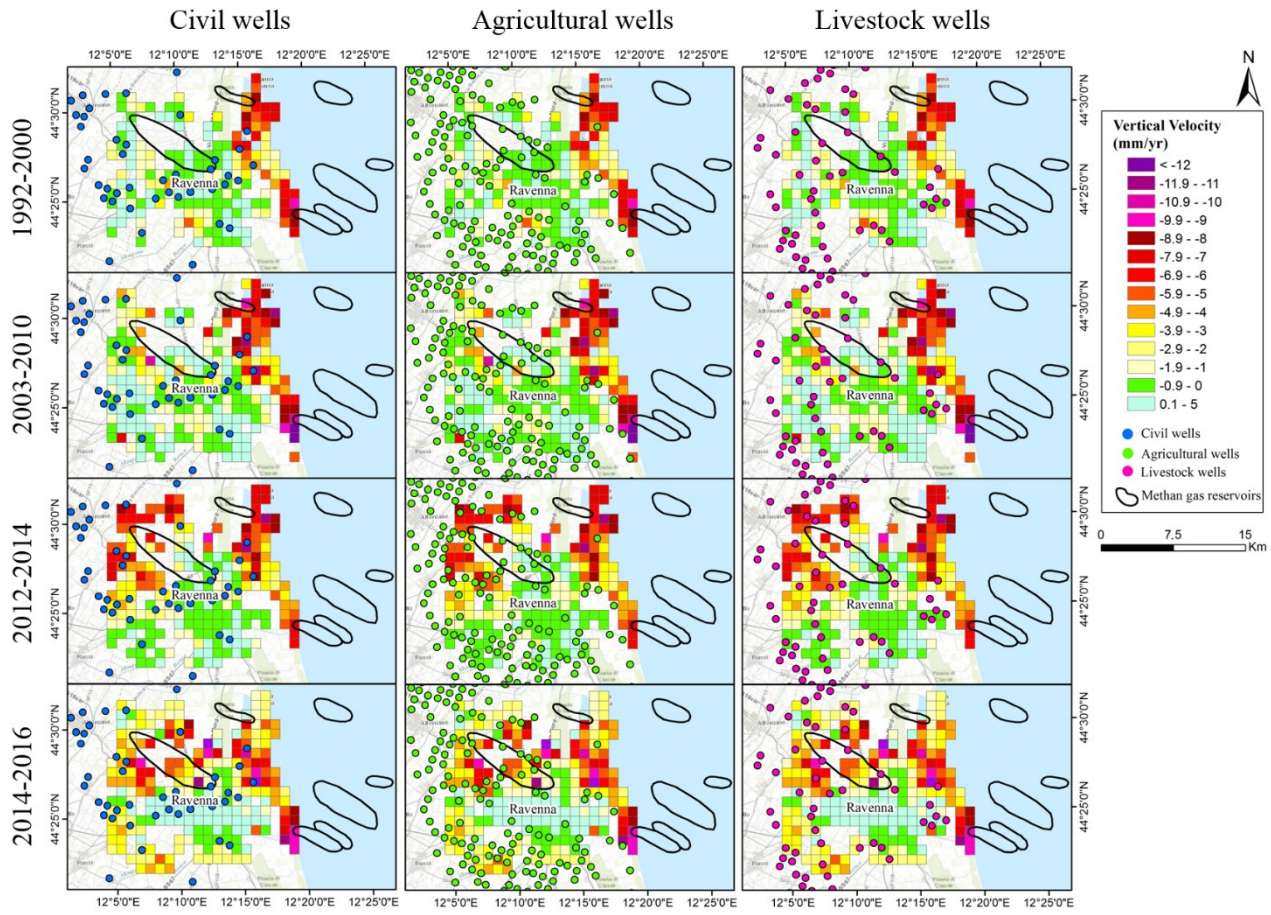

Figure 11. Average vertical velocities of deformation computed with a fishnet of 1 km x 1 km for each dataset. The location of the three categories of water wells and the extension of the methane gas fields are superimposed to the fishnet used in the statistical analyses.

The test does not show significant influence of the wells location on the subsidence velocities. A better correspondence was found only for the agricultural wells located in the northwestern part of the study area where agricultural activities continue to be prevalent.

In order to analyse the relationship between deformation and the gas extractions, the spatial correlation with the methane-gas field, the distance-velocity plots along with the gas production have been taken into account. We focused on Angela-Angelina and on Porto Corsini Terra gas fields.

Regarding Angela-Angelina (Figure 12), the average velocity values of the points closer to the reservoir are respectively of -1.1±1.1 mm/yr, -11.1±1.3 mm/yr, -6.9±1.3 mm/yr and -7.8±1.1 mm/yr for ERS-1/2, ENVISAT, TerraSAR-X and Sentinel-1A. The intercepts of the diagrams are of -9 mm/yr, -11 mm/yr, -6 mm/yr and -8 mm/yr for the four results.

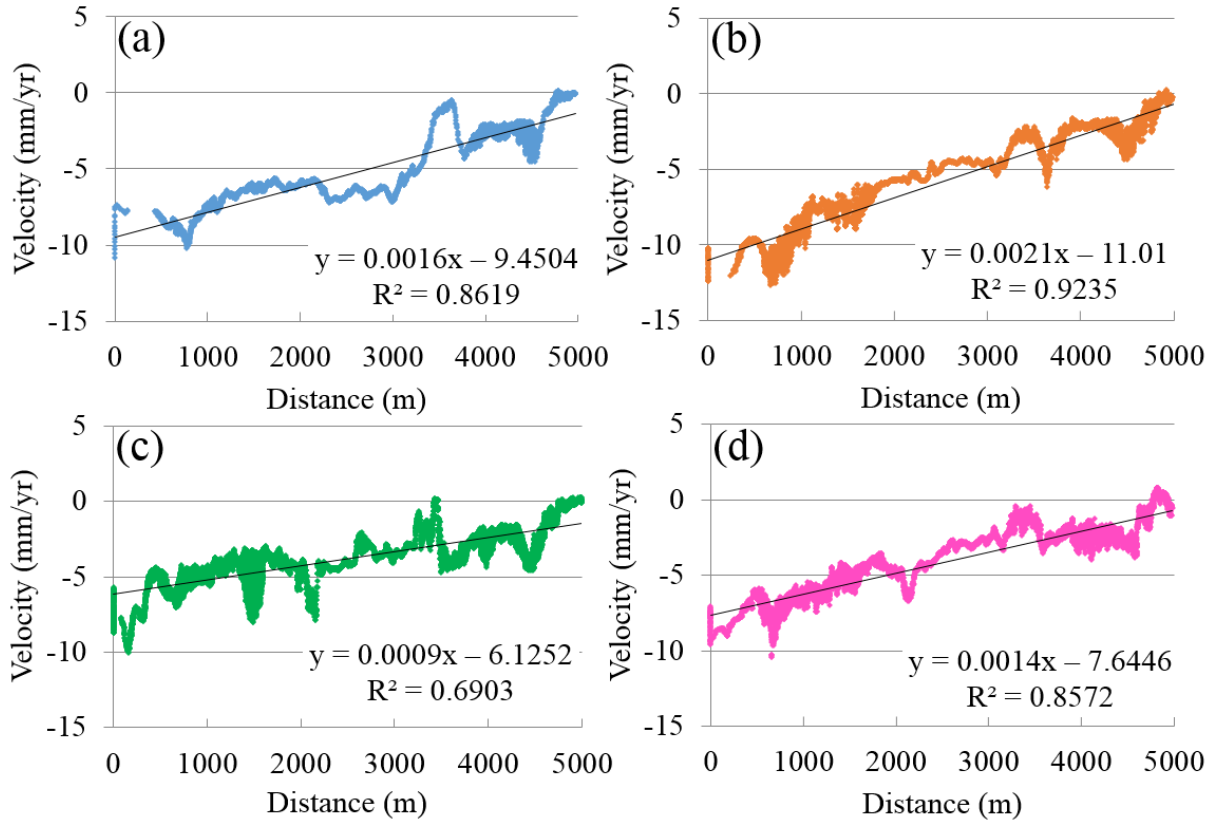

Figure 12. Velocity-distance plots for the Angela-Angelina gas field. (a) ERS-1/2 (b) ENVISAT (c) TerraSAR-X (d) Sentinel-1A.

It is possible to notice a general decrease of the measured deformations for increasing distances from the reservoir. Considering the average velocities of displacement in A3 and A4, there is an increase in the subsidence rates in the period 2003-2010 in respect to 1992-2000 and in the period 2014-2016 in respect to 2012-2014. The average velocity is higher in area A4 than in area A3. Considering the gas production activity in 1990-2016 (Figure 2), there is a quite good correlation with the measured deformations. The increase of the average velocity, detected using ENVISAT, can be related to the increase of the methane-gas extractions in 1998 (1748×10^6 Sm^3). In 2012-2014, the decrease of the average velocity can be correlated with a decrease in the methane-gas production from an annual average of 734×10^6 Sm^3 to 377×10^6 Sm^3. Conversely, the increase average velocity detected in the period 2014-2016 in both A3 and A4 is not correlated with the methane-gas production.

Even for the Porto Corsini Terra gas field, the analysis shows a general decrease of the deformations with increasing distance from the gas reservoir, especially in the northern side of the gas field (Figure 13) within a distance lower than 1 km.

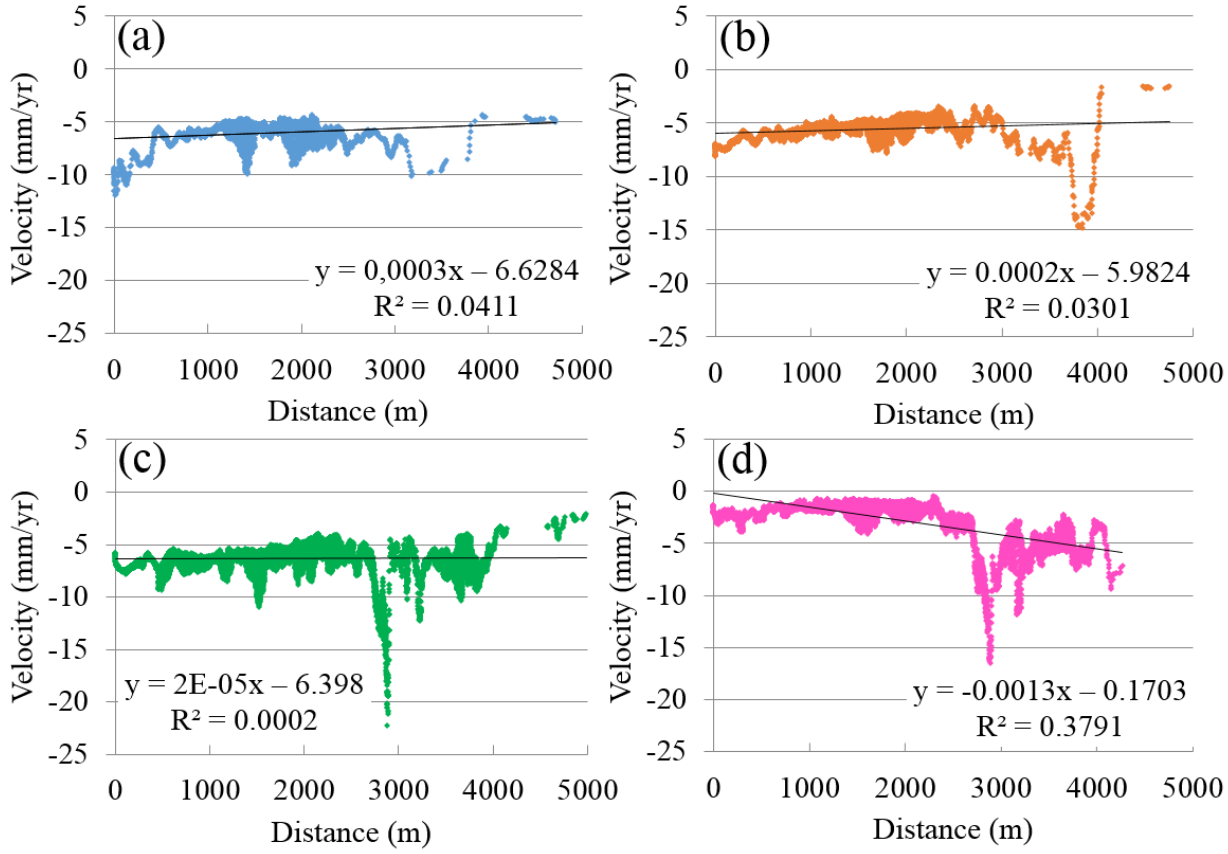

Figure 13. Velocity-distance plots for the Porto Corsini Terra gas field. (a) ERS-1/2 (b) ENVISAT (c) TerraSAR-X (d) Sentinel-1A.

The area closest to Porto Corsini Terra, A1, presents an increase of the average velocity from 2012-2014 to 2003-2010, while in 2014-2016 the velocity rapidly decreased until -2.09 mm/yr. The high average velocities found in 1992-2014 may correspond to the combined effects of the extraction activities taking place in the two gas reservoirs close to the area: Porto Corsini Terra and Porto Corsini Mare Ovest (Figure 1b). Despite the low production rates of the first, the proximity to A1 (around 1.5 km), may strongly influence the subsidence in the area. The maximum production in 2003 of 42.6 × 10^6 Sm^3 drastically lowered in the next years until ending in 2014. The Porto Corsini Mare Ovest reservoir is located around 5 km west of A1 and had a very high productivity in 2004-2008 with more than 260 × 10^6 Sm^3. In this case, the production ended in 2016. The decrease in the average velocity in 2014-2016 (-2.09 mm/yr) reflects the reduced methane-gas production in the two gas fields in those years.

4.5 Land-use change

The contribution that land-use changes may have on the detected displacement rates was evaluated by overlapping the six ground-motion areas with the CORINE Land Cover (CLC) inventory (EEA, 2007) corresponding to the period covered by each dataset (Figure 9). The ground-motion areas extracted from the ERS-1/2 results were compared with the 1990-2000 CLC changes. In A2, part of the subsidence occurs in areas which land-use changed from salt marshes and non-irrigated

arable land to industrial/commercial unit. The displacement observed with the ENVISAT data matches with the 2000-2006 CLC changes. A correlation between land use changes from arable land to industrial/commercial unit was detected in A3. Also in A2, the motion areas partly match with land-use that changed from arable land to construction unit. Therefore, in A2 part of the subsidence seems to be correlated to the sediments compaction caused by the load produced by the new constructions. Comparing the 2012-2013 CLC changes with the TerraSAR-X results, the same correlation was observed in a small area of A3 where the same land-use change occurred. The ground-motion area detected in A5 highlights a decrease of the average velocity from -6.10 mm/yr (1992-2000) to -2.72 mm/yr (2014-16). Unfortunately, no CLC changes are available for this area after 2006, but the comparison of the Google™ earth DigitalGlobe historic images Oct 17 2009 – Jun 7 2014 (Figure 14) shows new constructions in areas used as arable land. This may explain the relatively high average velocity (-5.23 mm/yr) registered in the area during 2012-2014. The ground-motion area detected at Savarna and Mezzano (A6) is characterized by a high increase of the average velocity from around -3.7 mm/yr of 1992-2010 to -10.11 mm/yr of 2012-2014; it follows a rapid decrease in 2014-2016 with -3.3 mm/yr. In this case, a strong correlation between the CLC change and subsidence did not result from the analysis. Only in few small areas of A6, the recent constructions that are visible comparing the Google™ earth DigitalGlobe historic images from 2006 to 2015 may explain local accelerations in the subsidence rates.

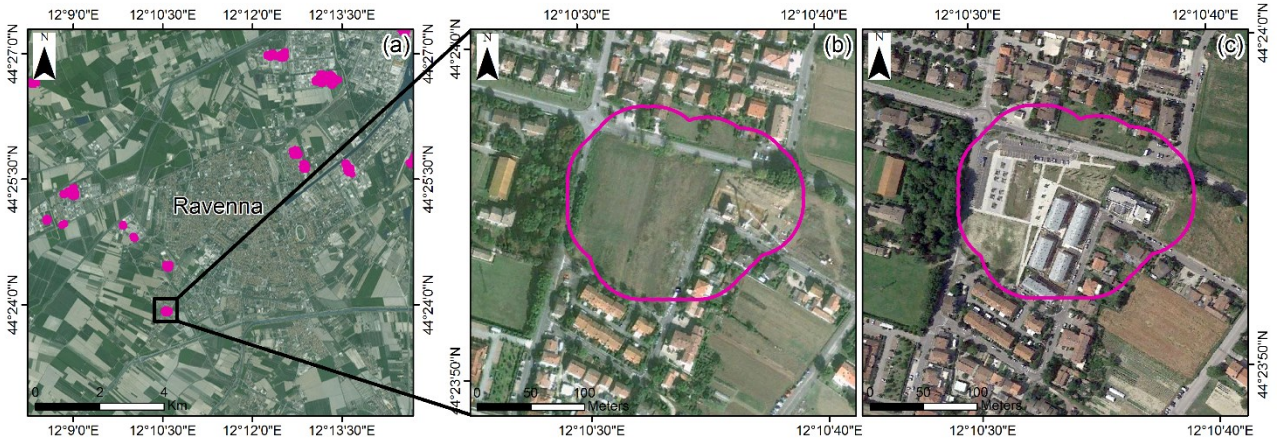

Figure 14. (a) Ground motion areas detected for the TerraSAR-X results. In (b) and (c), the comparison between the Google™ earth DigitalGlobe images Oct 17 2009 and Jun 7 2014 showing new urban development in A5.

5. Conclusions

The land subsidence affecting the city of Ravenna and its surrounding was measured using 25 years (1992-2016) of SAR data acquired by ERS-1/2, ENVISAT, TerraSAR-X and Sentinel-1A satellites. The A-DInSAR results reported as displacement maps projected to the vertical direction show subsidence up to -35 mm/yr affecting mainly the coastline and the industrial area of Ravenna. The analysis of the displacement time series was carried out over seven selected points that present mostly a linear trend. The points located along the coastline and in the industrial area present the highest displacement values in the 1992-2016 period, which was calculated as -250 mm and -280 mm, respectively. Statistical analyses were applied in order to better understand the behaviour of the

displacement over time and to assess the role of the main factors that control the subsidence. The analyses revealed that the main driving factor of the subsidence along the coastline can be related to the exploitation of the on- and off-shore methane-gas fields. There is no evident relationship between the water extraction and the detected displacements, while the correlation with the geology appears to be strong. One more factor considered was the land-use change that in many restricted areas explains the high rates of subsidence caused by the sediments consolidation under the loading of newly developed residential or industrial areas.

The results obtained with SBAS from the ENVISAT and TerraSAR-X images were cross-validated through the comparison with the CPT processing over the industrial area of Ravenna. The analysis of the time series of four control points showed that the displacement trends obtained with both techniques were very similar, confirming the validity of the SBAS results.

The study shows the benefits of a long term monitoring activity performed using A-DInSAR techniques thanks to which it is possible to monitor very large areas with metric resolution and millimetric accuracy. The availability of the new Sentinel-1A data, in particular, further improves the monitoring activity giving up to date information on the subsidence behaviour. The short revisiting time of 12 days of Sentinel-1A, not only permits to obtain better data coverage with increased points density, but also enhance the displacement time series analysis that now are sensible to seasonal trends, rainy periods or thermic variations. Furthermore, the launch in April 2016 of the twin satellite Sentinel-1B will reduce the revisiting interval to 6 days allowing us to perform near-real time and continuous monitoring activities.

Anyway, A-DInSAR results must always be integrated with other analyses in order to fully exploit their potential. In our case, the statistical analyses proved to be reliable tools that, applied to the deformation and velocity maps obtained with SBAS, allowed us to better understand the subsidence trends, its main driving factors, and the relationship with the exploitation of the underground resources in the area. Future work will regard the extension of the monitoring activity with the latest Sentinel-1A and 1B images along with the integration of other ancillary data to improve the statistical analyses.

Acknowledgments

ERS-1/2 and ENVISAT images are provided by the European Space Agency (ESA) through the project C1P.14280. The TerraSAR-X images are provided by the German Space Agency (DLR) through the proposals GEO2478 and GEO3016. The Sentinel-1A and Sentinel-2 images are freely available from the ESA's Sentinel Data Hub (https://scihub.copernicus.eu). Authors would like to thank Prof. J.J. Mallorquì (Remote Sensing Laboratory of the Universitat Politècnica de Catalunya of Barcelona) for providing the SUBSOFT processor software.

References

Amorosi, A., M.L. Colalongo, G. Pasini, and D. Preti. 1999. "Sedimentary response to Late Quaternary sea-level changes in the Romagna coastal plain (northern Italy)". *Sedimentology* 46: 99–121.

ARPA (Regional Agency *for the* Environmental Protection) Emilia-Romagna and Regione Emilia-Romagna. 2010. "Applicazione della modellistica matematica di simulazione. Fase II: analisi della subsidenza nelle zone costiere". Technical Report. Bologna, Italy. Accessed 12 June 2016. http://www.ARPA.emr.it/cms3/documenti/subsidenza/Relazione_FaseII.pdf

Berardino, P., G. Fornaro, R. Lanari, and E. Sansosti. 2002. "A new algorithm for surface deformation monitoring based on small baseline differential SAR interferograms". *IEEE Transactions on Geoscience and Remote Sensing* 40: 2375–2383. doi:10.1109/TGRS.2002.803792.

Berti, M., A. Corsini, S. Franceschini, and J.P. Iannacone. 2013. "Automated classification of Persistent Scatterers Interferometry time series". *Natural Hazards and Earth System Sciences* 13: 1945-1958.

Bertoni, W., G. Brighetti, G. Gambolati, G. Ricceri, and F. Vuillermin. 1995. "Land subsidence due to gas production in the on- and off-shore natural gas fields of the ravenna area, Italy". In *Land Subsidence,* Proceedings of the Fifth International Symposium on Land Subsidence, The Hague, IAHS 234.

Blanco, P., J.J. Mallorquí, S. Duque, and D. Navarrete. 2006. "Advances on DInSAR with ERS and ENVISAT data using the Coherent Pixels Technique (CPT)". In proceedings of *IEEE International Geoscience and Remote Sensing Symposium* 4: 1898-1901.

Bonì, R., G. Pilla, and C. Meisina. 2016. "Methodology for detection and interpretation of ground motion areas with the A-DInSAR time series analysis". *Remote Sensing 8* (8): 686. doi:10.3390/rs8080686.

Carbognin, L., and L. Tosi. 2002. "Interaction between climate changes, eustacy and land subsidence in the North Adriatic Region, Italy". *Marine Ecology* 23 (1): 38-50.

Carminati, E., G. Martinelli, and P. Severi. 2003. "Influence of glacial cycles and tectonics on natural subsidence in the Po Plain (Northern Italy): insights from 14C ages". *Geochemistry Geophysics Geosystems Journal* 4: 1082-1096.

Cascini, L., G. Fornaro, and D. Peduto. 2010. "Advanced low- and full-resolution DInSAR map generation for slow-moving landslide analysis at different scales". Engineering Geology 112: 29–42.

Chaussard, E., R. Bürgmann, M. Shirzaei, E.J. Fielding, and B. Baker. 2014. "Predictability of hydraulic head changes and characterization of aquifer-system and fault properties from InSAR-derived ground deformation". *Journal of Geophysical Research: Solid Earth* 119 (8): 6572-6590.

Chini, M., M. Albano, M. Saroli, L. Pulvirenti, M. Moro, C. Bignami, E. Falcucci, S. Gori, G. Modoni, N. Pierdicca, and S. Stramondo. 2016. "Coseismic liquefaction phenomenon analysis by COSMO-SkyMed: 2012 Emilia (Italy) earthquake". *International Journal of Applied Earth Observation and Geoinformation* 39: 65-78.

Costantini, M. 1998. "A novel phase unwrapping method based on network programming". *IEEE Transactions on Geoscience and Remote Sensing* 36 (3): 813-821.

Costantini, M., and P.A. Rosen. 1999. "A generalized phase unwrapping approach for sparse data". In proceedings of *IEEE International Geoscience and Remote Sensing Symposium*. 28 June-2 July 1999, Hamburg, Germany. 1: 267-269.

Di Martire, D., A. Novellino, M. Ramondini, and D. Calcaterra. 2016. "A-Differential Synthetic Aperture Radar Interferometry analysis of a Deep Seated Gravitational Slope Deformation occurring at Bisaccia (Italy)". *Science of The Total Environment* 550: 556-573. doi:10.1016/j.scitotenv.2016.01.102.

EEA (European Environmental Agency). 2007. Technical Report. Available online: http://land.copernicus.eu/user-corner/technical-library/CLC2006_technical_guidelines.pdf (accessed on 12 August 2016).

ENI (National Hydrocarbons Authority) S.p.A–AGIP and ARPA Emilia-Romagna. 2003. "Studio della Subsidenza Antropica generata dall'estrazione di acqua di falda lungo la costiera emiliano-romagnola". Technical report. Available online: http://www.ARPAe.it/cms3/documenti/subsidenza/Relfin_Agip_2003_rid.pdf (accessed on 13 June 2016).

Ferretti, A., C. Prati, and F. Rocca. 2000. "Nonlinear subsidence rate estimation using permanent scatterers in differential SAR interferometry". *IEEE Transactions on Geoscience and Remote Sensing* 38: 2202–2212. doi:10.1109/36.868878.

Ferretti, A., C. Prati, and F. Rocca. 2001. "Permanent Scatterers in SAR interferometry". *IEEE Transactions on Geoscience and Remote Sensing* 39 (1): 8–20. doi:10.1109/36.898661.

Fisher, R.A. 1942. *The Design of Experiments.* Third Edition, Edinburgh: Oliver & Boyd.

Gabriel, K., R.M. Goldstein, and H.A. Zebker. 1989. "Mapping small elevation changes over large areas: differential radar interferometry". *Journal of Geophysical Research* 94: 9183. doi:10.1029/JB094iB07p09183.

Gambolati, G., G. Ricceri, W. Bertoni, G. Brighenti, and E. Vuillermin. 1991. "Mathematical simulation of the subsidence of Ravenna". *Water Resources Research* 27: 2899-2918. doi:10.1029/91WR01567.

Gambolati, G., and P. Teatini. 1998. "Numerical analysis of land subsidence due to natural compaction of the Upper Adriatic Sea basin". In: *CENAS*, Coastline evolution of the upper Adriatic Sea due to sea level rise and natural and anthropogenic land subsidence. Kluwer Academic Publishing, Water Science & Technology Library 28: 103–131.

Gambolati, G., P. Teatini, L. Tomasi, and M. Gonella. 1999. "Coastline regression of the Romagna region, Italy, due to natural and anthropogenic land subsidence and sea level rise". *Water Resources Research* 35 (1): 163-184. doi:10.1029/1998WR900031.

Ghielmi, M., M. Minervini, C. Nini, S. Rogledi, M. Rossi, and A. Vignolo. 2010. "Sedimentary and tectonic evolution in the eastern Po-Plain and northern Adriatic Sea area from Messinian to Middle Pleistocene (Italy)". *Rendiconti Lincei* 21 (1): 131-166. doi:10.1007/s12210-010-0101-5.

Goldstein, R.M., and C.L. Werner. 1998. "Radar Interferogram Filtering for Geophysical Applications". *Geophysical Research Letters* 25 (21): 4035–4038. doi:10.1029/1998GL900033.

Herrera, G., R. Tomás, J.M. Lopez-Sanchez, J. Delgado, F. Vicente, J. Mulas, G. Cooksley, M. Sánchez, J. Duro, A. Arnaud, P. Blanco, S. Duque, J.J. Mallorquí, R. Vega-Panizo, and O. Monserrat. 2009. "Validation and comparison of advanced differential interferometry techniques: Murcia metropolitan area case study". *ISPRS Journal of Photogrammetry and Remote Sensing* 64: 501–512. doi:10.1016/j.isprsjprs.2008.09.008.

Iglesias, R., J.J. Mallorqui, and P. Lopez-Dekker. 2014. "DInSAR pixel selection based on sublook spectral correlation along time". *IEEE Transactions on Geoscience and Remote Sensing* 52 (7): 3788–3799. doi:10.1109/TGRS.2013.2276023.

Lanari, R., O. Mora, M. Manunta, J.J. Mallorquì, P. Berardino, and E. Sansosti. 2004. "A small-baseline approach for investigating deformations on full-resolution differential SAR interferograms". *IEEE Transactions on Geoscience and Remote Sensing* 42 (7): 1377-1386. doi:10.1109/TGRS.2004.828196.

Massonnet, D., M. Rossi, C. Carmona, F. Adragna, G. Peltzer, K. Feigl, and T. Rabaute. 1993. "The displacement field of the Landers earthquake mapped by radar interferometry". *Nature* 364: 138–142. doi:10.1038/364138a0.

Massonnet, D., P. Briole, and A. Arnaud. 1995. "Deflation of Mount Etna monitored by spaceborne radar interferometry". *Nature* 375: 567–570. doi: 10.1038/375567a0.

Meisina, C., F. Zucca, D. Notti, A. Colombo, A. Cucchi, G. Savio, C. Giannico, and M. Bianchi. 2008. "Geological interpretation of PSInSAR data at regional scale". *Sensors* 8 (11): 7469–7492.

Meyer, F.J., D.B. McAlpin, W. Gong, O. Ajadi, S. Arko, P.W. Webley, and J. Dehn. 2015. "Integrating SAR and derived products into operational volcano monitoring and decision support systems". *ISPRS Journal of Photogrammetry and Remote Sensing* 100: 106-117.

Mora, O., J.J. Mallorqui, and A. Broquetas. 2003. "Linear and Non-linear Terrain Deformation Maps from a Reduced Set of Interferometric SAR Images". *IEEE Transactions on Geoscience and Remote Sensing* 41: 2243–2253. doi:10.1109/TGRS.2003.814657.

Notti, D., F. Calò, F. Cigna, M. Manunta, G. Herrera, M. Berti, C. Meisina, D. Tapete, and F. Zucca. 2015. "A User-Oriented Methodology for DInSAR Time Series Analysis and Interpretation: Landslides and Subsidence Case Studies". *Pure and Applied Geophysics* 172 (11): 3081-3105. doi:10.1007/s00024-015-1071-4.

Snedecor, G.W., and W.G. Cochran. 1967. *Statistical Methods*. Sixth Edition, Ames: Iowa State University Press.

Soergel, U. (Ed.). 2010. *Radar Remote Sensing of Urban Areas*. vol. 15. Springer Science & Business Media. Springer Dordrecht Heidelberg London New York.

Teatini, P., M. Ferronato, G. Gambolati, W. Bertoni, and M. Gonella. 2005. "A century of land subsidence in Ravenna, Italy". *Environmental Geology* 47: 831–846.

Tessitore, S., J.A. Fernández-Merodo, G. Herrera, R. Tomás, M. Ramondini, M. Sanabria, J. Duro, J. Mulas, and D. Calcaterra. 2016. "Comparison of water-level, extensometric, DInSAR and simulation data for quantification of subsidence in Murcia City (SE Spain)". *Hydrogeology Journal* 24 (3): 727-747.

Tomás, R., Y. Márquez, J.M. Lopez-Sanchez, J. Delgado, P. Blanco, J.J. Mallorquí, M. Martínez, G. Herrera, and J. Mulas. 2005. "Mapping ground subsidence induced by aquifer overexploitation using advanced Differential SAR Interferometry: Vega Media of the Segura River (SE Spain) case study". *Remote Sensing of Environment* 98 (2–3): 269-283. dx.doi.org/10.1016/j.rse.2005.08.003.

Tomás, R., R. Romero, J. Mulas, J.J. Marturià, J.J. Mallorquí, J.M. Lopez-Sanchez, G. Herrera, F. Gutiérrez, P.J. González, J. Fernández, S. Duque, A. Concha-Dimas, G. Cocksley, C. Castañeda, D. Carrasco, and P. Blanco. 2014. "Radar interferometry techniques for the study of ground subsidence phenomena: a review of practical issues through cases in Spain". *Environmental Earth Sciences* 71: 163-181. doi:10.1007/s12665-013-2422-z.

CHAPTER 2

Testing the potential of Sentinel-1A TOPS interferometry for the detection and monitoring of landslides at local scale.

S. Fiaschi [1], M. Mantovani [2], S. Frigerio [2], A. Pasuto [2] and M. Floris [1]

[1] University of Padova, Department of Geosciences, Padua, Italy.
[2] CNR-IRPI: National Research Council of Italy - Research Institute for Geo-Hydrological Protection, Padua, Italy.

Abstract

The recent Sentinel-1 mission, started by the European Space Agency (ESA) in April 2014, provides to the scientific community new capabilities for the monitoring of the Earth surface. In particular, the Terrain Observation by Progressive Scans (TOPS) imaging technique used in the Interferometric Wide swath (IW) acquisition mode, permits to acquire data over very wide areas (250 km of swath extension) at 20 m spatial resolution, with 12-day revisit time, making it suitable for ground displacement monitoring applications. With more than one year of SAR images available, it is now possible to carry out monitoring activities of slow moving phenomena such as landslides at both regional and local scales. In this work, the potential of Sentinel-1A for the monitoring of shallow landslides occurring in the North-Eastern Italian Pre-Alps was tested. Two stacks of Sentinel-1A scenes acquired in both ascending and descending orbits were processed using the Permanent Scatter Interferometry (PSI) technique. The results, analysed in terms of PS density and quality, were compared with the ERS-1/2 and ENVISAT PSI database available from the Italian National Cartographic Portal to assess the capabilities of Sentinel-1A in detecting and monitoring landslides in respect to the previous satellite missions. The results of this work show the great potential of Sentinel-1A in the continuous monitoring of landslides-prone territories even at local scale. The achievable results can provide information that are useful to delineate the spatial and temporal evolution of landslides and precisely assess their rates of deformation.

1. Introduction

In the last years, Advanced Differential Synthetic Aperture Radar Interferometry (A-DInSAR) techniques have been widely used to detect, monitor and characterize displacements triggered by natural processes such as subsidence (Tomás et al., 2014), earthquakes (Wright et al., 2006), deflation and inflation of volcanoes (Biggs et al., 2009) and slope movements (Wasowski and Bovenga, 2014). In the case of landslides, the results obtained from A-DInSAR analyses are often not completely satisfying (Cascini et al., 2010). The reasons are to be found in both the technique and in the

deformation process itself. On one hand, the geometry of acquisition of the space-borne SAR sensors coupled with the topography of the area of interest cause shadowing effects and geometric distortions (i.e. foreshortening and overlay); on the other, the typology of the investigated landslide, in terms of slope, aspect, activity and the presence of vegetation, decorrelate the signal between the acquisitions (Chaabane et al., 2005; Colesanti and Wasowski, 2006; Wasowski and Bovenga, 2014; Wasowski et al., 2014). To tackle some of these limitations, the exploitation of dataset acquired by missions with more suited wavelengths and shorter revisiting time has been proposed (Tosi et al., 2016; Wasowski and Bovenga, 2014). Furthermore, to detect and monitor landslides occurring over vegetated areas or to measure large displacement rates and ignore phase decorrelation, new algorithms based on the amplitude off-set tracking were developed (Casu et al., 2011; Manconi et al., 2014; Michel et al., 1999; Singleton et al., 2014).

The Sentinel-1A mission, operated by European Space Agency (ESA) since April 2014, provides to the scientific community new capabilities for the quasi-continuous monitoring of the Earth surface. The Terrain Observation by Progressive Scans (TOPS) imaging technique, used in the Interferometric Wide swath (IW) acquisition mode, permits to generate SAR images over very wide areas (250 km swath dimension) at 20 m spatial resolution, with 12-day of revisiting time. Since April 2016, the launch of the twin satellite Sentinel-1B enhanced this temporal sampling capability by reducing the revisiting time to 6 days. With these increased interferometry-oriented design capabilities, the Sentinel-1 mission represents a very promising tool for ground displacement monitoring applications and at present, with almost two years of data acquisition, it is possible to carry out A-DInSAR analyses of landslides at both regional and local scales. Some Authors have already successfully tested the potential of Sentinel-1A data in updating landslide inventory maps and monitoring landslide activity (Barra et al., 2016; Lazecky et al., 2016; Wasowski et al., 2016). Even if different methods to assess the a-priori effectiveness of interferometric techniques have been proposed (Cascini et al., 2009; Colombo et al., 2006; Plank et al., 2012, 2013), additional tests in different geo-environmental scenarios are needed, because the quality of the results, in particular for landslide analyses purposes, depends on several factors related to the geo-environmental features of the area under investigation and to the processing technique (Hanssen, 2005; Mahapatra et al., 2012), which can limit the reproducibility of the interferometric results in different areas (Wasowski and Bovenga, 2014).

In this work, the potential of Sentinel-1A acquisitions to detect and monitor landslide phenomena affecting a densely vegetated area located in the North Eastern Italian Pre-Alps is tested. More than 40 images acquired from ascending and descending orbits were processed using the Persistent Scatterer Interferometry (PSI) technique (Ferretti et al. 2001). The results were compared with the ERS-1/2 and ENVISAT PSI database available from the Italian National Cartographic Portal (www.pcn.minambiente.it). The quality of the outcomes was assessed in terms of persistent reflectors density and measurement accuracy (Colesanti and Wasowski, 2006) over the entire study area; in particular, the observations on two specific active slopes are reported and discussed. The strengths and weaknesses of the Sentinel-1A TOPS mode interferometry emerged during this study were likewise pointed out.

2. Study Area

The Municipality of Trissino, covers an area of about 22 km^2 in the Province of Vicenza (Veneto Region, Italian Pre-Alps, NE Italy) (Figure 1). The territory is characterized by elevations ranging from 800 m a.s.l. (West) to 100 m a.s.l. (South) with typical hillslope morphologies. The main geology consists of volcanic deposits such as lavas, pyroclastites and ignimbrites, which are overlaid by eluvial and colluvial deposits originated from the alteration of the volcanic substratum. The entire area is affected by a large number of different ground instabilities, which have been detected and classified according to Cruden and Varnes (1996) combining the information provided by the Italian Landslide Inventory (IFFI) archive compiled in 2008 and the geomorphological map produced by the 2013 Italian Territory Development Plan (PAT) project. This information was updated through the analysis and interpretation of the available aerial photographs and orthophotos acquired from 1954 to 2010. A total of 64 landslides, affecting the 18% of the Municipality of Trissino have been reported and classified by three main types of movement (Figure 1): earth flow, roto/translational slide and complex. Such instabilities are generally triggered by intense rain events as occurred in November 2010, when an exceptional event (up to 500 mm of cumulated rainfall in 3 days) hit the Vicenza Province and the entire NE Italy causing several floods and triggering a very large number of mass movements. During the floods, the Soil Protection Division of the Vicenza Province received more than 500 warnings of instability phenomena (Floris et al., 2012) and in the Municipality of Trissino the activation of 12 landslides were documented (Figure 1).

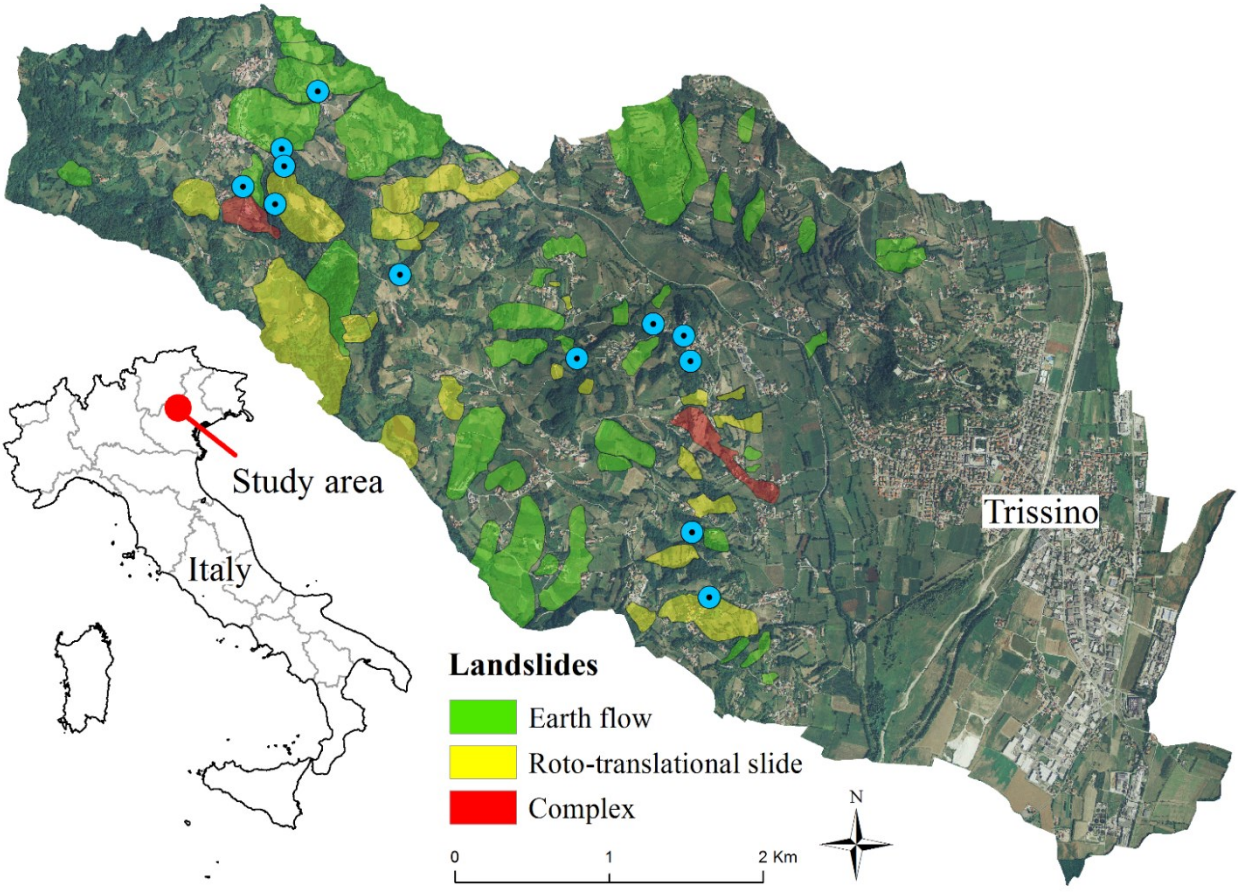

Figure 1. Location of the study area, the boundaries of the Municipality of Trissino, and the landslides within its territory. The blue dots are the location of the landslides occurred after the November 2010 exceptional rainfall event.

Mass movements generally involve the debris coverage or the terrain up to a maximum depth of 8 m, and occur mainly between 250 m and 400 m a.s.l. in the central section of the study area and between 450 m and 600 m a.s.l. in the western section. Most of the landslides occur along the N-S and E direction, while only few along the W direction. The average velocity of movement that characterize the instabilities over large areas is generally below 10 mm/yr, while smaller landslides generally occur suddenly with no warning signs. Even if these slope instabilities are not very large, they often occur near the urbanized areas damaging the buildings and the infrastructure, in particular the road network, and causing significant disruptions of daily life and high economic losses (Figure 2). Landslides prevention and control works such as the installation of drainage systems were carried in the most critical areas and are constantly monitored by the local Authorities.

Figure 2. Typical landslides occurring in the study area. In evidence the damage to the road network. (a) earth flow, (b) rotational slide/flow.

3. Data and data processing

The Sentinel-1A datasets processed in this study consist of 46 scenes acquired from 12/2014 to 09/2016 with descending orbit number 95 and 42 scene acquired from 03/2015 to 09/2016 with ascending orbit number 117. The ground resolution achievable with the Sentinel-1A C-band sensor is around 20 m x 20 m applying a multi-look factor of 5 in Range and 1 in Azimuth. In order to reduce processing time, save disk space and, at the same time, to produce results that can be easily managed in a Geographic Information System (GIS) environment for the post processing analyses, the acquisitions were resized to comprehend exclusively the study area (the Municipality of Trissino). The processing of the available images has been carried out through the PSI technique using the Precise Orbit Ephemerides (POE) to reduce the errors related to the satellite orbit inaccuracies. The main steps of the processing can be synthesized as follows: i) first, the images are connected to create a network of master and slave pairs, using a single master image (Figure 3); ii) the images are coregistered onto the master acquisition and the coherence image, the interferograms and the related intensity images are generated. The interferograms are then flattened removing the constant phase (due to the acquisition geometry) and the topographic phase. For the latter, the Shuttle Radar Topography Mission (SRTM) Digital Elevation Model (Rabus at al., 2003) with 30 m pixel size was

used; iii) the phase-height pair-by-pair proportionality factors are estimated and removed from the flattened interferograms. The Persistent Scatterers (PS) candidates are then generated and the displacement information (i.e. velocity) is estimated using the linear model:

$$Disp = V * (t - t0)$$

where Disp is the displacement at time t and V is the displacement velocity; iv) the spatial and temporal variations related to the atmospheric phase are estimated and subtracted from the interferograms in order to calculate the final displacements. The atmospheric correction is performed applying two filtering methods: the Low Pass filtering, which accounts for the spatial distribution of the atmospheric variations and is implemented by using a square window of 1200 m; and the High Pass filter, which accounts for the temporal distribution of the atmospheric variations and uses a temporal window of 365 days. The PS candidates are then selected considering the coherence value, which identifies the level of backscattering that the targets on the ground maintain between two consecutive acquisitions. In this case, the coherence threshold was set to 0.80; v) finally, all PS candidates are projected onto the adopted Geographic Coordinate System (GCS) WGS84. To improve results quality, the PS candidates can be further filtered in this step considering the amplitude dispersion index (μ/σ), which represents the ratio between the average SAR intensity (μ) and the standard deviation (σ). In this case, the adopted threshold was 3.2.

The obtained results were compared with the ERS-1/2 and ENVISAT PSI database available from the National Cartographic Portal (PCN) that were produced in the framework of the Special Remote Sensing Environment Plan, promoted by the Italian Ministry of Environment. Within the study area, the PSI results obtained from the following datasets were available: 79 descending ERS-1/2 images (04/1992 - 11/2000); 29 ascending ERS-1/2 images, (05/1992 - 06/2000); 34 descending ENVISAT images (01/2003 - 06/2010); 34 ascending ENVISAT images, (12/2003 - 07/2010).

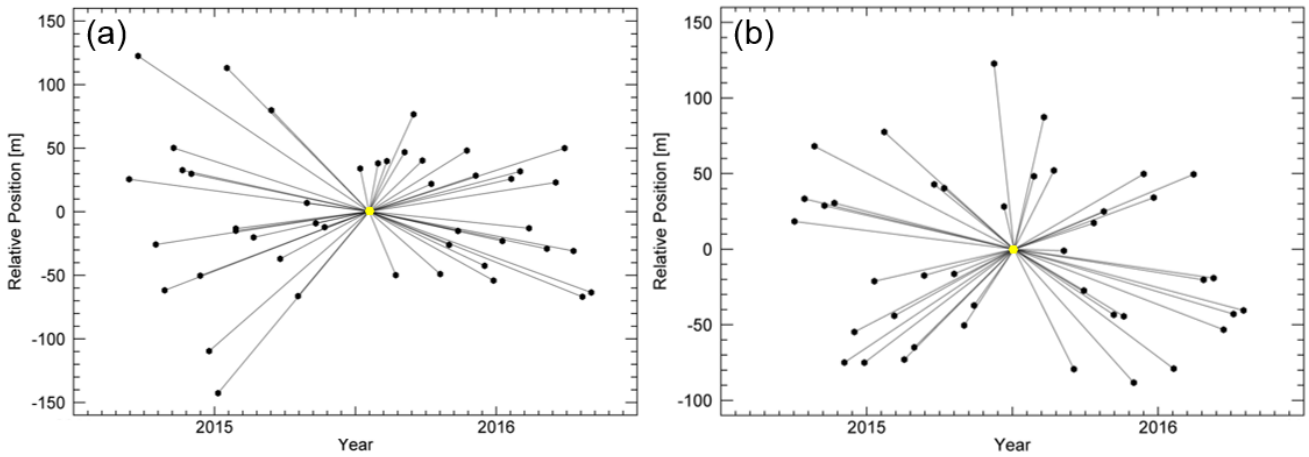

Figure 3. Connection network between master (yellow dot) and slaves (black dots) images obtained from (a) 46 Sentinel-1A descending scenes and (b) 42 ascending scenes.

4. Results

The results obtained from the PSI analysis applied to the Sentinel-1A images are reported in terms of mean linear displacement velocity along the sensor Line of Sight (LOS) in Figure 4. Positive values are colour coded in blue and refer to natural radar targets (the PS) moving towards the satellite, while negative values (in red), testify a displacement far from the satellite. Although the selected parameters were quite restrictive, 6203 PS candidates were generated with the descending dataset, and 5855 with the ascending one. PSI analysis detects several areas affected by displacements, in particular in the north-west and the central sections of the Trissino Municipality. The range of the displacement velocities is generally low, with rates ranging from 2 mm/yr to 7 mm/yr, values that are in accordance with the type of instabilities affecting the area. As it can be noticed from Figure 4, most of the small urban agglomerates in the area are recording deformation patterns as consequence of the mobilization of the weak deposits triggered by intense rainfall. The use of images acquired in descending and ascending orbits permits a better characterization of the prevalent direction of the displacements allowing us to assess the components of plano-altimetric change. Furthermore, since the backscattering properties change with the satellite viewing geometry, the analysis of descending and ascending datasets increases the number and the spatial distribution of the PS within the area of interest.

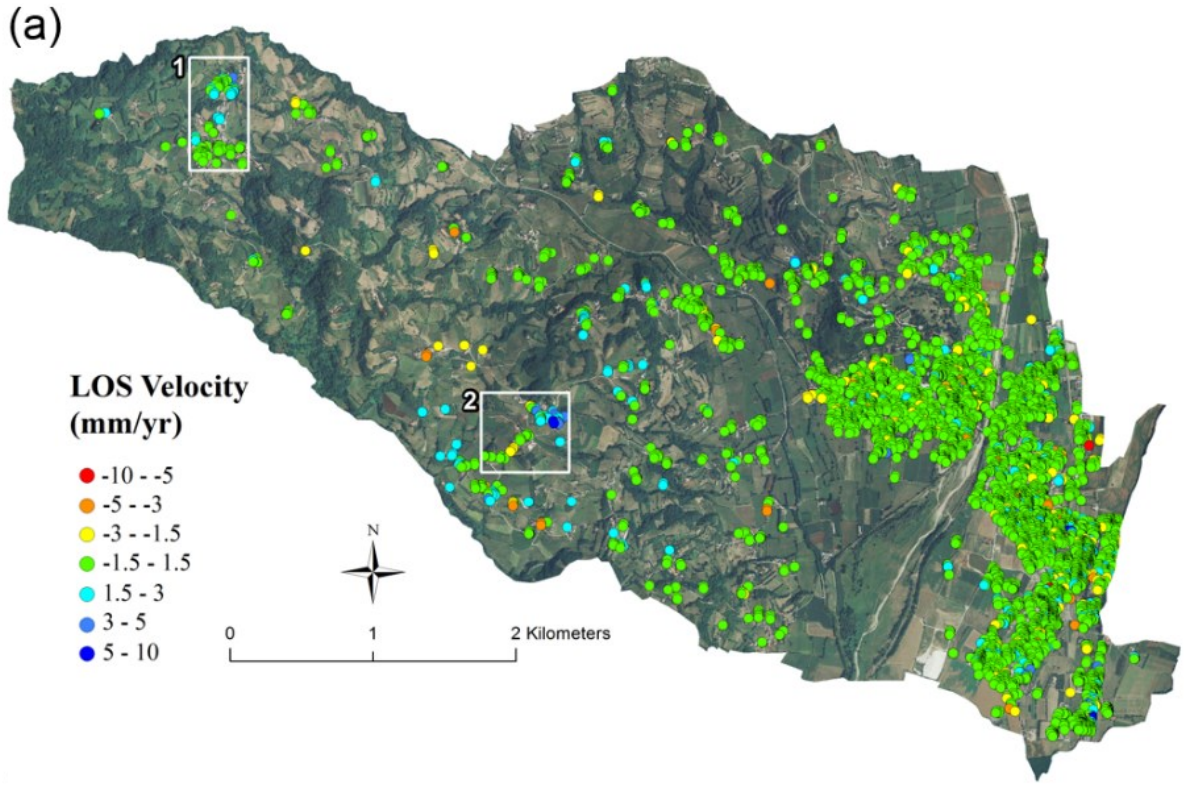

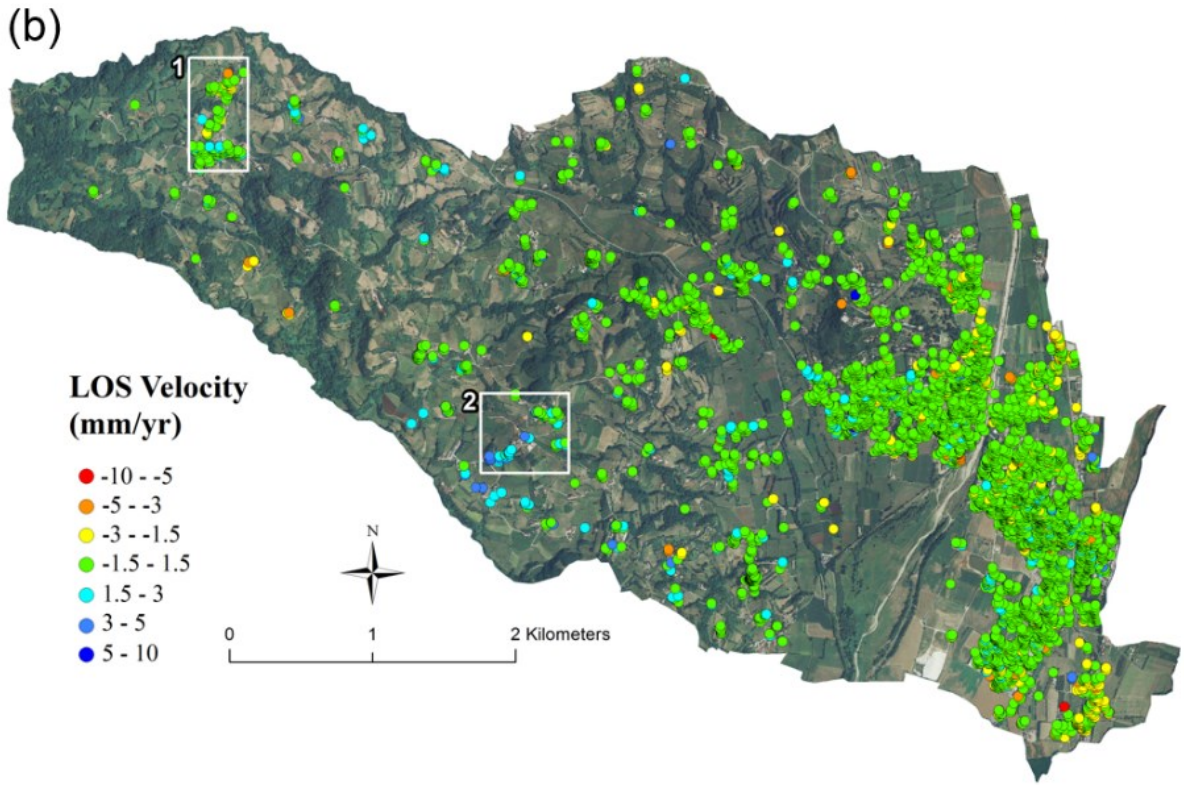

Figure 4. LOS velocity maps obtained from descending (a) and ascending (b) Sentinel-1A data processing. White boxes indicate the specific unstable slopes reported in Figures 5 and 6.

The shorter revisit time of Sentinel-1A in respect to ERS-1/2 and ENVISAT (12 vs 35 days) allowed us to obtain a much higher PS density (Table 1) that positively reflects not only on the quantity but also on the quality of the measurements. Despite the restrictive processing thresholds adopted, the Sentinel-1A results are still affected by a moderate level of noise generated by an overall low signal-to-noise ratio, which is probably consequence of the short temporal extent of the available images stack (Hanssen, 2005; Mahapatra et al., 2012). The presence of noise in the results can be noticed in Figure 4 from the moving PS (red and blue dots) in the stable area (green dots) in the section occupied by the city of Trissino.

Table 1. Comparison between the PS results obtained with Sentinel-1A, ENVISAT and ERS-1/2: image acquisition geometry; total number of PS; PS density; velocity standard deviation (σ); percentage of moving PS.

Satellite	Geometry	N. of PS	PS/Km^2	Velocity σ (mm/yr)	Moving PS (Vel ≠ ±1.5 mm/yr)
Sentinel-1A	Descending	6203	283	0.54	12%
ENVISAT	Descending	1204	54	0.69	6%
ERS-1/2	Descending	1305	59	0.35	7%
Sentinel-1A	Ascending	5855	267	0.69	18%
ENVISAT	Ascending	992	45	0.44	2%
ERS-1/2	Ascending	803	36	0.43	7%

The comparison with the ERS-1/2 and ENVISAT PSI database shows a good agreement in the rates of movement and location of the landslides detected by each sensor (Figure 5 and 6). Figure 5, shows the displacements detected by the PSI analysis over area 1 of Figure 4. As reported by the people living in this area, several houses have recently shown fissures and displacements of walls and sidewalks as sign of the terrain mobilization. Moreover, the complexity of the movements and the lack of geomorphological evidences, makes difficult to precisely map the extension of the landslide.

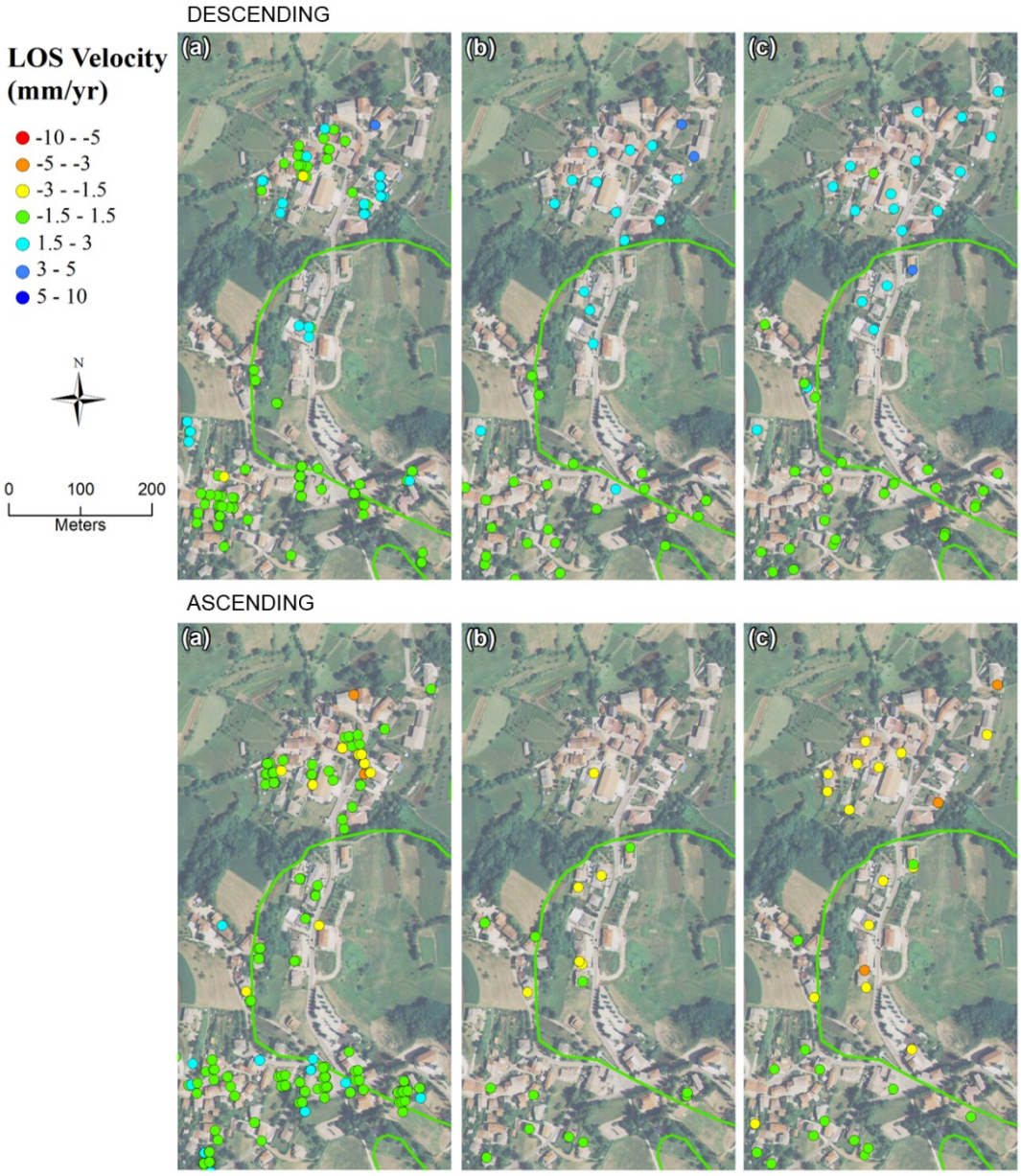

Figure 5. LOS velocity maps of the north section of the study area (area 1 of Figure 4) obtained from Sentinel-1A (a), ENVISAT (b) and ERS-1/2 (c) datasets. The green lines indicate the mapped landslides.

The opposite colour shift in the two datasets (blue for the descending acquisitions and orange for the ascending) witnesses a prevalent planimetric displacement toward E-SE of the buildings in the northern sectors; this direction of movement is in accordance with the one of the instability phenomenon. This result clearly shows the landslides distribution of activity (marked retrogressive) suggesting the necessity of reviewing its limits.

Figure 6, displays in detail another area affected by movement (area 2 of Figure 4). In the SW sector, the direction of displacement toward W revealed by the ascending orbit (positive values) is coherent with a retrogressive activity distribution of the instability. Furthermore, in the NE sector where no landslides were mapped before, it is clearly visible the toward satellite movement of the area mainly in the E direction given by the positive values of the detected PS in descending orbit. In this case, of the 29 PS measured, 27 of them registered velocities in the range from 1.6 mm/yr to 3.6 mm/yr, while only two present higher velocities of 5.4 mm/yr and 7.1 mm/yr, which is the maximum value registered in the entire study area. Thus, also in this case, the landslides delimitation should be updated and more in depth remote and ground based analyses are needed to characterize the landslide detected by the PSI analysis in the NE sector of Figure 6.

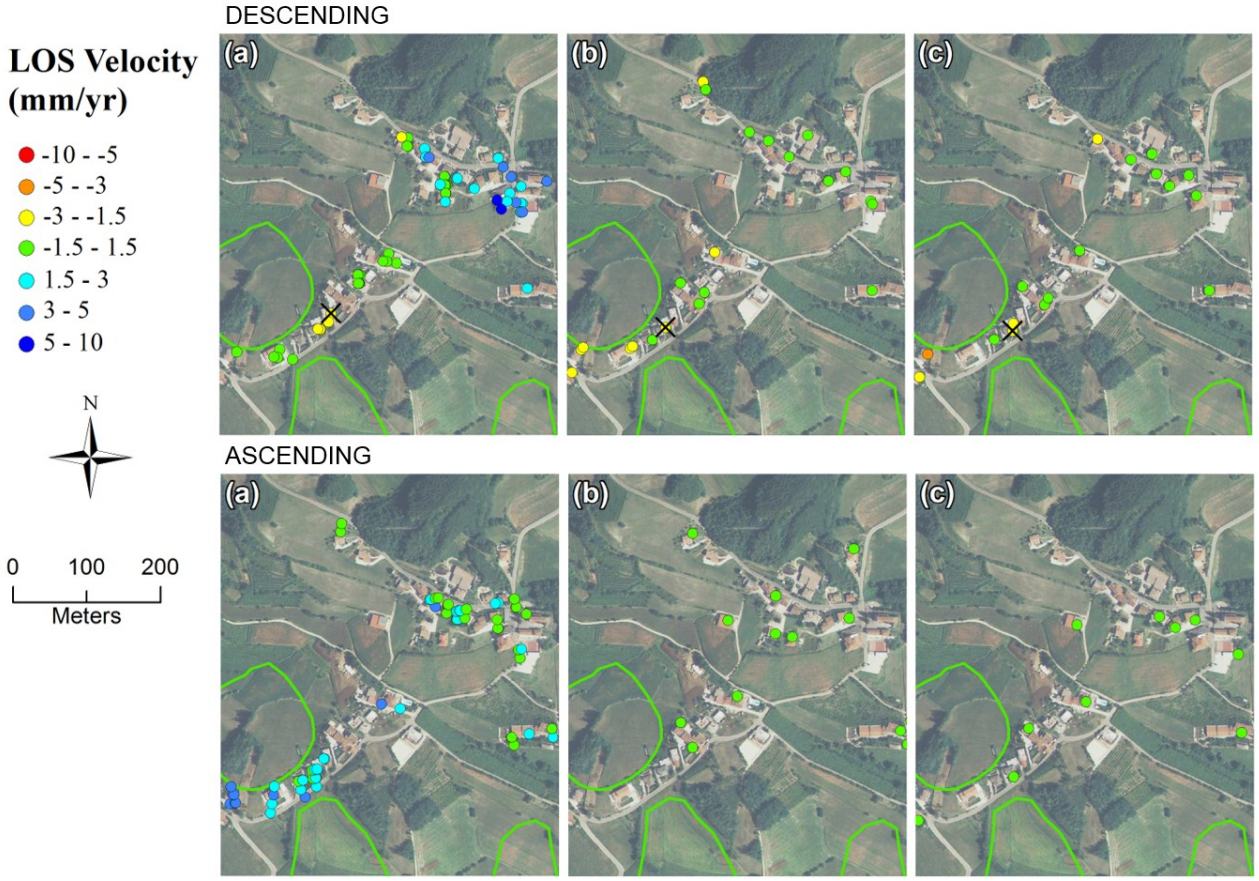

Figure 6. LOS velocity maps of the middle section of the study area (area 2 of Figure 4), obtained from Sentinel-1A (a), ENVISAT (b) and ERS-1/2 (c) datasets. The green lines indicate the mapped landslides. The displacement time series for the selected PS (black cross) are reported in Figure 8.

In order to assess the capabilities of the Sentinel-1A for landslide monitoring in such environment, the number of Sentinel-1A, ENVISAT and ERS-1/2 PS falling inside the mapped instabilities has been calculated (Table 2) considering a buffer of 50 m around each landslide. This buffer was adopted to compensate possible geocoding inaccuracies of the PS and unprecise delimitations of the instability phenomena. Assuming a threshold of PS≥4 as the minimum to monitor the temporal evolution of mass movements (Cigna et al., 2013; Herrera et al., 2013; Notti et al., 2010), the results are quite encouraging: up to 45% of the landslides contain a number of PS above the threshold. More than the 50% of the landslides (64% in the case of ascending orbit) has at least one PS falling inside their limits. According to these results, the descending orbit is more suitable to detect

flow type landslides than the slides, probably because of the morphological conditions of the investigated territory. The results obtained with Sentinel-1A represent a great improvement in respect to the performance obtained with ERS-1/2 and ENVISAT and are comparable to the results achieved by some Authors in other geomorphological contexts using medium and high resolution SAR data (Cigna et al., 2013; Herrera et al., 2013; Notti et al., 2010; Wasowski and Bovenga, 2014).

Table 2. Number of PS falling in the mapped landslides. In brackets the percentage respect to the total of the instability phenomena (41 flows and 23 slides).

Satellite	Track	Landslides with PS≥4	Flows with PS≥4	Slides with PS≥4	Landslides with 1≤PS<4	Flows with 1≤PS<4	Slides with 1≤PS<4
Sent.-1A	Desc.	23 (36%)	17 (41%)	6 (26%)	13 (20%)	10 (24%)	3 (13%)
ENVISAT	Desc.	10 (16%)	8 (19%)	2 (9%)	29 (45%)	18 (44%)	11 (49%)
ERS-1/2	Desc.	17 (26%)	13 (32%)	4 (17%)	28 (44%)	18 (44%)	10 (43%)
Sent.-1A	Asc.	29 (45%)	19 (46%)	10 (43%)	12 (19%)	8 (19%)	4 (17%)
ENVISAT	Asc.	4 (6%)	2 (5%)	2 (9%)	26 (41%)	17 (41%)	9 (39%)
ERS-1/2	Asc.	8 (12%)	5 (12%)	3 (13%)	24 (37%)	16 (39%)	6 (26%)

The displacement trends of target reflectors selected in the stable area of the town of Trissino (Figure 7) and in an unstable area (Figure 8) are analysed in detail to further demonstrates the great improvement brought by the Sentinel-1A data for ground displacement monitoring purposes. In order to make the all the results comparable with the Sentinel-1A time series (624 days in total), a 630 days stretch was extracted from the original ENVISAT and ERS-1/2 time series: from January 2007 to October 2008 for ENVISAT, and from December 1996 until September 1998 for ERS-1/2. These stretches were chosen among those with the largest number of ENVISAT and ERS-1/2 acquisitions, covering the seasonal periods enclosed in the Sentinel-1A datasets (December 2014 – September 2016). As it can be noticed from Figure 7, the number of measurements plays and important role in the interpretation of the time series. If from one hand the 47 Sentinel-1A acquisitions clearly define the stability of the PS in the investigated period, on the other, the 10 ENVISAT measurements resulted in a very noisy scattered plot. Better results were obtained by the ERS-1/2 dataset from which the stability of the area can be assumed even if some seasonal variations are evident. Assuming an expected value equal to 0 (no displacement) the standard deviations of the three measurements are 0.76 mm, 5.03 mm and 2.16 mm respectively for the Sentinel-1A, ENVISAT and ERS-1/2 datasets.

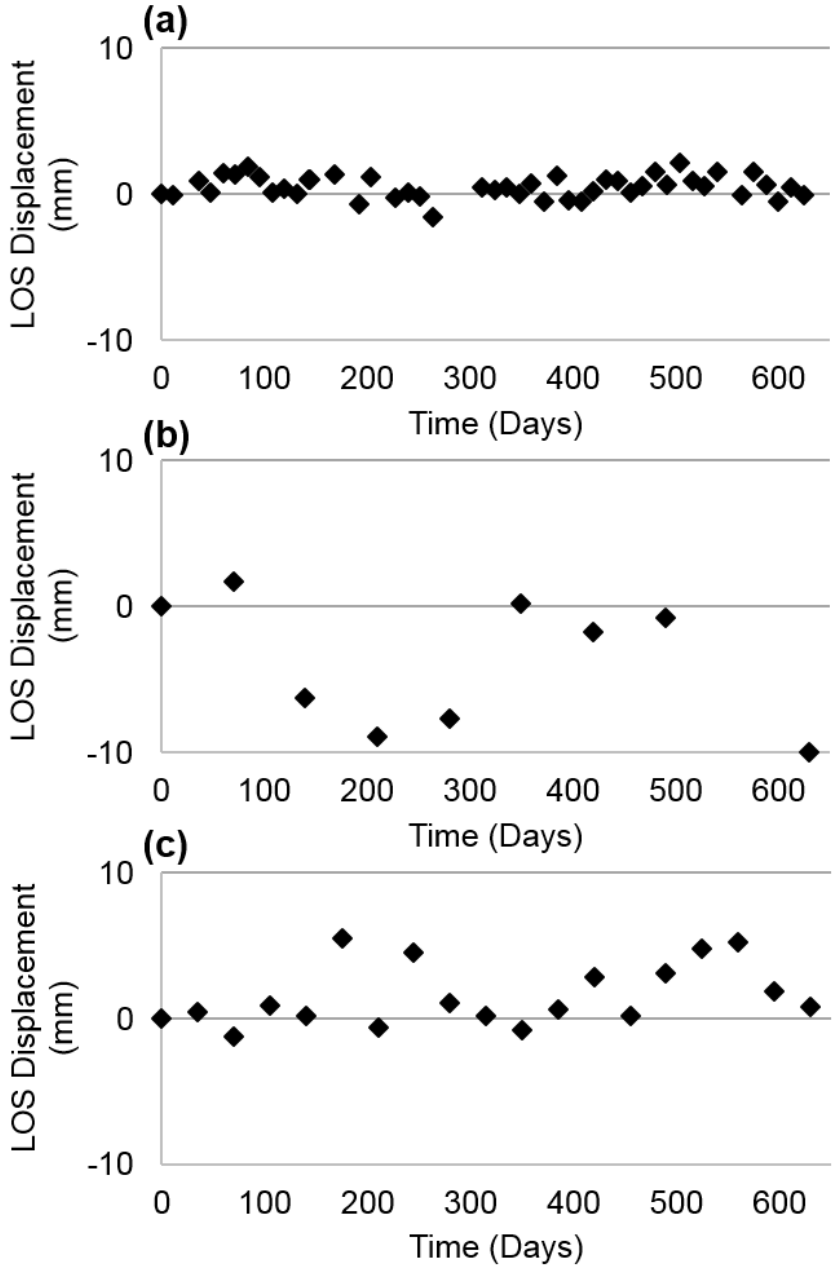

Figure 7. Time series of a stable target selected in the town of Trissino: (a) Sentinel-1A, (b) ENVISAT, (c) ERS-1/2.

Figure 8 shows that the displacement trend of a point located inside the landslide body of Figure 6, chosen as example, is evident with Sentinel-1A measurements (besides a clear unwrapping error in the fourth interferogram), while with ENVISAT and ERS-1/2 the noise is predominant, making difficult the correct interpretation of the movement trend. In the latter case, only by analysing a longer time series, as reported in Figure 8 d and e, the deformation trends can be correctly inferred.

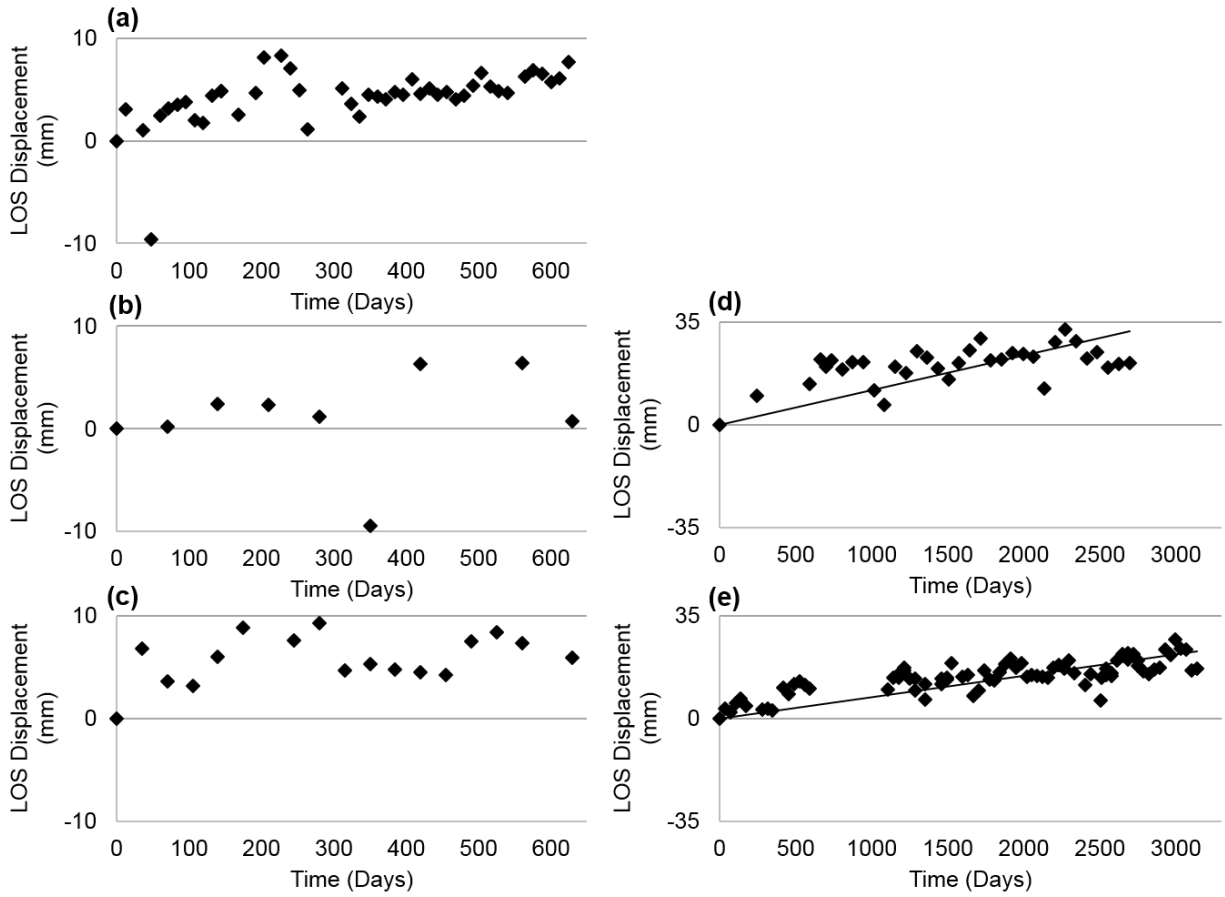

Figure 8. Time series of moving targets selected over a landslide body obtained with Sentinel-A (a), ENVISAT (b), ERS-1/2 (c); (d) and (e) show the full-length time series respectively of ENVISAT and ERS-1/2.

5. Conclusions

In this work, we tested the potential of the new Sentinel-1A satellite SAR data in the monitoring of a densely vegetated area in the northern Italy affected by small to medium size landslides. To this end, 46 descending and 42 ascending Sentinel-1A images acquired respectively from 12/2014 to 09/2016 and from 03/2015 to 09/2016 have been processed using the PSI technique. The results were compared with those of the ERS-1/2 (1992-2000) and ENVISAT (2003-2010) PSI archive available from the National Cartographic Portal of the Ministry of Environment, in order to verify their quality and applicability. Sentinel-1A results show that among the 64 mapped landslides, the 45% have more than 4 measured PS falling inside their limits, and the 64% have at least 1 PS. The movement rates are generally low, reaching at maximum 7 mm/yr. The obtained results show the great potential of the Sentinel-1A data in the continuous monitoring of landslides-prone territories not only limiting the activity at the regional scale, but also focusing on local scale phenomena. The high number of PS obtained with Sentinel-1A and the high temporal sampling rate of the measurements can help to better characterize the movements in the area, to delineate the extent of several landslides, and to detect new instability phenomena. Such results represent a great improvement in the detection and monitoring of landslides in respect to the previous ERS-1/2 and ENVISAT C-band satellites and they can be comparable to the results achievable by using high resolution X-band SAR data. Even if there are

only less than two years of acquisitions available, the measurements carried out with Sentinel-1A can correctly assess the rate of deformation of natural target reflectors. These results, as demonstrated, are hardly achievable in such a short period of time from previous satellite missions (e.g. ERS-1/2 and ENVISAT). The availability of new images and the extension of the temporal coverage, will increase the overall quality of the achievable results. Moreover, the twin Sentinel-1B satellite launched in April 2016 will supply the scientific community with an additional set of SAR images that will permit, combining the data from both satellites, to lower the image frequency to 6 days, with great benefits in terms of detection capabilities and quality of the results.

Sentinel-1 exploitation can provide very useful information about the spatial and temporal evolution of landslides. A continuous monitoring activity is crucial especially in critical areas to keep track of the landslides movement over time and to assess abrupt changes in the deformation rates. However, since the PS are limited to high backscattering object (namely, the buildings), it is not possible to rely only on A-DInSAR techniques to precisely delineate the extension of an active landslide, which limits may interest vegetated areas where no measure points are available. For this reason, geological surveys are always necessary in order to check the presence of geomorphological evidences that are sign of active movements.

Acknowledgements

ERS-1/2 and ENVISAT datasets were processed by Tele-Rilevamento Europa (TRE S.r.l.) in the framework of the Special Remote Sensing Environment Plan, promoted by the Italian Ministry of Environment. These results are available from the National Cartographic Portal (PCN) at www.pcn.minambiente.it. Sentinel-1A images are freely available from the European Space Agency (ESA) Sentinel-1 Scientific Data Hub (https://scihub.copernicus.eu/).

References

Barra, A., O. Monserrat, P. Mazzanti, C. Esposito, M. Crosetto, and G. Scarascia Mugnozza. 2016. “First insights on the potential of Sentinel-1 for landslides detection”. *Geomatics, Natural Hazards and Risk* 7 (6): 1874-1883. doi: 10.1080/19475705.2016.1171258.

Biggs, J., E.Y. Anthony, and C.J. Ebinger. 2009. “Multiple inflation and deflation events at Kenyan volcanoes, East Africa Rift”. *Geology* 37 (11): 979-982. doi: 10.1130/G30133A.1.

Cascini, L., G. Fornaro, and D. Peduto. 2009. “Analysis at medium scale of low-resolution DInSAR data in slow-moving landslide affected areas”. *ISPRS Journal of Photogrammetry and Remote Sensing* 64 (6): 598–611. http://dx.doi.org/10.1016/j.isprsjprs.2009.05.003.

Cascini, L., G. Fornaro, and D. Peduto. 2010. “Andvanced low- and full-resolution DInSAR map generation for slow-moving landslide analysis at differential scales”. *Engineering Geology* 112 (1-4): 29-42. doi: 10.1016/j.enggeo.2010.01.003.

Casu, F., A. Manconi, A. Pepe, and R. Lanari. 2011. “Deformation time-series generation in areas characterized by large displacement dynamics: The SAR amplitude pixel-offset SBAS technique”. *IEEE Transactions on Geoscience and Remote Sensing* 49 (7): 2752-2763.

Chaabane, F., F. Tupin, and H. Maitre. 2005. “An empirical model for interferometric coherence”. Proceedings of SPIE - The International Society for Optical Engineering 5980, art. no. 59800E. doi: 10.1117/12.627341.

Cigna, F., S. Bianchini S, and N. Casagli. 2013. “How to assess landslide activity and intensity with Persistent Scatterer Interferometry (PSI): the PSI-based matrix approach”. *Landslides* 10 (3): 267–283. doi: 10.1007/s10346-012-0335-7.

Colesanti, C., and J. Wasowsky. 2006. “Investigating landslides with space-borne Synthetic Aperture Radar (SAR) interferometry”. *Engineering Geology* 88 (3-4): 173-199. doi: 10.1016/j.enggeo.2006.09.013.

Colombo, A., L. Mallen, R. Pispico, C. Giannico, M. Bianchi, and G. Savio. 2006. “Mappatura regionale delle aree monitorabili mediante l'uso della tecnica PS”. Proceedings of *10th National Conference ASITA*, November 14-17, 2006, Bolzano, Italy (ISBN/ISSN: 88-900943-0-3-2006).

Cruden, D.M., and D.J. Varnes. 1996. “Landslide types and processes”. In: Special Report 247 - Landslides: Investigation and mitigation. Washington DC: Transportation Research Board.

Ferretti, A., C. Prati, and F. Rocca. 2001. “Permanent scatterers in SAR interferometry”. *IEEE Transactions on Geoscience and Remote Sensing* 39 (1): 8–20.

Floris, M., A. D’Alpaos, A. De Agostini, G. Stevan, G. Tessari, and R. Genevois. 2012. “A process-based model for the definition of hydrological alert systems in landslide risk mitigation”. *Natural Hazards and Earth System Sciences* 12: 3343–3357. doi:10.5194/nhess-12-3343-2012.

Hanssen, R. 2005. “Satellite radar interferometry for deformation monitoring: a priori assessment of feasibility and accuracy”. *International Journal of Applied Earth Observation and Geoinformation* 6: 253–260. doi:10.1016/j.jag.2004.10.004.

Herrera, G., F. Gutiérrez, J.C. García-Davalillo, J. Guerrero, D. Notti, J.P. Galve, J.A. Fernández-Merodo, and G. Cooksley. 2013. “Multi-sensor advanced DInSAR monitoring of very slow landslides: the Tena Valley case study (Central Spanish Pyrenees)”. *Remote Sensing of Environment* 128: 31–43. doi: 10.1016/j.rse.2012.09.020.

Lazecky, M., F. Canaslan Comut, E. Nikolaeva, M. Bakon, J. Papco, A.M. Ruiz-Armenteros, Y. Qin, J.J.M. de Sousa, and P. Ondrejka. 2016. “Potential of Sentinel-1A for nation-wide routine updates of active Landslide maps”. *ISPRS Archives* XLI-B7:775-781. doi:10.5194/isprsarchives-XLI-B7-775-2016.

Mahapatra, P., S. Samiei-Esfahany, and R. Hansen. 2012. “Towards repeatability, reliability and robustness in time-series InSAR”. Proceedings of *Fringe 2011 Workshop*, September 19–23, 2011, Frascati, Italy. ESA Special Publication, SP-697 (January 2012, CD. ISBN 978-92-9092-261-2, ISSN 1609-042X).

Manconi, A., F. Casu, F. Ardizzone, M. Bonano, M. Cardinali, C. De Luca, E. Gueguen, I. Marchesini, M. Parise, C. Vennari, R. Lanari, and F. Guzzeti. 2014. “Brief communication: Rapid mapping of landslide events: the 3 December 2013 Montescaglioso landslide, Italy”. *Natural Hazards and Earth System Sciences* 14: 1835–1841. doi: 10.5194/nhess-14-1835-2014.

Michel, R., and J.P. Avouac. 1999. “Measuring ground displacement from SAR amplitude images: application to the Landers earthquake”. *Geophysical Research Letters* 26 (7): 875-878. doi: 10.1029/1999GL900138.

Notti, D., J.C. Davalillo, G. Herrera, and O. Mora. 2010. “Assessment of the performance of Xband satellite radar data for landslide mapping and monitoring: Upper Tena valley case study.” *Natural Hazards and Earth System Sciences* 10: 1865–1875. doi:10.5194/nhess-10-1865-2010.

Plank, S., J. Singer, and K. Thuro. 2012. “Estimation of the persistent scatterer density using optical remote sensing data and land cover data”. Proceedings of *Fringe 2011 Workshop*, September 19–23, 2011, Frascati, Italy. ESA Special Publication, SP-697, January 2012, CD. ISBN 978-92-9092-261-2, ISSN 1609-042X.

Plank, S., J. Singer, and K. Thuro. 2013. “Assessment of number and distribution of persistent scatterers prior to radar acquisition using open access land cover and topographical data”. *ISPRS Journal of Photogrammetry and Remote Sensing* 85: 132–147. doi: 10.1016/j.isprsjprs.2013.09.001.

Rabus, B., M. Eineder, A. Roth, and R. Bamler. 2003. “The shuttle radar topography mission - A new class of digital elevation models acquired by spaceborne radar”. *ISPRS Journal of Photogrammetry and Remote Sensing* 57: 241–262.

Singleton, A., Z. Li, T. Hoey, and J.P. Muller. 2014. “Evaluation sub-pixel offset techniques as an alternative to D-InSAR for monitoring episodic landslide movements in vegetated terrain”. *Remote Sensing of Environment* 147: 133–144. doi: 10.1016/j.rse.2014.03.003.

Tomás, R., R. Romero, J. Mulas, J.J. Marturià, J.J. Mallorquí, J.M. Lopez-Sanchez, G. Herrera, F. Gutiérrez, P.J. González, J. Fernández, S. Duque, A. Concha-Dimas, G. Cocksley, C. Castañeda, D. Carrasco, and P. Blanco. 2014. “Radar interferometry techniques for the study of ground subsidence phenomena: a re-view of practical issues through cases in Spain”. *Environmental Earth Sciences* 71 (1): 163–181. doi: 10.1007/s12665-013-2422-z.

Tosi, L., C. Da Lio, T. Strozzi, and P. Teatini. 2016. “Combining L- and X-Band SAR Interferometry to Assess Ground Displacements in Heterogeneous Coastal Environments: The Po River Delta and Venice Lagoon, Italy”. *Remote Sensing* 8: 308. doi:10.3390/rs8040308.

Wasowski, J., and F. Bovenga. 2014. “Investigating landslides and unstable slopes with satellite Multi Temporal Interferometry: Current issues and future perspectives”. *Engineering Geology* 174: 103-138. doi: 10.1016/j.enggeo.2014.03.003.

Wasowski, J., F. Bovenga, D.O. Nitti, and R. Nutricato. 2012. “Investigating landslides with Persistent Scatterers Interferometry (PSI): current issues and challenges”. In: Eberhardt E, Froese C, Turner AK, Leroueil S (Eds.). Proceedings of the *11th International and 2nd North American Symposium on Landslides*, Banff (Canada), 3–8 June, 2012. Landslides and Engineered Slopes, vol. 2. CRC Press/Balkema, Leiden, The Netherlands, 1295–1301.

Wasowski, J., F. Bovenga, R. Nutricato, D.O. Nitti, M.T. Chiaradia, A. Refice, and G. Pasquariello. 2016. “Exploring the potential of Sentinel-1 data for regional scale slope instability detection using multi-temporal interferometry”. *Geophysical Research Abstracts* 18.

Wright, T.J., C. Ebinger, J. Biggs, A. Ayele, G. Yirgu, D. Keir, and A. Stork. 2006. “Magma-manteined tirf segmentation at continental rupture in the 2005 Afar dyking episode”. *Nature* 442. doi: 10.1038/nature04978.

CHAPTER 3

The monotonous rising of the Lisan diapir revealed by 25 years of DInSAR observations. Dead Sea, Jordan.

Simone Fiaschi [1], Damien Closson [2], Najib Abou Karaki [3] and Mario Floris [1]

[1] Department of Geosciences, University of Padua, Padua, Italy.
[2] Eurosense, Wemmel, Belgium.
[3] Applied and Environmental Geology Department, Faculty of Science, The University of Jordan, Amman, Jordan.

Abstract

This article presents and analyses the results obtained from Differential Interferometric Synthetic Aperture Radar (DInSAR) techniques applied to ERS-1/2, ENVISAT, ALOS-PALSAR, COSMO-SkyMed, and Sentinel-1A datasets over the Lisan Peninsula, located in the southern part of the Dead Sea, Jordan. The novelty comes from the integration of three different frequencies to study the dynamics of a salt dome. The monitoring activity entirely covers the period extending from 1992 to 2016. Five displacement maps have been produced, calibrated and then fused to provide a total cumulated map of the displacements in the area. The ground movements have been analysed by comparison with in-situ tectonic observations collected by various Authors since the mid-1980s. The study shows a monotonous rising of the Lisan diapir. The presented results can be useful to update the knowledge of the displacement rates occurring in the area and to better comprehend the complex dynamics of the Lisan Peninsula.

1. Introduction

The Dead Sea (DS) region (Figure 1a) is one of the best examples of the negative impacts that the over-exploitation of fresh water and mineral resources may have on the environment. Since the 1950s, the DS' main feeder, the Jordan River, has been diverted for civil and agricultural purposes in the region and as far as the Negev desert, in southern Israel. Nowadays, more than 90% of its water does not supply the terminal lake anymore. The natural evaporation rates of 1500 mm/year (Dayan and Morin, 2006) and the annual precipitations of only 60 mm/year (Klein, 1985) also contribute to the negative water balance. Consequently, the DS water level has dropped at an increasing pace: from 395 m below Mean Sea Level (bMSL) in the 1960s to about 430 m bMSL in 2016 when the rate exceeded 120 cm/yr (Abou Karaki et al., 2016). Up to now, the cumulated water level dropped by 35 m and the lake shrunk by more than one-third. During the last five decades, secular equilibrium such as the meromictic state disappeared with a complete overturn of the water column during 1978-

1979 (Steinhorn et al., 1979). In addition to this water depletion, an increasing amount of salt minerals is extracted from the water of the DS by the potash industries located in the southern shallow basin of the lake. On average, about one third of the DS water lost each year, is pumped into salt evaporation ponds to permit the harvesting of the potash minerals. Below the coastal zones, the seaward and downward migration of the fresh/saline groundwater interface, forces the riparian freshwater to flow at various pace through the underlying evaporitic layers mainly made of salt minerals and gypsum (Salameh and El-Naser, 2000; Closson and Abou Karaki, 2009; Yechieli et al., 2016). Dissolution-related phenomena such as subsidence and sinkholes have appeared all along the former shoreline causing damage to the landscape and to the infrastructures such as bridges, roads, earthen dikes of the desalinization ponds, houses, hotels, resorts, and factories. The most active subsidence has occurred in the exposed lake bottom surrounding the Lisan Peninsula (LP) (Baer et al., 2002; Shimoni et al., 2002; Closson et al., 2003; Closson and Abou Karaki, 2009), located in the southern part of the DS (Figure 1b). Besides, the LP is also characterized by the activity of an underlying salt diapir, the biggest in the whole DS basin. The latter has been extensively studied by geophysicists in order to detect either oil reservoirs (deep surface) in relation with salt diapirs, or sinkholes and subsidence (near surface) to determine if assets along the coast are exposed to damage. Regarding the near surface studies, different surveying methods have been used such as: gravimetry (Abou Karaki, 1995; Choi et al., 2011), multidisciplinary geophysical approach (Frumkin et al., 2011), ground penetrating radar (Batayneh et al., 2002), seismic data interpretation (Mechie et al., 2009) and satellite interferometry (Baer et al., 2002; Shimoni et al., 2002; Abelson et al., 2003; Closson et al., 2003, 2011; Nof et al., 2012, 2013; Yechieli et al., 2016). Despite the large number of published papers, only a few focused on the movements affecting the LP and its surroundings (e.g. Shimoni et al., 2002). Moreover, since Closson et al. (2011), there is no attempt to monitor the entire LP area with satellite interferometry techniques. This article aims to fill this gap by giving an updated overview of the ground displacements occurring in the area. Differential Interferometric Synthetic Aperture Radar (DInSAR) techniques have been applied to five independent SAR datasets covering the period from 1992 to 2016. The images have been acquired by ERS-1/2, ENVISAT, ALOS-PALSAR, COSMO-SkyMed, and Sentinel-1A platforms. Five velocity and displacement maps have been produced and analyzed. Then, the five outputs have been combined to compute a cumulated displacement map of the last 25 years.

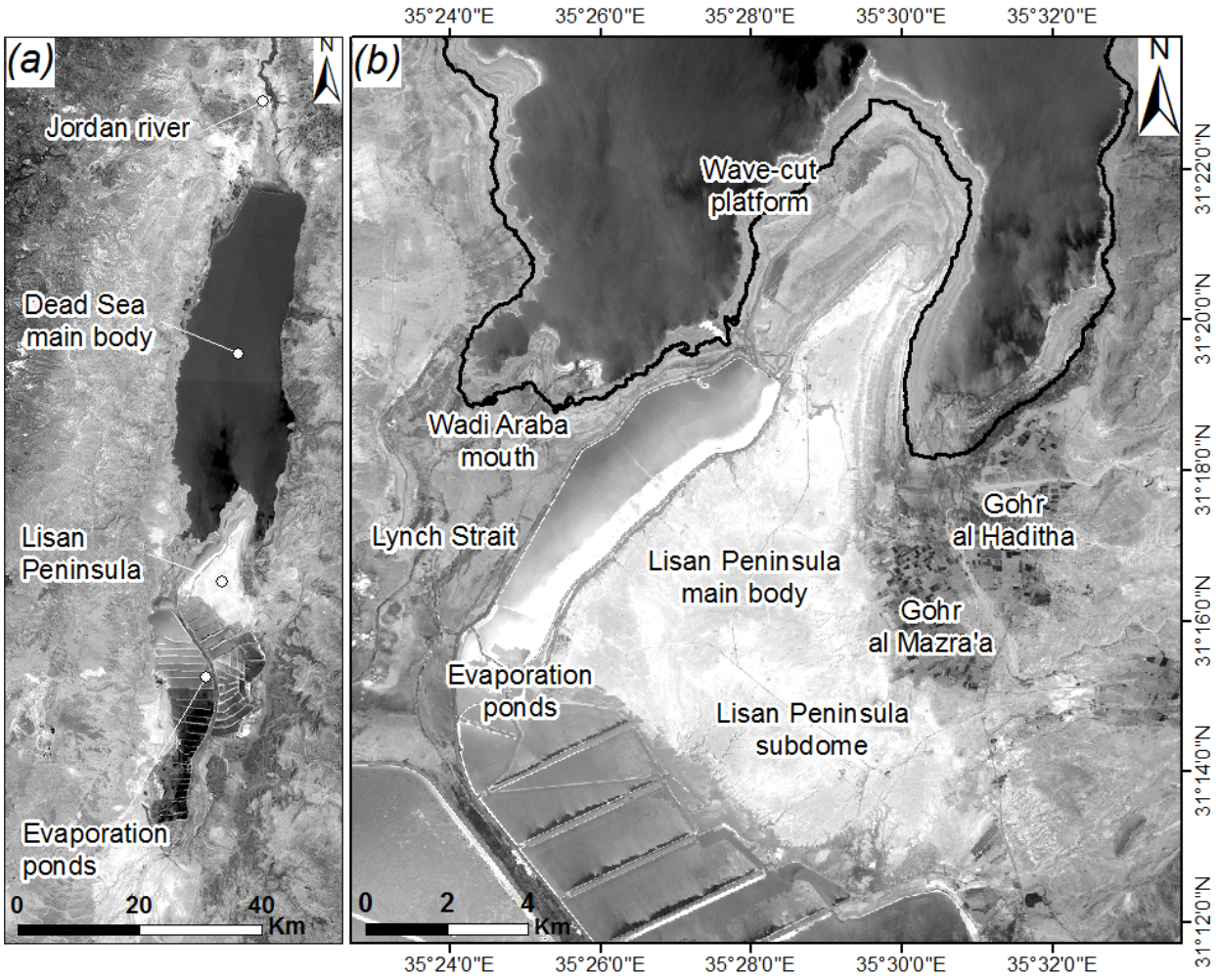

Figure 2. a) Location of the Dead Sea. b) Study area and the main locations discussed in the text. The black line refers to the 415 m bMSL contour line derived from the February 2000 SRTM DEM. Basemap: 20/07/2016 Sentinel-2 image.

2. Geological Setting

The DS is a hypersaline terminal lake located in the lowest point on continental Earth, at ~430 m bMSL, in 2016. It formed in a pull-apart basin along the strike-slip Dead Sea fault (Mechie et al., 2009). The basin is 150 km long, ≤15 km wide, <8.5 km deep (ten Brink and Flores 2012) and, in the southern part, comprises 10 km-thick sediments accumulated in the last 4-6 Ma (Garfunkel and Ben-Avraham, 1996; Al-Zoubi and ten Brink, 2001; Bartov et al., 2006; Ben-Avraham and Schubert, 2006). During the Miocene until the Holocene, the accumulated sediments had mainly lacustrine and terrestrial origin (Picard, 1943; Zak, 1967; Baer et al., 2002). Two main formations occupy the first tens of meters along the DS shoreline: the Lisan Formation formed in late Pleistocene and the Holocene Ze'elim Formation (Begin et al., 1974; Sneh, 1979; Yechieli et al., 2016). According to (Sunna, 1986; Bartov et al., 2002; Closson et al., 2007), the Lisan Formation can be divided in three main Members: Upper, Middle and Lower. The Upper Member has a total thickness of 10 m and is made of alternating laminae of aragonite and detritus; the Middle Member has a total thickness of 12 m, it includes layers of gypsum, detritus and alternating laminae of aragonite and detritus topped by

a 50 cm thick gypsum layer; the Lower Member is similar to the upper one and consists mainly of laminae of aragonite and detritus, with 1-2 cm thick salt layers, that alternates for a total of 8 meters. Three prominent gypsum layers of 50 cm in thickness cap this Member. The Ze'elim Formation mainly consists of layers of alternating laminae of aragonite and clastic material such as clay, sand and gravel (Baer et al., 2002; Yechieli et al., 2016).

The LP, located entirely in Jordanian territory, is a salty desert 18 km long and 10 km wide. The highest elevation point is at ~318 m bMSL. This strip of land separates the two sections of the DS, the main body of water to the north (sea bottom at 730 m bMSL) and the shallower section to the south (sea bottom at 402 m bMSL) now entirely occupied by the evaporation ponds which construction started in early 1960s (Closson and Abou Karaki, 2014). These two sections were connected until 1978 by the Lynch strait that dried up as a consequence of the water level drop. The main body of the LP is formed by the Lisan Formation while the margins belong to the Ze'elim formation (Bartov, 1999; Baer et al., 2002). The sediments outcrop for a total thickness of 100 m, of which 40 m consists of the Lisan Formation (Closson et al., 2007). The Lisan diapir, a salt diapir elongated in the north-south direction, underlies the LP. The extension of this diapir has been discussed in different studies: Al-Zoubi and ten Brink (2001) using magnetic, gravity, seismic and boreholes data determined its size to be 13 km × 10 km with an average thickness of 6 km; Choi et al. (2011) calculated with gravimetric data a size of 20 km × 15 km and an average thickness of 5.5 km; Meqbel et al. (2013) found a size of 17 km × 12 km and a maximum thickness of 5-6 km through magnetotelluric data; Hofstetter and Dorbath (2014) estimated through seismic data a size of 23 km × 13 km and average thickness of 4.3 km. The roof of the salt dome is located at 125 m below the surface (Bender, 1974). The Lisan diapir comprises different subdomes and a structural depression (Bartov, 1999). Two main sets of lineaments, related to different fault systems, are present in the peninsula: the first set with north-south direction, is located in the east; the second, with east–southeast and west–northwest direction, is located in the south (Sunna, 1986). The surface in the southern part of the peninsula, presents structurally controlled semi-circular cracks and depressions presumably in correspondence of the diapir margins. According to Baer et al. (2002), their formation may be related to one or the combination of the following factors: dissolution of a specific layer; collapse of layers at the margins of the dome; dissolution of salt at the margins of the dome at 100-250 m of depth. The presence of these depressions may also indicate the possible occurrence of a major plunging anticline (Sunna, 1986; Closson et al., 2007). A normal fault also bounds the peninsula in the north-western side (Bartov, 1999).

3. Methodology and datasets

An area of about 18 km x 22 km that covers the LP was selected as region of interest (Figure 1b). The available SAR datasets (Table 1) consist of: 24 ERS-1/2 covering the period 06/1992-06/2000 and 32 ENVISAT covering 01/2003-06/2010, both acquired in C-band by the European Space Agency (ESA); 10 L-band ALOS-PALSAR acquired by the Japan Aerospace Exploration Agency (JAXA) from 11/2007 to 02/2011; 20 X-band COSMO-SkyMed (CSK) for the period 12/2011-05/2014 acquired by the Italian Space Agency (ASI). Finally, we exploited 32 Sentinel-1A images acquired by ESA and covering the period 10/2014-05/2016. In addition, another Sentinel-1A dataset made of 30 images acquired in ascending geometry over the same period was processed and used to

assess the predominant component of the movements in the area. In order to retrieve the ground displacements information collected by each sensor, the Small Baseline Subset (SBAS) (Berardino et al., 2002) DInSAR technique was applied through the SARscape® software package. The SBAS relies on the combination of images pairs that have short temporal and spatial baselines to produce a stack of interferograms from which it is possible to calculate the deformation of each measured point on the ground. The generated interferograms were filtered using the Goldstein adaptive filter (Goldstein and Werner, 1998) and the interferometric fringes were unwrapped using the Delaunay minimum cost flow (MCF) algorithm (Costantini, 1998). The removal of the topographic component of the phase was carried out using the Shuttle Radar Topographic Mission (SRTM) digital elevation model (DEM) with a ground resolution of 1 arc second (30 m x 30 m pixel size). All the datasets were multi-looked differently in order to obtain the same ground resolution with a pixel size of ~20 m x 20 m (Table 1). The areas along the shore that were exposed year by year by the DS lowering, were masked out in all the images using the 415 m bMSL contour line of the SRTM DEM, that refers to the water level in February 2000 at the time the DEM was produced (Figure 1b).

Table 1. Main features of the available SAR datasets used in this study.

Satellite	Band/ λ (cm)	Acquisition geometry	Revisit time (days)	Multi-look Rg/Az	Look angle
ERS-1/2	C/5.6	Desc	35	1/5	23°
ENVISAT	C/5.6	Desc	35	1/5	23°
ALOS-PALSAR	L/23.8	Asc	46	2/6	39°
CSK	X/3.1	Desc	16	10/9	41°
Sentinel-1A	C/5.6	Desc/Asc	12	5/1	39°

The selection of an appropriate reference point located over an area with zero vertical displacement or with known deformation is crucial to obtain reliable results. Considering the complexity of the movements affecting the LP and the lack of Global Position System (GPS) stations in the area, an a-priori knowledge of the movement rates is necessary to identify the areas that can be used as reference. The identification of the stable areas was based on the information obtained from the work done by Shimoni et al. (2002) in which are reported the differential interferograms of the LP for several time intervals from July 1992 to March 1999, and by Nof et al. (2012) that presented the LOS velocity map of the entire DS basin for the period 1993-2001. Thanks to the modules implemented in SARscape®, several reference points (≥7) were selected in the identified stable areas highlighted in Figure 2. In this way, it is possible to reduce the errors in the estimation of the displacement velocity due to a misplaced single reference point.

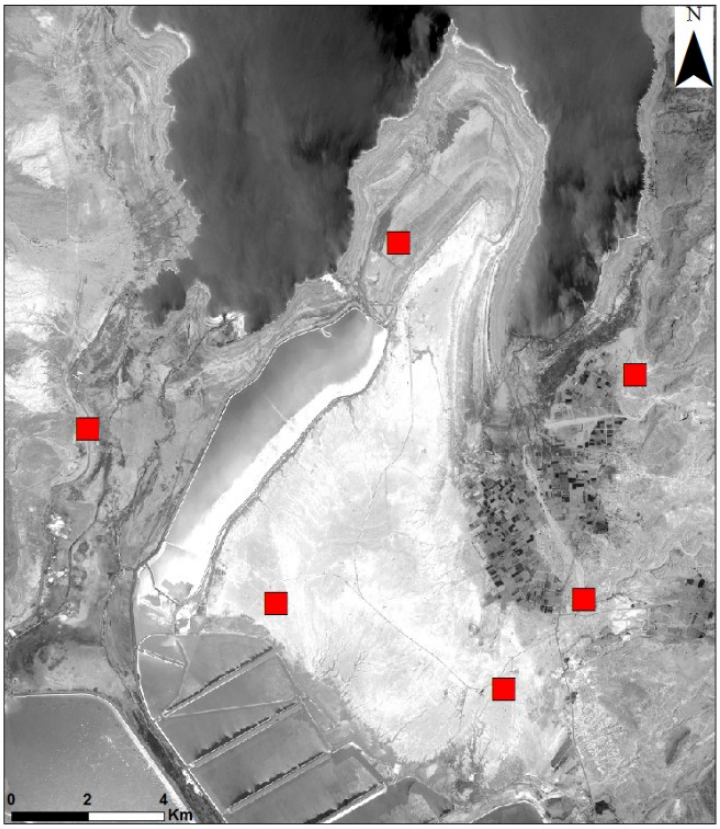

Figure 2. The red squares are the location of the stable areas used as reference for the SAR images processing. Basemap: 20/07/2016 Sentinel-2 image.

To get knowledge of the displacements in the LP area starting from the early 1990s until 2016, several SAR images acquired by sensors working with C, X and L bands have been exploited. The use of different spectral bands in the monitoring of the same territory may lead to obtain results that differ in terms of data coverage and overall quality. Such a difference is the consequence of the different interactions between the incident energy coming from the radar antenna and the characteristics of the illuminated ground surface. The amount of radar energy returned to the antenna that is used to produce the amplitude image and to compute the variations of distance between antenna and ground scatters, is mainly a function of the physical and geometric characteristics of the irradiated surface. The main parameters influencing the backscattered signature (backscattering radar cross section or backscattering coefficient) include surface roughness, dielectric constant (moisture and temperature), and spatial structure. The backscattering signal is also controlled by the radar frequency, the polarization and the incidence angle. Figure 3 illustrates, as example, the difference between the LP “landscapes” when observed in X, C and L band.

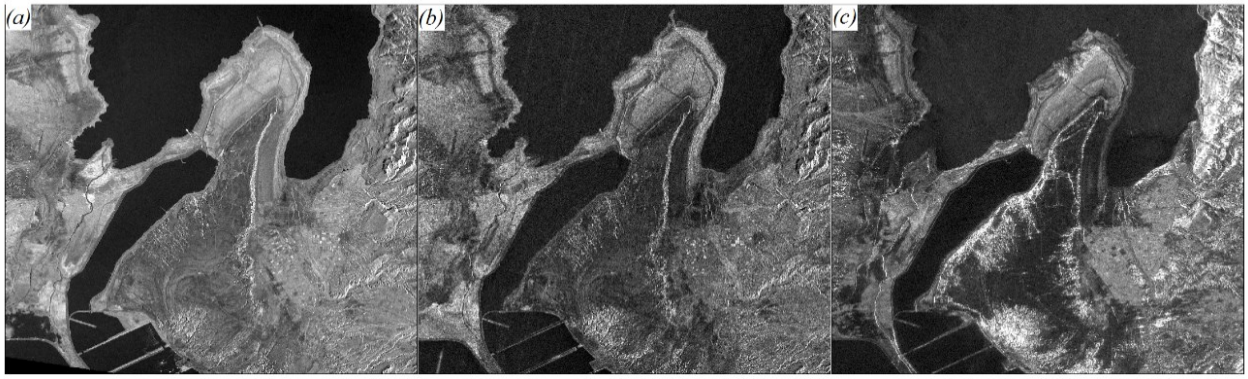

Figure 3. Backscattered energy of the LP with regards to: a) X, b) C, and c) L wavelengths. The colours range is from black (low) to white (high). Black colour means that all the energy transmitted is reflected away from the antenna and there is no information, neither in the amplitude, nor in the phase. White colour means the opposite. In this case, the grey level depends on the surface roughness, which is a parameter related to the incident wavelength. This is illustrated in a very convincing way by comparing the amplitude images of the peninsula in X-band (light grey) and L-band (black).

In the LP area, the amplitude value is inversely proportional to the wavelength used: the shorter wavelength of X-band scatters back to the antenna more energy over smoother surfaces such as the peninsula main body, while the longer L-band does not, at the exception of the southern and eastern areas where an incised drainage system developed and created canyons. As a consequence, in that context, X-band images provided the best signal, followed by C-band, and L-band. However, since the subsidence in the DS area can be extremely rapid with the appearance of sinkholes, the quality of the outputs is reverse as L-band is able to manage a wider range of ground displacements than C-band and X-band. In particular, in the Lynch Strait, X-band has provided the deformation field associated with strong subsidence related to sinkholes; while L-band was able to perform measurements in the most affected zones at the exception of the ground collapse itself. Furthermore, over the areas of the peninsula corresponding to the salt domes, the range of ground movement is very wide, with displacement velocities that vary from few millimetres per year to tens of centimetres per year. The exploitation of each sensor has, in this case, its advantages and drawbacks: X-band is more sensitive to subtle deformations but leads to a complete loss of information where the movements are too fast; L-band is recommended to map the areas with very fast movements, but losing the sensibility to smaller deformations. C-band is closer in wavelength to X-band but being less sensitive, it provides a good compromise.

4. SBAS processing results and discussion

The exploitation of five different SAR datasets with DInSAR SBAS technique allowed us to produce detailed maps of the movements along the radar Line Of Sight (LOS) affecting the LP area for more than two decades. The location, extension and evolution of the displacement areas along with the subsidence and uplift rates were studied analysing the time series for each monitored period. The LOS velocity and displacement maps are presented in Figure 4 and 5, respectively. In the adopted colour scale, positive values, in blue, represent uplift while negative values, in red, represent subsidence. The stable areas are in green. The range of displacement considered as stable was set to

correspond to a mean velocity threshold of around ±1.5-2 mm/yr accordingly to the duration of the period covered by each dataset: ±12 mm for ERS-1/2 and ENVISAT, ±5 mm for ALOS-PALSAR, ±3 mm for CSK and Sentinel-1A. This, allowed us to better distinguish between the moving and stable areas even for short monitoring periods such as the one covered by the CSK and Sentinel-1A datasets, 17 months and 19 months, respectively.

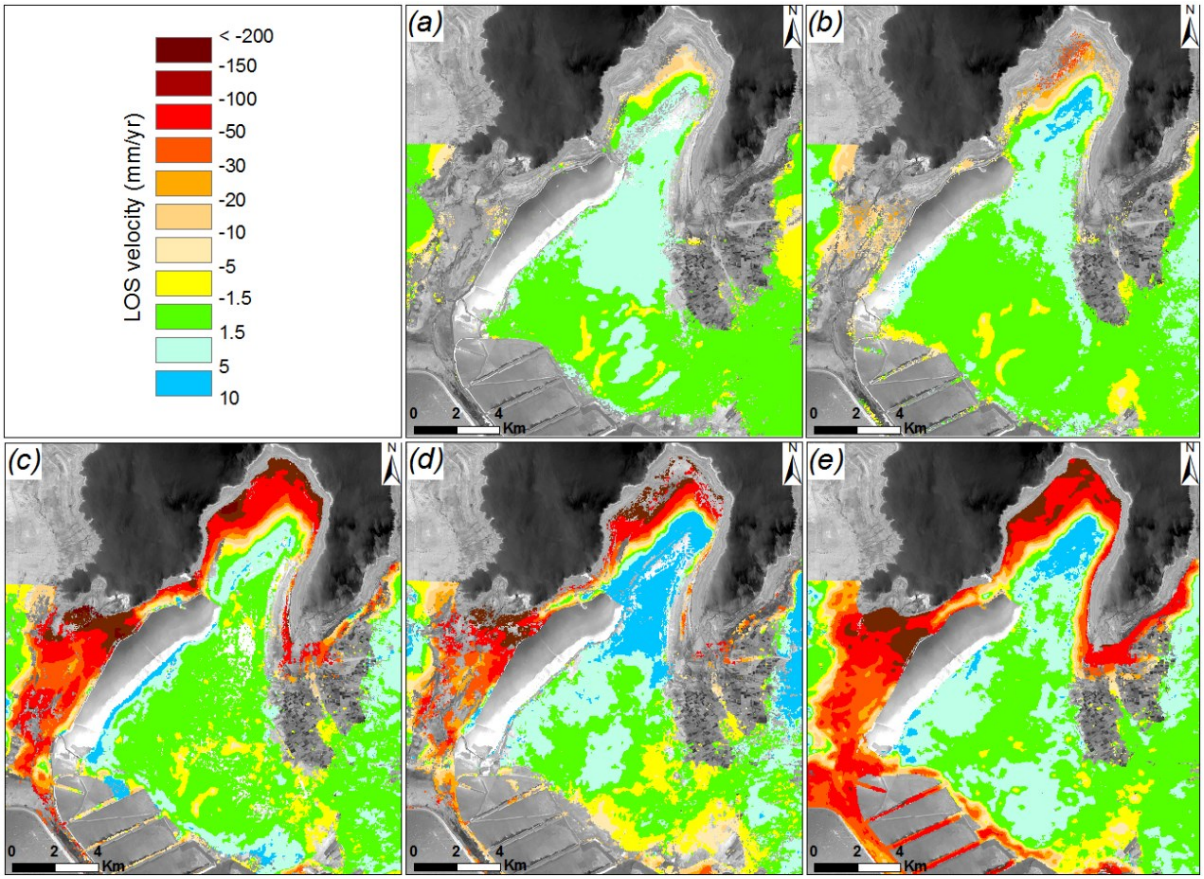

Figure 4. LOS velocity maps: a) 1992-2000 (ERS-1/2); b) 2003-2010 (ENVISAT); c) 2007-2010 (ALOS-PALSAR); d) 2011-2014 (CSK); e) 2014-2016 (Sentinel-1A). Basemap: 20/07/2016 Sentinel-2 image.

From the velocity maps presented in Figure 4, it is possible to delineate two distinct movement areas: the peninsula, characterized by low velocities, and the coastal and peripheral areas affected by more intense deformations. Both subsidence and uplift are present in the first, while only subsidence is present in the second. In the peninsula, maximum subsidence rates of -7.3 mm/yr were registered in the south during 2007-2010, while maximum uplift values of 15.6 mm/yr were registered in the northern part during 2011-2014. Along the coastline, the maximum rates of displacement registered were of -181.7 mm/yr in correspondence of the Wadi Araba mouth during 2014-2016. Similar rates of subsidence up to -181 mm/yr were detected in 2007-2010 along the northern coastline close to the LP wave-cut platform. Considering the C-band datasets only (Figure 4 a, b and e), it is possible to notice a general increase with time of the deformation velocities in the wave-cut platform where the subsidence rates went from -13 mm/yr (1992-2000) to -41 mm/yr (2003-2010) and reached -87 mm/yr (2014-2016).

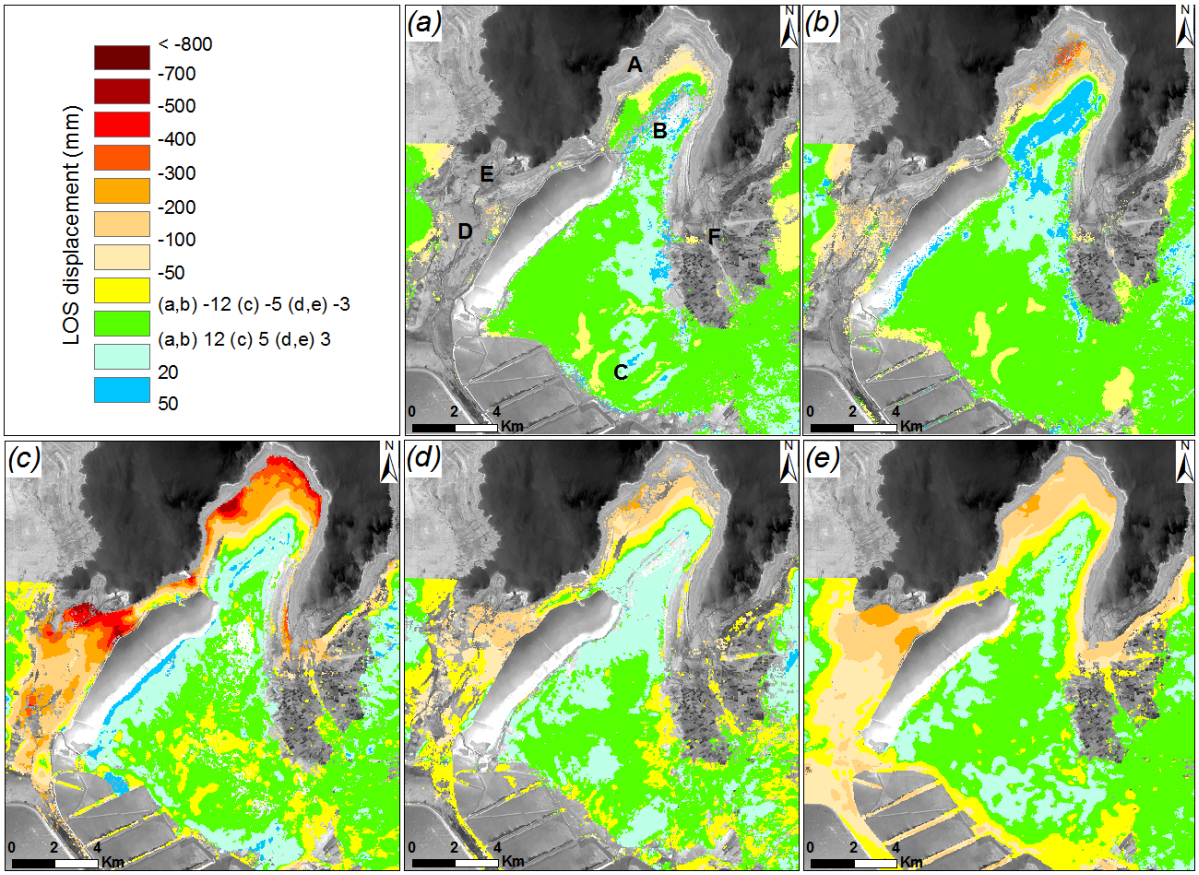

Figure 5. LOS displacement maps: a) 1992-2000 (ERS-1/2); b) 2003-2010 (ENVISAT); c) 2007-2010 (ALOS-PALSAR); d) 2011-2014 (CSK); e) 2014-2016 (Sentinel-1A). In a) the letters are the locations of the main areas affected by displacement: (A) wave-cut platform; (B) northern tip; (C) southern body; (D) Lynch strait; (E) Wadi Araba mouth; (F) Gohr Al Haditha and Gohr Al Mazra'a. Basemap: 20/07/2016 Sentinel-2 image.

Considering the displacement maps of Figure 5, six main deformation zones were detected (Figure 5a): the wave-cut platform (A); the northern tip (B); the southern body (C); the Lynch strait (D); the Wadi Araba mouth (E); Ghor Al Haditha and Ghor al Mazra'a (F).

The results obtained with the ERS-1/2 images (1992-2000), show subsiding areas mainly in A, with maximum values of -150 mm, and in D with -170 mm. Moderate subsidence up to -50 mm, affected narrow and elongated semi-circular areas in C. Uplift occurred mainly in the eastern side of the peninsula with the highest values in B (60 mm). Uplift was detected in C between the semi-circular depressions as result of the differential movement of the salt diapir subdome. Large areas not covered by data, corresponding to territories with very low temporal coherence, were located in the mud plains of D and in the agricultural fields of F.

ENVISAT (2003-2010) results show strong subsidence up to -430 mm affecting the north-western shore of A. Subsidence up to -53 mm was detected in C. High values of subsidence (-230 mm) were registered also in D. Despite most of the cultivated land in F remained not covered by data, increasing subsidence values up to -83 mm were detected moving north towards the shoreline. The area in B reached a maximum uplift of 62 mm.

L-band ALOS-PALSAR (2007-2011) results presented an increased data coverage that extended over most of the monitored area. Very high subsidence values were detected in the northeast (-700 mm) and northwest (-806 mm) margins of A. In C the maximum subsidence registered was -35 mm.

Very strong subsidence was recorded in D (-394 mm) and E (-830 mm). Data coverage extended also over the shoreline in F and partly over the cultivated lands, where increasing subsidence up to -485 mm was detected moving closer to the shoreline. Uplift occurred along the western border of the LP. A maximum uplift of 38 mm was registered in B.

The location and distribution of the subsiding areas resulted from the CSK dataset (2011-2014), were in accordance with the ALOS-PALSAR results, even if the detected rates were lower due to the shorter band used by the CSK sensor (3.1 cm) in respect to the ALOS-PALSAR (23.8 cm). The shore in A registered the highest subsidence value of -332 mm, while E was affected by subsidence up to -282 mm. Most of B presented strong uplift up to 32 mm. Uplift was also registered in C and in the western side of the peninsula (around 15 mm).

Sentinel-1A (2014-2016) results presented the best data coverage, thanks to the combination of the C-band and the short revisit time (12 days). The north-western section of A and E registered the highest subsidence values of -365 mm and -403 mm, respectively. Increasing subsidence occurred also in F moving from the cultivated fields (-20 mm) to the shoreline (-245 mm). Uplift up to 49 mm was registered in B. Uplift with lower values also occurred in C and in the western side of the peninsula.

In order to assess the evolution of the displacement in the LP area, the cumulated displacement maps of the five time intervals covered by the SAR datasets were produced. Since the deformation calculated along LOS varies depending on the incidence angle, the direct use of the displacement values obtained with different satellites is not recommended for the production of cumulated displacement maps. For this reason, the deformation rates were projected to the vertical direction assuming a zero horizontal component of the movement in the study area. This assumption was confirmed by the comparison between the results obtained with the Sentinel-1A images acquired in descending and ascending geometries that shows very similar rates of deformation over the peninsula and along its coastline with no change in the sign of the velocity vector, which implies the predominance of vertical movements. Moreover, a dominant vertical component of movement along the DS shoreline is also described in Baer et al. (2002). The vertical deformation (V_{def}) was then extracted using the equation:

$$V_{def} = LOS_{def} / \cos \theta$$

where, for each measured point, LOS_{def} is the deformation calculated along LOS and θ is the incidence angle. Using the first available ERS-1/2 image (11/06/1992) as starting date, the time intervals considered were: 06/2000 – 06/2010 – 02/2011 – 05/2013 – 05/2016, corresponding to the ERS-1/2, ENVISAT, ALOS-PALSAR, CSK and Sentinel-1A datasets. The stacking procedure was carried out only for the pixels overlapping in each displacement map. The adopted classification is similar to the one described previously, but in this case the range of displacement chosen as stable was fixed at ±20 mm. The five different displacement maps were combined into one (Figure 6) in order to assess the total displacement in the 25-year period (1992-2016). The measured values of displacement, despite the inaccuracies and the errors related to the adopted technique, may be lower than the real one, since the displacement occurring in the time gaps between the datasets was not taken into account.

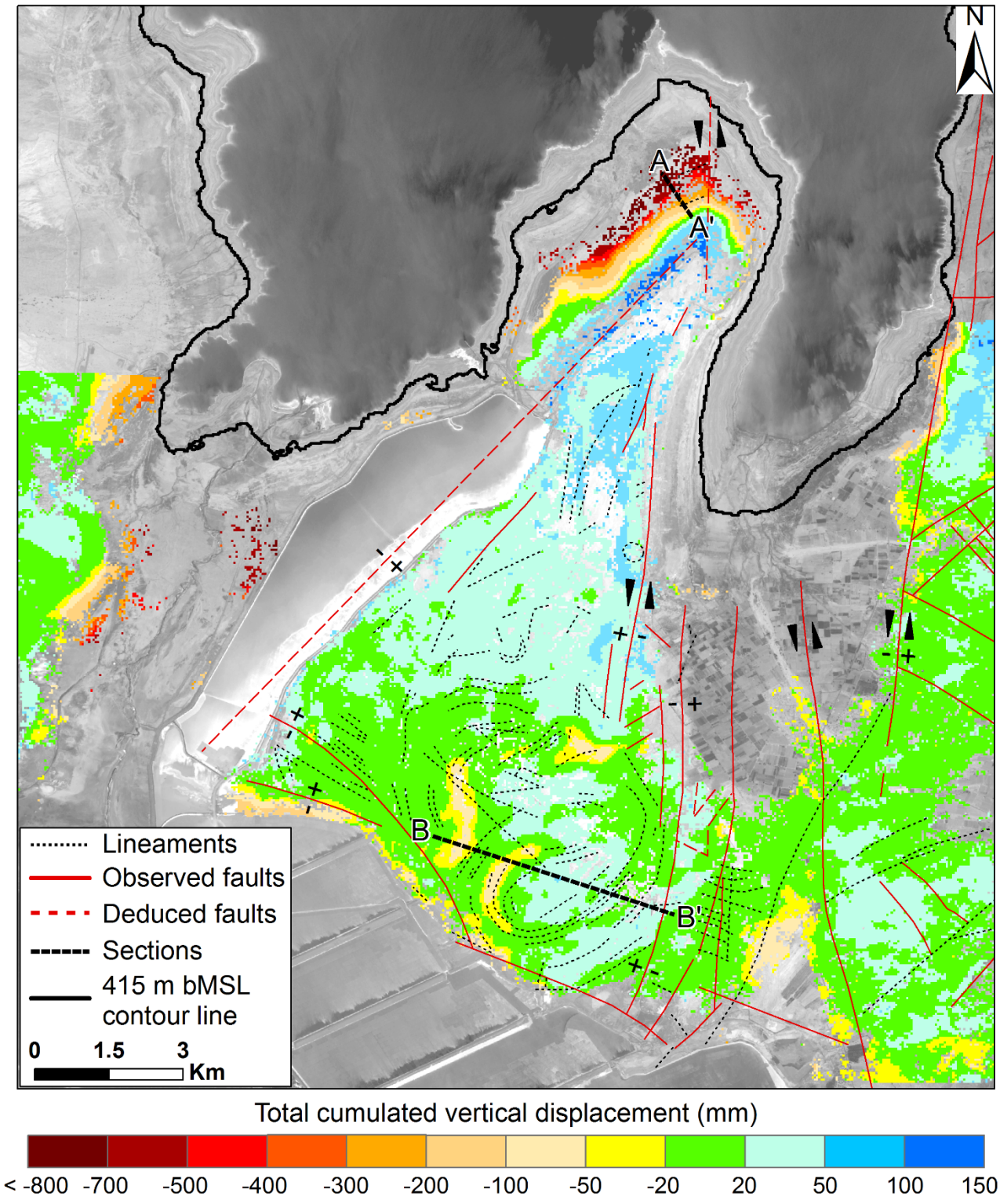

Figure 6. Total vertical cumulated displacement map for the period 1992-2016. Basemap: 25/07/2016 Sentinel-2 image.

The results were validated overlapping the main lineaments and faults of the LP to the 1992-2016 cumulated displacement map (Figure 6). The reported geological features are based on the field work done by Sunna (1986) and Bartov et al. (2006) imported in a Geographic Information System (GIS). The visual inspection of the map shows a good accordance between the SBAS results and the

field data: the very high values of uplift registered in the northern area can be explained with the presence of the fault that strikes with southwest-northeast direction on the west side of the LP. Furthermore, the semi-circular depressions and the uplifting zones located in the southern area match perfectly with the pattern of the lineaments delimiting the salt diapir subdome.

The displacements occurring in the area were also described through two sections drawn over the northern and southern part of the peninsula. Section 1 (Figure 7) is located on the northern margin of the wave-cut platform, and starts from the shoreline (A) to a stable area at the top of the platform (A') just before the uplifting zone. In 1992-2000 the displacement reached almost -100 mm at the shoreline, then the rates increased more than four times and reached around -440 mm in 2010, -500 mm in 2011, -700 mm in 2013 and a maximum value of -940 mm in 2016. It is worth noting that the section starts in proximity of a large collapsed area. Here, the Arab Potash Company constructed during the late 1990s a salt evaporation pond to increase the potash productivity. In March 2000, the pond was completely destroyed by the collapse of 1650 m of the earthen dike as consequence of the severe increase of the subsidence activity in the area (Closson and Abou Karaki 2009, 2014b).

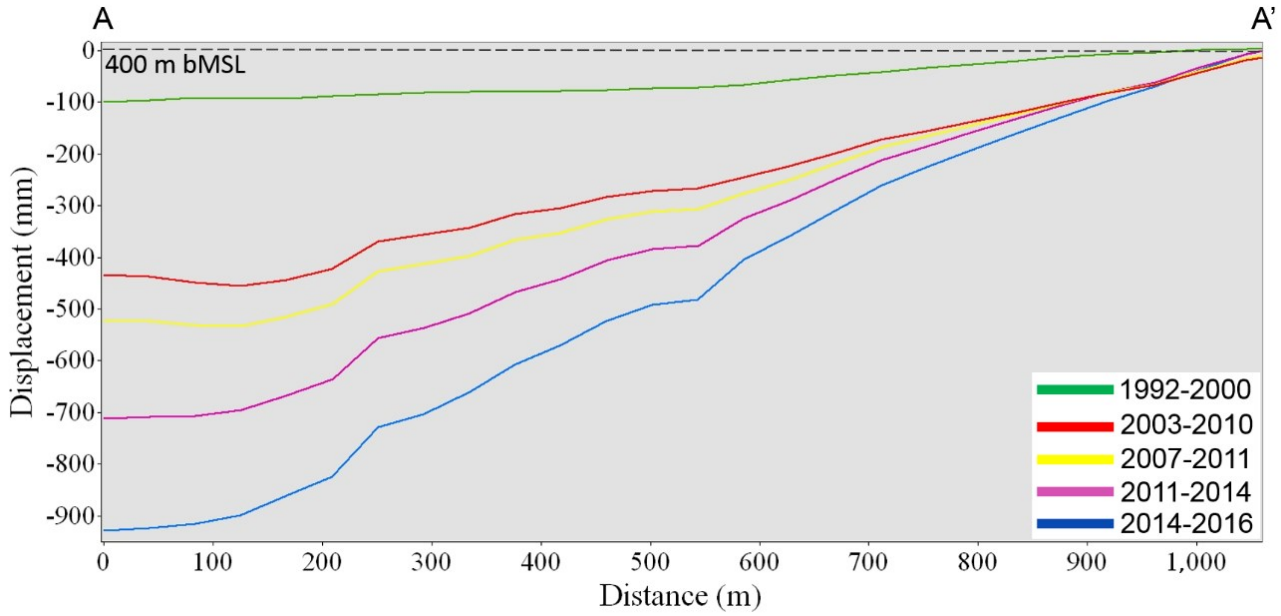

Figure 7. Vertical displacement values calculated over the section located in the northern part of the LP, from A to A'. The dashed black line represents the topography elevation extracted from the SRTM DEM along the section.

Section 2 (Figure 8) was drawn in the southern part of the peninsula over the two main semi-circular depressions and the two distinct uplifting areas, from B to B'. According to Figure 4, the two depressions are located in the section at a distance of 450 m and 1250 m while the main uplifting areas are at 2200 m and 4000 m. From 1992 to 2000 the displacement values in the two depressions were -41 mm and -36 mm, while in the two uplifting areas 20 mm and 22 mm, respectively. After 2000 the displacement rates increased drastically: but while the subsidence stopped in 2011 after reaching a maximum value of -75 mm, the uplift increased over the entire period, reaching 35 mm in 2010, 44 mm in 2013 and almost 50 mm in 2016. These values correspond to velocities that are steady around 2-2.4 mm/yr. The results, showed a steady uplift that characterized the LP during the entire monitored period (1992-2016): this is in contrast with the findings of previous studies in which the

authors describe the Lisan diapir uplift as episodic and not monotonous (Shimoni et al., 2002; Closson et al., 2011).

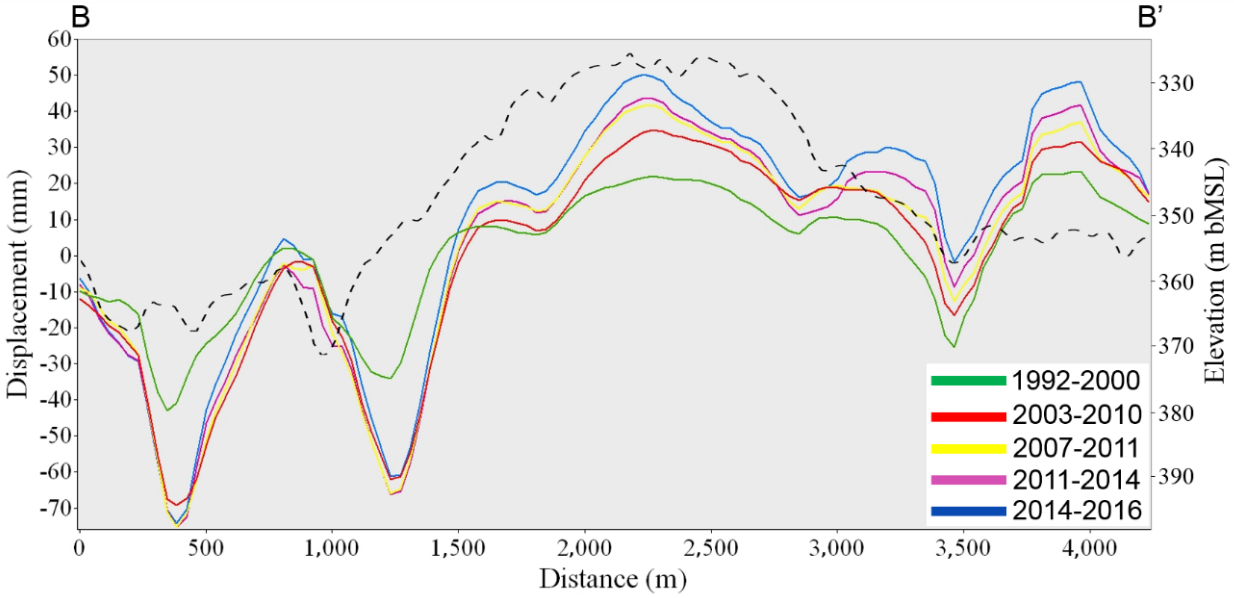

Figure 8. Vertical displacement values calculated over the section located in the southern part of the LP, from B to B'. The dashed black line represents the topography elevation extracted from the SRTM DEM along the section.

Assessing the mechanisms that control the displacements in the DS area is beyond the scope of this study, but few considerations can be drawn from the presented results. Combining the information provided by the scientific literature and the DInSAR results of this study, four main controlling mechanism can be identified: dissolution, tectonic, diapirsm, compaction or, more likely, their combination.

Dissolution related phenomena could explain the high rates of subsidence found along the coastline in the Gohr Al Haditha area and in the wave-cut platform. In the latter, the subsidence could be enhanced by the Lisan diapir upward movement that forces the salt to migrate from the periphery to feed the rising mass, as explained in Shimoni et al. (2002). The coastal subsidence could also be caused by the compaction of the marl layers as consequence of the DS level lowering (Baer et al., 2002).

The combination of sediments compaction and salt dissolution can explain the very high subsidence rates found in the Lynch Strait, where the entrenchment of the Wadi Araba in the erodible sediments lowers the brackish water table and causes the dissolution of the buried salt layer (Closson et al., 2010), and in the Wadi Araba mouth where the transported sediments accumulate rapidly loading the underlying layers.

The displacements in the peninsula are mainly controlled by the diapirism, even if the high rates of uplift detected with DInSAR cannot be entirely explained by the diapir upward movement itself. Hence, other controlling factors must be considered. The formation and rising of the diapir subdomes may explain the presence of semi-circular depressions around the diapir margins. A large number of faults and lineaments serve as preferential paths for the water flow that controls the localized dissolution of the salt layers.

5. Conclusions

In this work, we monitored the evolution of the Lisan Peninsula area over a period of 25 years, from 1992 to 2016, through the SBAS DInSAR technique. SBAS revealed to be extremely useful to measure the entity of the movements occurring in the area and, at the same time, to detect and map the most affected areas. The results show an increase in the displacement rates, for both the subsidence and uplift, starting from the 2000. The area most affected by subsidence is the shoreline, where every year the constant dropping of the DS level exposes new portion of territory. The uplift occurring in the north part of the peninsula is probably caused by the displacements of the faults striking in the area. Semi-circular depressions occur around minor uplifting areas in the southern part of the peninsula as consequence of the salt diapir upward movement. The validity of the SBAS results is confirmed by the good agreement with the concealed tectonic features and lineaments reported in literature. The Sentinel-1A satellite used in this study demonstrated its great potential as a tool for continuous monitoring activity over areas affected even by very fast displacements. The obtained results updated the knowledge of the karst dynamics in the Lisan Peninsula, and could be used as the starting point for further studies in the area. DInSAR techniques showed to be a very useful tool for assessing geological and geomorphological features, especially in areas characterized by bad environmental conditions (not easily accessible) and with very few (or none at all) field data available. Further studies are necessary to better understand the mechanisms that control the displacements in the area and their interactions. Future work will regard the DInSAR mapping of the after-2000 emerged DS shore using Digital Surface Models (DSM) generated with long baseline interferometric pairs. This will allow us to correctly calculate the deformation rates of the coastal areas recently exposed and to better characterize the subsidence phenomena that are strictly related to the DS water level decline.

Acknowledgements

This project was carried out using: CSK® Products © ASI (Italian Space Agency), delivered under an ASI licence.

Funding

This work was partially supported by the University of Padua under the grant: “University Cooperation Initiatives” (ICU) 2014. Part of the work of Najib Abou Karaki was done during a sabbatical year supported by the University of Jordan.

References

Abelson, M., G. Baer, V. Shtivelman, D. Wachs, E. Raz, O. Crouvi, I. Kurzon, and Y. Yechieli. 2003. “Collapse-sinkholes and radar interferometry reveal neotectonics concealed within the Dead Sea basin”. *Geophysical Research Letters* 30: 1545. doi:10.1029/2003GL017103.

Abou Karaki, N. 1995. “The gravity survey: assessment of the hazard of subsidence and sinkholes in Ghor Al-Haditha area - Final report”. In El-Isa et al., Centre for Consultation, Technical Services and Studies, University of Jordan, unpublished, 117-124.

Abou Karaki, N., S. Fiaschi, and D. Closson. 2016. “Sustainable development and Anthropogenic induced geomorphic hazards in subsiding areas”. *Earth Surface Processese and Landforms*. Published online (Wileyonlinelibrary.com), doi: 10.1002/esp.4047.

Al-Zoubi, A., and U.S. ten Brink. 2001. “Salt diapirs in the Dead Sea basin and their relationship to Quaternary extensional tectonics”. *Marine and Petroleum Geology* 18 (7): 779–797.

Baer, G., U. Schattner, D. Wachs, D. Sandwell, S. Wdowinski, and S. Frydman. 2002. “The lowest place on Earth is subsiding: an InSAR (interferometric synthetic aperture radar) perspective”. *Geological Society of America Bulletin* 114 (1): 12–23.

Bartov, Y. 1999. “The Geology of the Lisan formation in Massada Plain and the Lisan peninsula”. PhD thesis, The Hebrew University of Jerusalem, Israel.

Bartov, Y., M. Stein, Y. Enzel, A. Agnon, and Z. Reches. 2002. “Lake levels and sequence stratigraphy of Lake Lisan, the late Pleistocene precursor of the Dead Sea”. *Quaternary Research* 57: 9–21.

Bartov, Y., A. Agnon, Y. Enzel, and M. Stein. 2006. “Late Quaternary faulting and subsidence in the central Dead Sea basin”. *Israel Journal of Earth Sciences* 55: 17–31.

Batayneh, A.T., A.A. Abueladas, and K.A. Moumani. 2002. “Use of ground-penetrating radar for assessment of potential sinkhole conditions: an example from Ghor al Haditha area, Jordan”. *Environmental Geology* 41: 977–983.

Begin, B., A. Ehrlich, and Y. Nathan. 1974. “Lake Lisan, the Pleistocene precursor of the Dead Sea”. *Geological Survey of Israel Bulletin* 63: 30 pages.

Bender, F.K. 1974. “Geology of Jordan” (supplementary edition of volume 7). Gebrüder Borntraeger, ISBN: 3-443-11707-4, Berlin-Stuttgart, Germany.

Ben-Avraham, Z. and G. Schubert. 2006. “Deep ‘‘drop down’’ basin in the southern Dead Sea”. *Earth and Planetary Science Letters* 251: 254–263.

Berardino, P., G. Fornaro, R. Lanari, E. and Sansosti. 2002. “A new algorithm for surface deformation monitoring based on small baseline differential interferograms”. *IEEE Transactions on Geoscience and Remote Sensing* 40: 2375–2383.

Choi, S., H.-J. Gotze, U. Meyer, and DESIRE Group. 2011. “3-D density modelling of underground structures and spatial distribution of salt diapirism in the Dead Sea Basin”. *Geophysical Journal International* 184: 1131–1146.

Closson, D., N. Abou Karaki, H. Hansen, D. Derauw, C. Barbier, and A. Ozer. 2003. “Space-borne Radar interferometric mapping of precursory deformations of a dyke collapse - Dead Sea area, Jordan”. *International Journal of Remote Sensing* 24 (4): 843-849.

Closson, D., P.E. LaMoreaux, N. Abou Karaki, and H. al-Fugha. 2007. “Karst system developed in salt layers of the Lisan Peninsula, Dead Sea, Jordan”. *Environmental Geology* 52 (1): 155–172.

Closson, D., and N. Abou Karaki. 2009. “Human-induced geological hazards along the Dead Sea coast”. *Environmental Geology* 58: 371. doi:10.1007/s00254-008-1400-3.

Closson, D., N. Abou Karaki, and F. Hallot. 2010. “Landslides along the Jordanian Dead Sea coast triggered by the lake level lowering”. *Environmental Earth Sciences* 59 (7): 1417-1430.

Closson, D., N. Abou Karaki, N. Milisavljević, F. Hallot, and M. Acheroy. 2011. "Salt Tectonics of the Lisan Diapir Revealed by Synthetic Aperture Radar Images" in *Tectonics*, Dr. Damien Closson ed. InTech. doi:10.5772/13133.

Closson, D., and N. Abou Karaki. 2014. "Earthen Dike Leakage at the Dead Sea". In Engineering Geology for Society and Territory - Volume 5. G. Lollino, A. Manconi, F. Guzzetti, M. Culshaw, P. Bobrowsky, F. Luino (eds). Springer International Publishing, Switzerland, 461-464. doi: 10.1007/978-3-319-09048-1_92.

Closson, D., and N. Abou Karaki. 2014b. "Dikes Stability Monitoring Versus Sinkholes and Subsidence, Dead Sea Region, Jordan" in *Land Applications of Radar Remote Sensing*, Dr. Damien Closson ed. InTech. doi: 10.5772/57277.

Costantini, M. 1998. "A novel phase unwrapping method based on network programming". *IEEE Transactions on Geoscience and Remote Sensing* 36 (3): 813-821.

Dayan, U., and E. Morin. 2006. "Flash flood–producing rainstorms over the Dead Sea: A review". *Geological Society of America Special Paper* 401.

Frumkin, A., M. Ezersky, A. Al-Zoubi, E. Akkawi, and A.R. Abueladas. 2011. "The Dead Sea sinkhole hazard: Geophysical assessment of salt dissolution and collapse". *Geomorphology* 134: 102–117.

Garfunkel, Z., and Z. Ben-Avraham. 1996. "The structure of the Dead Sea basin". *Tectonophysics* 266: 155–176.

Goldstein R.M., and C.L. Werner. 1998. "Radar Interferogram Filtering for Geophysical Applications". *Geophysical Research Letters* 25 (21): 4035–4038.

Hofstetter, A., and C. Dorbath. 2014. "Teleseismic travel times residuals across the Dead Sea Basin". *Journal of Geophysical Research - Solid Earth* 119. doi: 10.1002/2014JB011357.

Klein, C. 1985. "Fluctuations of the level of the Dead Sea and climatic fluctuations in the country during historical times". In: International association of hydrological sciences, symposium, scientific basis for water resources management, Jerusalem, September 1985, Israel, 197–224.

Mechie, J., K. Abu-Ayyash, Z. Ben-Avraham, R. El-Kelani, I. Qabbani, M. Weber, and DESIRE Group. 2009. "Crustal structure of the southern Dead Sea basin derived from project DESIRE wide-angle seismic data". *Geophysical Journal International* 178: 457–478.

Meqbel, N., O. Ritter, and DESIRE Group. 2013. "A magnetotelluric transect across the Dead Sea basin: Electrical properties of geological and hydrological units of the upper crust". *Geophysical Journal International* 193: 1415–1431.

Nof, R.N., A. Ziv, M.P. Doin, G. Baer, Y. Fialko, S. Wdowinski, Y. Eyal, and Y. Bock. 2012. "Rising of the lowest place on Earth due to Dead Sea water-level drop: Evidence from SAR interferometry and GPS". *Journal of Geophysical Research* 117. doi: 10.1029/2011JB008961.

Nof, R.N., G. Baer G, A. Ziv, E. Raz, S. Atzori, and S. Salvi. 2013. "Sinkhole precursors along the Dead Sea Israel, revealed by SAR interferometry". *Geology* 41 (9): 1019-1022. doi:10.1130/G34505.1.

Picard, L. 1943. "Structure and evolution of Palestine with comparative notes on neighboring countries". *Bulletin of the Geological Department, Hebrew University* 4 (2–4): 1–187.

Salameh, E., and H. El-Naser. 2000. "Changes in the Dead Sea Level and their Impacts on the Surrounding Groundwater Bodies" *Acta Hydrochimica et Hydrobiologica* 28 (1): 24-33.

Shimoni, M., R.F. Hanssen, F. Van Der Meer, B.M. Kampes, E. Ben Dor. 2002. “Salt Diapir movements Using SAR interferometry in the Lisan Peninsula, Dead Sea Rift”. *Proceeding of Society of Photo-optical Instrumentation Engineers* 4543: 151–160.

Sneh, A. 1979. “Late Pleistocene fan-deltas along the Dead Sea Rift”. *Journal of Sedimentary Petrology* 49: 541–552.

Steinhorn, I., G. Assaf, J.R. Gat, A. Nishry, A. Nissenbaum, M. Stiller, M. Beyth, D. Neev, R. Garber, G. M. Friedman, and W. Weiss. 1979. "The Dead Sea: deepening of the mixolimnion signifies the overture to overturn of the water column". *Science* 206 (4414): 55-57.

Sunna, B.F. 1986. “The geology of salt deposits in the Lisan peninsula- Dead Sea”. Seminar on salt in the Arab World, Ministry of Energy and Mineral Resources, Natural Resources Authorities, May 4–6, Amman, Jordan.

Ten Brink, U., and C. Flores. 2012. “Geometry and subsidence history of the Dead Sea basin: A case for fluid-induced mid-crustal shear zone?”. *Journal of Geophysical Research* 117. doi:10.1029/2011JB008711.

Yechieli, Y., M. Abelson, and G. Baer. 2016. “Sinkhole formation and subsidence along the Dead Sea coast, Israel”. *Hydrogeol. J.* 24: 601–612. doi:10.1007/s10040-015-1338-y.

Zak, I. 1967. “The geology of Mount Sedom”. Ph.D. thesis, Hebrew University, Jerusalem, 208 pages (in Hebrew, English abstract).

CHAPTER 4

The contribution of local land subsidence to coastal flooding hazard along the U.S. Atlantic coast.

S. Fiaschi [1] and S. Wdowinski [2]

[1] Department of Geosciences, University of Padua, Padua, Italy.
[2] Department of Earth and Environment, Florida International University, Miami, USA.

Abstract

The Atlantic coast of U.S. is one of the most vulnerable areas to Sea Level Rise (SLR) due to its low elevation, large population, and economic importance. The effect of SLR has felt mostly in low-lying coastal communities, such as the City of Miami Beach and Norfolk, Virginia that are facing in the last years the occurrence of more frequent flooding as consequence of the increasing rates of the relative SLR. However, some of the increased flooding frequency might have caused by land subsidence affecting only some sections of the cities. In this short paper, Differential Synthetic Aperture Radar Interferometry (DInSAR) techniques are used to assess the contribution of localized land subsidence to the increasing flooding hazard in Miami Beach and Norfolk, Virginia. ERS-1/2 images are exploited using the Permanent Scatterers (PS) and the Small Baseline Subset (SBAS) techniques in order to retrieve the velocity maps of the two study areas, and detect which part of the cities are more affected by subsidence. Results yield localized subsidence at a rate of -2 - -3 mm/yr, mostly along the western section of the city of Miami Beach and up to -5 mm/yr is some areas of Norfolk. This study shows the importance in considering the local subsidence in the flooding hazard assessment and mitigation plans.

1. Introduction

Climate changes are causing the warming of the oceanic water and the melting of glaciers and ice-sheets that contribute to the rise of the water level at global scale. Sea Level Rise (SLR) increased dramatically since last century: the rates that were estimated to be about 1.2 mm/yr for the period 1901-1990, more than doubled during 1996-2010 reaching 3.1 mm/yr (Hay et al., 2015). One of the most evident effects of global SLR is the increase of the flooding hazard in many countries in the World, in particular in low-lying coastal areas such as the Atlantic regions of U.S (Figure 1a). The U.S. Atlantic coast is, in fact, one of the most vulnerable areas to SLR due to its low elevation, large population concentrations, and economic importance (Wdowinski et al., 2016). Here, around 2 million people are living on land below 1 m of the high tide threshold and are at high risk of flooding hazard (Strauss et al., 2012). Flooding hazard is particularly intense in areas characterized by local

accelerations of the relative SLR that can be produced by land subsidence: since sea level is measured by a local tide gauge relatively to a single location on the land surface, if the land is sinking the relative sea level rises faster than the global seal level. The cities of south Florida and of the mid-Atlantic regions are particularly vulnerable to relative SLR acceleration as they are experiencing an increasing occurrence of flooding events in the last years.

In south Florida, Miami and Miami Beach (Figure 1b) are among the economically most vulnerable city to SLR in the world (Melillo et al., 2014). A recent flooding hazard study of Miami Beach have shown that since 2006 the flooding frequency increased by 400% in respect to the previous decade (Figure 2) (Wdowinski et al., 2016). The study attributed the flooding frequency increase to a decadal-scale accelerating rates of SLR that occurred most likely due to the weakening of the Florida Current/Gulf Stream system. However, some of the increased flooding frequency might have caused due to local land subsidence occurring in sections of the city built over reclaimed swamps. Even the communities in the Chesapeake Bay area, such as Norfolk, Virginia, (Figure 1c) are facing increasing flooding events due to relative SLR accelerations. The sea level in the Chesapeake Bay area is monitored by the National Oceanic and Atmospheric Administration (NOAA) (Zervas, 2009) through 15 tide gauge stations that provide hourly measure of tide level. The Sewells Point gauge station, located at the Norfolk Naval Base (Figure 2b), is collecting data since 1928 showing relative SLR rates of approximately 5 mm/yr over the past decades (Boon et al., 2010; Atkinson et al., 2013). The consequence of these rates can be dramatic considering the low elevations and the flat topography of Norfolk and its surroundings. Local SLR in the Bay is enhanced by regional and local subsidence with rates ranging from about -1.3 mm/yr to -4.0 mm/yr (Boon et al., 2010).

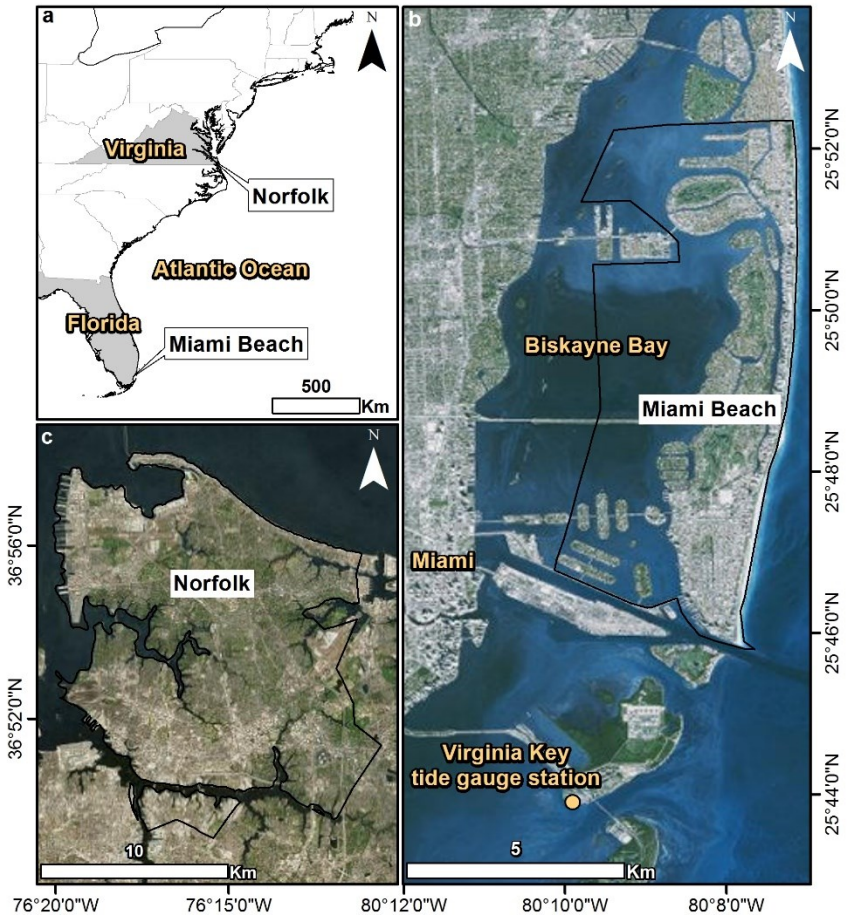

Figure 1. a) U.S. Atlantic coastline. b) Miami Beach area. c) Norfolk area.

The precise assessment of the flooding hazard in a particular area requires the knowledge of the factors that have influence on the flooding frequency, such as tide level, topography and land movement. Since data distribution and quality is usually not uniform across the territory, some areas may lack of one or more information. Moreover, the datasets used for the production of flooding hazard maps can be inaccurate and incomplete. In the case of Norfolk, despite the good amount of sea level data provided by the tidal gauge stations in the Chesapeake Bay area, the subsidence and its impacts on local SLR rates are still not well-documented (McFarlane, 2012). In the Miami Beach area, only one tide gauge station is available and is located at Virginia Key (Figure 1b), 5 km southwest of the city. No other data about local subsidence are available.

In both examples, the lack of monitoring instruments such as Continuous Global Positioning System (CGPS) stations limits the knowledge of land subsidence affecting those areas. Furthermore, with conventional ground based survey methods is difficult to achieve a high density of measured points over very large areas, limiting the possibility to detect localized subsidence. In this study, we assess the contribution of localized land subsidence to the increasing flooding occurrence in the cities of Miami Beach and Norfolk through Differential Interferometric Synthetic Aperture Radar (DInSAR) techniques.

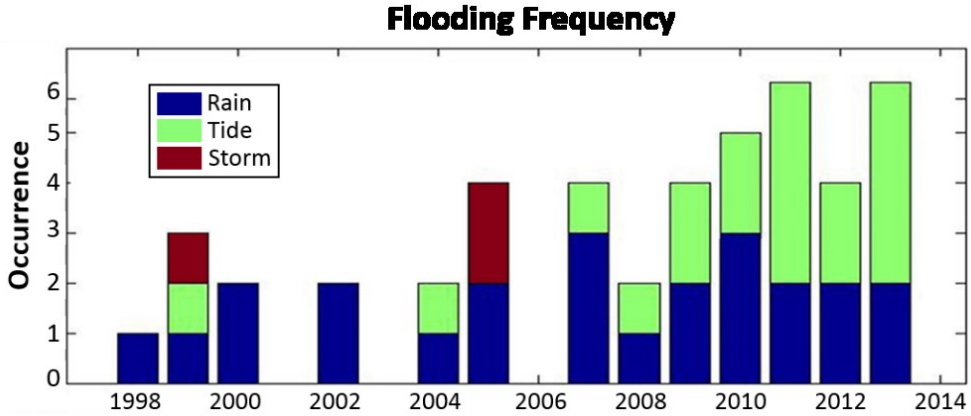

Figure 2. Flooding frequency in Miami Beach by type of cause. It is possible to notice a significant increase in tide flooding events since 2006.The reported events were collected from different sources: media reports, claims and city documentation. (after Wdowinski et al., 2016).

2. Study areas

2.1. Miami Beach

Miami Beach is a densely populated strip of land, around 10 km long and 2.5 km wide at its largest point, located between the Biscayne Bay and the Atlantic Ocean, few kilometres away from the South Florida coastline. It extends for 18.2 km^2, and, as of 2016, has a population of around 92,000 inhabitants. The construction of Miami Beach started in the 1870s with the drainage of mangrove swamps and the reclamation of new land over which the city growth and became one of the most important vacation locality in the U.S. Miami Beach is historically an area affected by flooding events related to heavy rain, storm surges and high tide. Since the last decade, the increasing frequency and magnitude of these events is cause of major discomfort to the population and damage

to the properties. Flooding events have affected mostly the neighbourhoods located in the western part of the city, that presumably were built over reclaimed land around 80-90 years ago. In 2014 the Municipality started a five-year project in order to protect the city from the flooding: with a total expense estimated in 600-700 million of dollars, the plan is to install up to 80 water pumps in the most critical areas and to raise roads and seawalls across the city.

2.2. Norfolk

The city of Norfolk, Virginia, is a densely populated area of around 250,000 inhabitants, located in the lower Chesapeake Bay, the largest estuary in the U.S. The geology of the area is mainly made of late Plesistocenic deposits of marine origin; Holocenic alluvium and beach deposits can be found along the northern coastline, while swamps and lagoons in the south (Scott et al., 2010 and references therein). The entire Chesapeake Bay area is affected by subsidence caused by two main factors: Glacial Isostatic Adjustment (GIA) and underground water extraction. A third contribution to the subsidence may also be given by the compaction of the fill sediments within the Chesapeake Bay Impact Crater (Powars and Bruce, 1999), but the rates at Norfolk are minimum (Egglestone and Pope, 2013) and can be neglected. GIA is the response of the Earth crust to the deglaciation of the Laurentide ice sheet started at the end of the last ice age, around 20,000 years ago. The postglacial rebound manifests as uplift in the areas around the Hudson Bay and as subsidence south of it (Sella et al 2007). In the Chesapeake Bay area, GIA is estimated to generate subsidence rates in the order of -0.6 - -1.8 mm/yr (Engelhart and Horton, 2012). The Subsidence caused by groundwater extraction activities acts more locally in respect to GIA. Localized water pumping contributes to the sediments compaction with rates estimated in -3.8 mm/r and -4.8 mm/yr in two cities close to Norfolk, and its effect extends in the Norfolk area with rates of -2.8 mm/yr (Egglestone and Pope, 2013; Ezer and Atkinson, 2016). Considering the total contribution of GIA and water extraction, the land subsidence in the Chesapeake Bay area causes more than half of the observed relative SLR (Egglestone and Pope, 2013). The Norfolk community is experiencing flooding events with increasing frequency and duration that is cause of growing concern for the authorities and the population. Lately, many local- and state-level initiatives were taken as a response to the increased flooding hazard in Virginia with particular attention to communities like Norfolk, bringing together researches, local authorities, professionals and the population to discuss about the increasing flooding risk and to develop mitigation and adaptation strategies (Ezer and Atkinson, 2016).

3. Methodology

Interferometric Synthetic Aperture Radar (InSAR) is a remote sensing technique that uses two or more SAR images to generate maps of surface deformation. A SAR image is generated when a microwave beam, emitted by an antenna mounted on a satellite, reaches a target on the Earth surface and bounces back to the receiver containing information of the amplitude and phase of the signal. InSAR uses the phase shift between two SAR images acquired over the same area at different times to generate an interferogram and calculate the movement of the targets on the Earth surface. The interferometric phase (φ_{int}) is given by different contributions:

$$\varphi_{int} = \varphi_f + \varphi_{topo} + \varphi_{displ} + \varphi_{atm} + \varphi_{err}$$

where, φ_{f} is a constant phase value generated by an ideally flat Earth, φ_{topo} is the phase given by the topography, usually removed using an external Digital Elevation Model (DEM), φ_{displ} is the phase of the ground deformation, φ_{atm} is the phase of the atmospheric effects, and φ_{err} is the non-linear phase considered as error given by the noise. When multiple SAR image acquisitions are made over long periods (months or years), using the DInSAR technique it is possible to measure and keep track over time of the surface displacements. DInSAR is nowadays widely used in a broad range of applications, in particular for the monitoring of the Earth surface and its processes such as landslides, land subsidence, volcanic activity, earthquakes, ice-sheets motion etc. A comprehensive review of the technique and its applications can be found in Ouchi (2013). In this study, we used two main DInSAR techniques: the Permanent Scatterers (PS) (Ferretti et al., 2001) and the Small Baseline Subset (SBAS) (Berardino et al., 2002). Both techniques use stacks of interferograms to generate displacement maps calculated along an inclined direction of observation, the Line of Sight (LOS). While PS relies on point targets with stable reflectivity over time and works well on urbanized areas only, the SBAS takes into account the distributed scatterers and works well even in open areas. One of the key point of DInSAR is the possibility to perform the time series analysis for each point measured on the ground.

4. Datasets and data processing

We analysed two sets of SAR images available from the European Space Agency (ESA) archives, both acquired in C-band (5.6 cm wavelength) by the ERS-1/2 satellites (Table 1). The first dataset, covering the Miami Beach area, consists of 23 scenes acquired from 1993 to 2005; the second, covering the city of Norfolk, is made of 27 scenes acquired from 1993 to 1998. The maximum ground resolution achievable through the ERS-1/2 images is 20 m x 20 m applying a multi-look of 1 - 5 in Range and Azimuth, respectively. The exploitation of the available datasets was carried out through the PS and SBAS techniques. In the case of Miami Beach, the PS technique provided the best results, since the sinking areas are only limited to localized features (i.e. buildings) along the coastline, and the application of SBAS resulted in a loss of sensitivity to the very small deformation values that characterize this area (~ -2 mm/yr). This effect can be explained considering that PS physically represents the motion of the dominant scatterer in the resolution element, while SBAS the average motion of the several scatterers in the resolution element (Shanker et al., 2011). On the other hand, in the Norfolk area, the SBAS gave the best results, with data coverage much higher than PS. For the PS processing, using a single master date (16 Jan 1997), 22 interferograms were generated (Figure 3a). Only the points with a spatial correlation values (coherence), from 0 (minimum) to 1 (maximum) higher than 0.75 were used. With the SBAS, we generated 133 interferograms (Figure 3b) using a temporal baseline of 1200 days and a spatial baseline of 60% (in respect to the critical baseline). In this case, the correlation threshold adopted was 0.35. To remove the topographic component of the phase, the Shuttle Radar Topography Mission (SRTM) DEM with a ground resolution of 30 m has been used. Since the deformations in both areas are the consequence of sediments compaction that can be assumed to be prevalently vertical, the measurements obtained with DInSAR were projected from the LOS to the vertical direction according to the incidence angle of each measured point on the

ground, around 23.3° for ERS-1/2. The results, reported as velocity maps, were classified in a Geographic Information System (GIS) using a colour scale from blue to red, in which positive values, in blue, are the points moving towards the satellite (i.e. uplift), while negative values, in red, the points moving far from the satellite (i.e. subsidence). The stable points, in green, are the ones with velocities in the range of ±1.5 mm/yr.

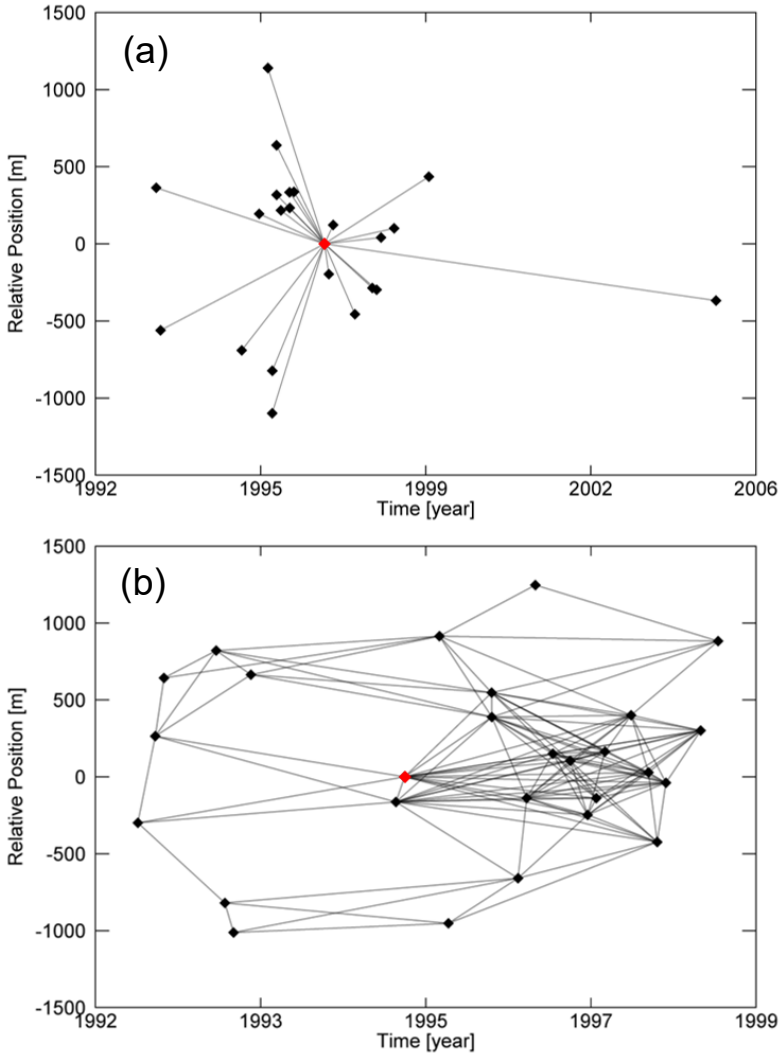

Figure 3. Connection network (black lines) between the available SAR scenes (black dots) obtained for a) Miami Beach with the PS technique and b) Norfolk with the SBAS technique. The red dot corresponds the image used as master.

Table 1. Available SAR datasets

Study Area	Period	N° of images	Revisit time	Orbit
Miami Beach	03/05/1993-01/09/2005	23	35 days	240d
Norfolk	19/06/1992-09/11/1998	27	35 days	192d

5. Results and discussion

5.1 Miami Beach

The results obtained from the PSI processing over the Miami Beach area, are reported as vertical velocity map in Figure 4a. The results, yield to localized subsidence with rates ranging from -1.6 mm/yr to -3.8 mm/yr in particular over the western coastal areas. The time series analysis of four selected points shows the linearity of the deformations in the monitored period (Figure 5). One of the most affected areas is located in the middle section of the city built over reclaimed swamps. In this area, the buildings were classified by their construction year, showing that most of them were built in the ‘20s and the ‘30s and from the ‘40s to the ‘50s, while only few are of more recent construction, from the ‘60s to 2015. The sinking of these buildings is mainly related to the compaction of the underneath sediments used to fill the swampy areas as consequence of the overload produced by the structures themselves. If we consider the age of the oldest houses in the area, around 80-90 years, the total rate of settlement can be calculated using a linear model of deformation: only the first years after the application of the load are, in fact, the most critical and are well represented by a hyperbolic consolidation model instead of a linear one (Tan et al., 1991; Chung et al., 2009; Kim et al., 2010). Considering the mean subsidence velocity in the area of -2.27 mm/yr, the total displacement estimated from the year of construction up to 2016 is around 18-20 cm. Because of this, taking into account the combined effect of SLR and subsidence, the houses that were originally built on higher ground at 1 m m.s.l., are now exposed to higher flooding hazard than the rest of the city. The comparison between the location of flood claims between 1998 and 2012 in the Miami Beach area (Figure 4b) and the 1993-2005 velocity map depicts the good correlation between the reported flooding events and the areas affected by subsidence detected by DInSAR. This suggests the possible contribution of localized subsidence to the increased flooding hazard in some areas of the city.

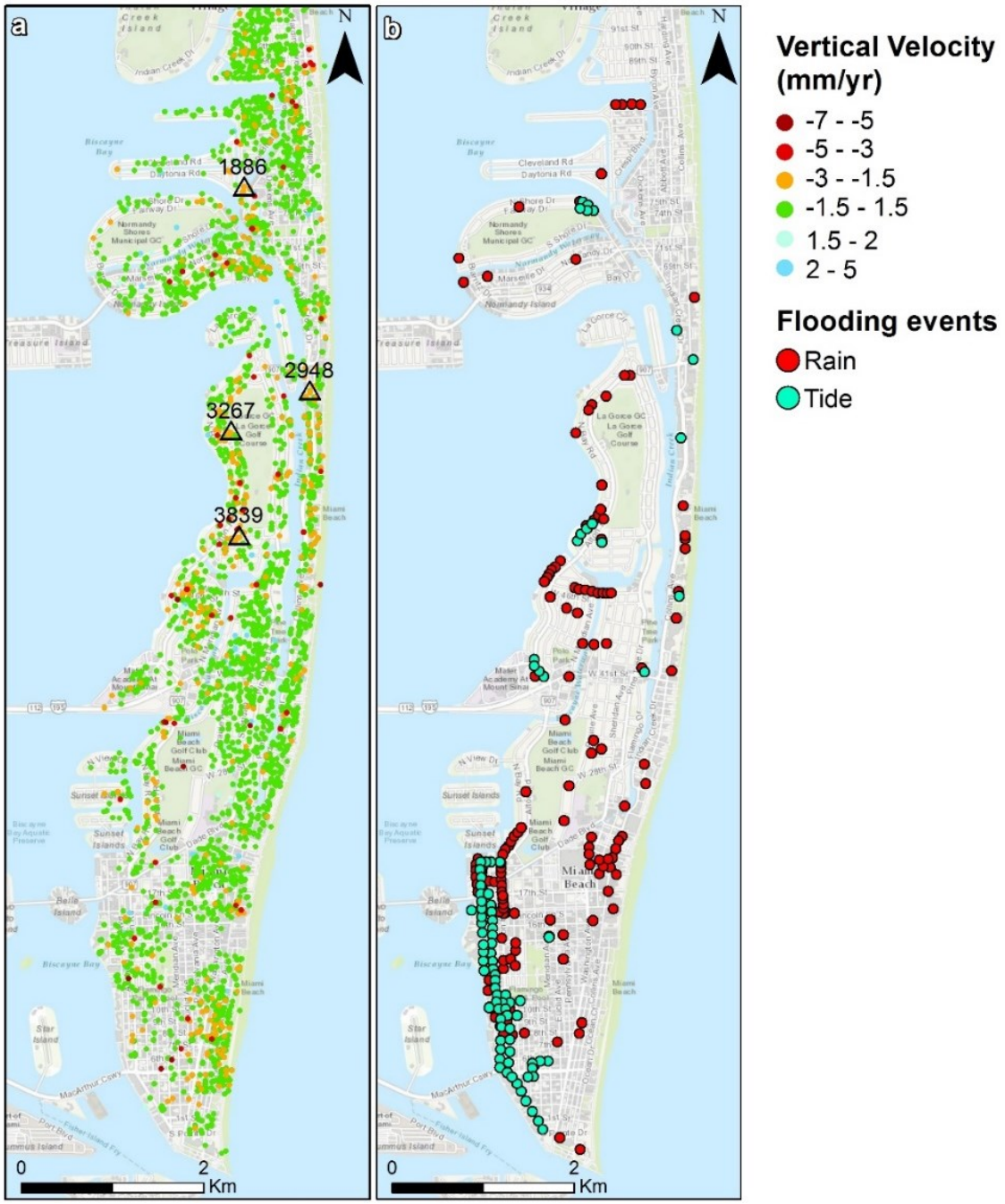

Figure 4: a) Vertical velocity map of the Miami Beach area obtained with the PS technique. b) Location of flood claims during the years 1998-2012 (after Wdowinski et al., 2016). For the selected points (triangles), the time series are shown in Figure 5.

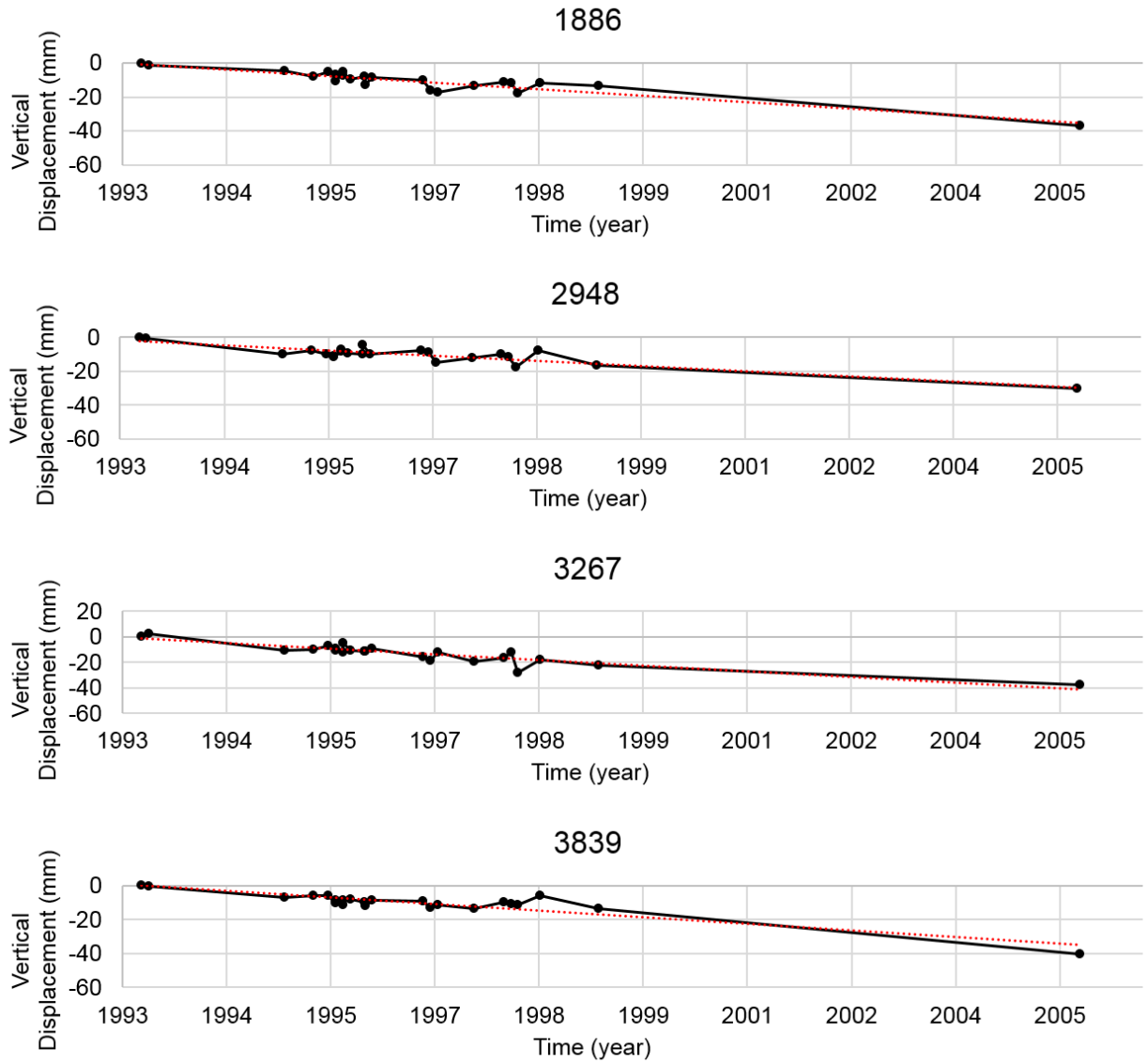

Figure 5. Vertical displacement time series of the points selected in four representative areas of Miami Beach affected by subsidence.

5.2) Norfolk

Considering that the entire Chesapeake Bay area is subject to subsidence, the results obtained from the SBAS processing over city of Norfolk are the expression of the differential movements of the measured points in respect to the sinking land surface. To obtain the real entity of the subsidence in the area, the contribution of the regional subsidence must be added to the DInSAR measurements. The results obtained from the SBAS analysis are reported as vertical velocity map in Figure 6: most of the city lies over a relatively stable territory; only few localized areas are affected by subsidence up to -5 mm/yr. In particular, 2,500 m in length of the Hampton Roads Beltway close to the Norfolk International Airport shows subsidence rates ranging from -2 mm/yr to -4 mm/yr (Figure 7a). This is one of the main designated hurricane evacuation route for people in vehicle to flee the Virginia Beach and Norfolk areas, as reported from the Virginia Department of Emergency Management. The presence of subsiding areas along the route may increase the flooding hazard in case of storm surges

making very difficult for the authorities to properly plan an evacuation. Localized subsidence occurs also in the surroundings of the bridges that cross the Wayne Creek (Figure 7b), north of the city. Here, the settlement rates ranges from -2 mm/yr to -4.8 mm/yr. Similar rates of subsidence affect the tip of the peninsula in the northern section of the city and the west flank of the man-made island where the entrance to the tunnel that connects Norfolk to Hampton is located (Figure 7c). Localized subsidence up to -4.3 mm/yr affects also the Lamberts Point coal terminal, while the subsidence is more evident in the near Naval Base of Portsmouth where the rates reach -4.8 mm/yr (Figure 7d). The displacement time series of the points selected for each area are reported in Figure 8.

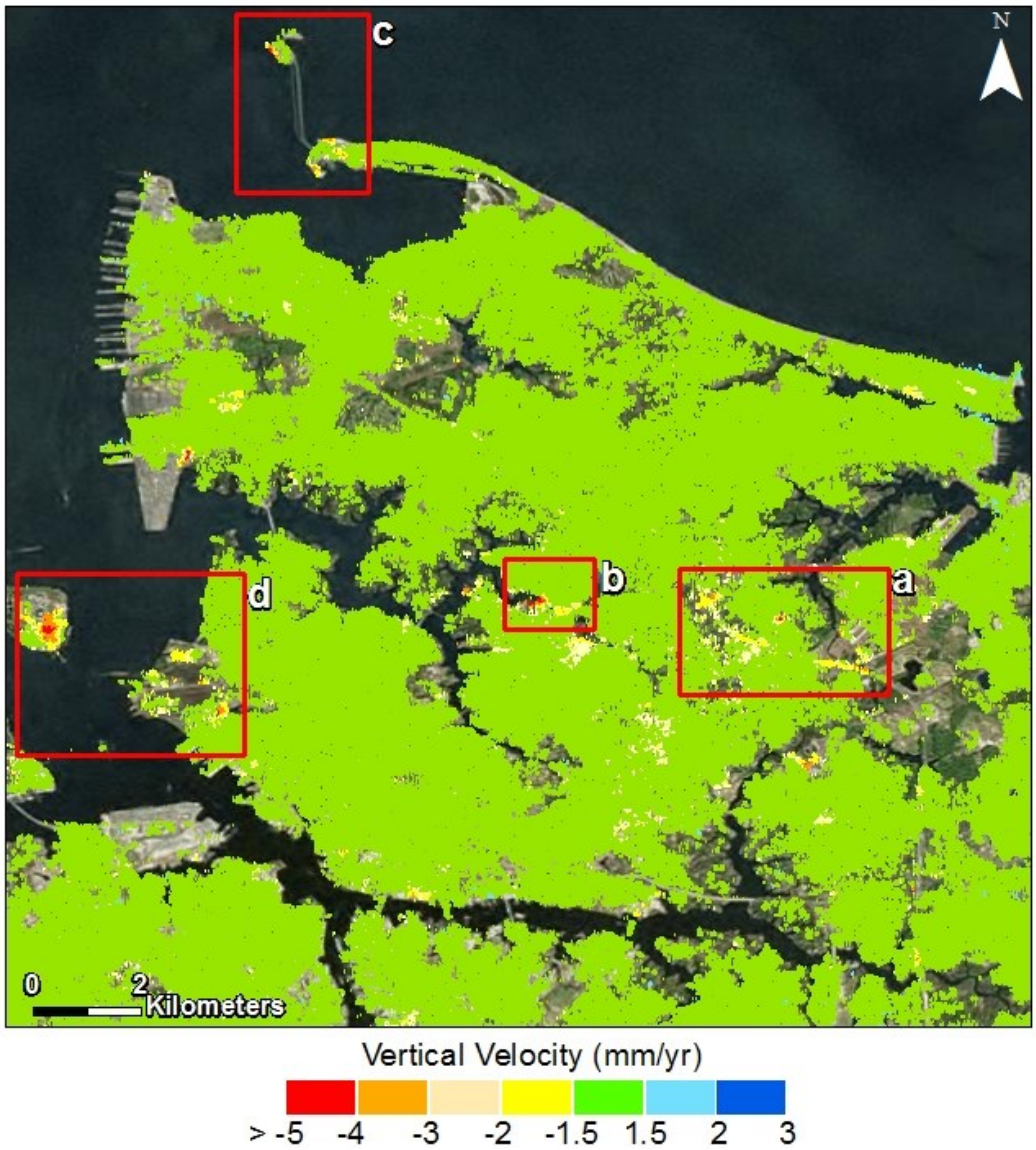

Figure 6: Vertical velocity map of the Norfolk area obtained with the SBAS technique. The red squares are the main areas affected by land subsidence reported in Figure 7.

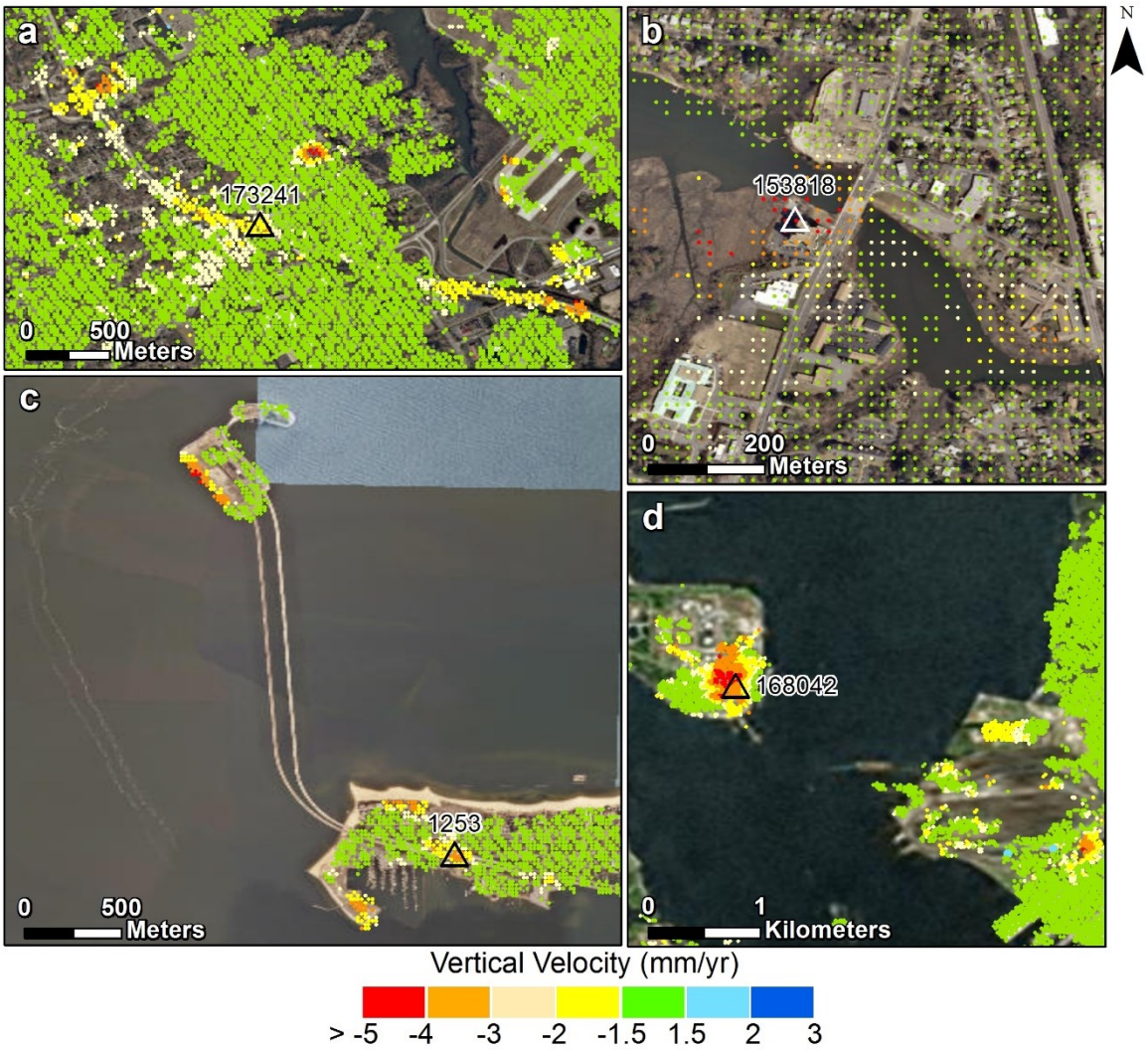

Figure 7. Localize subsidence in the city of Norfolk. a) Hampton Road Beltway. b) Bridge area at the Wayne Creek. c) Peninsula tip and tunnel island. d) Lamberts Point terminal (right) and Portsmouth naval base (left). For the selected points (triangles) the time series are shown in Figure 8.

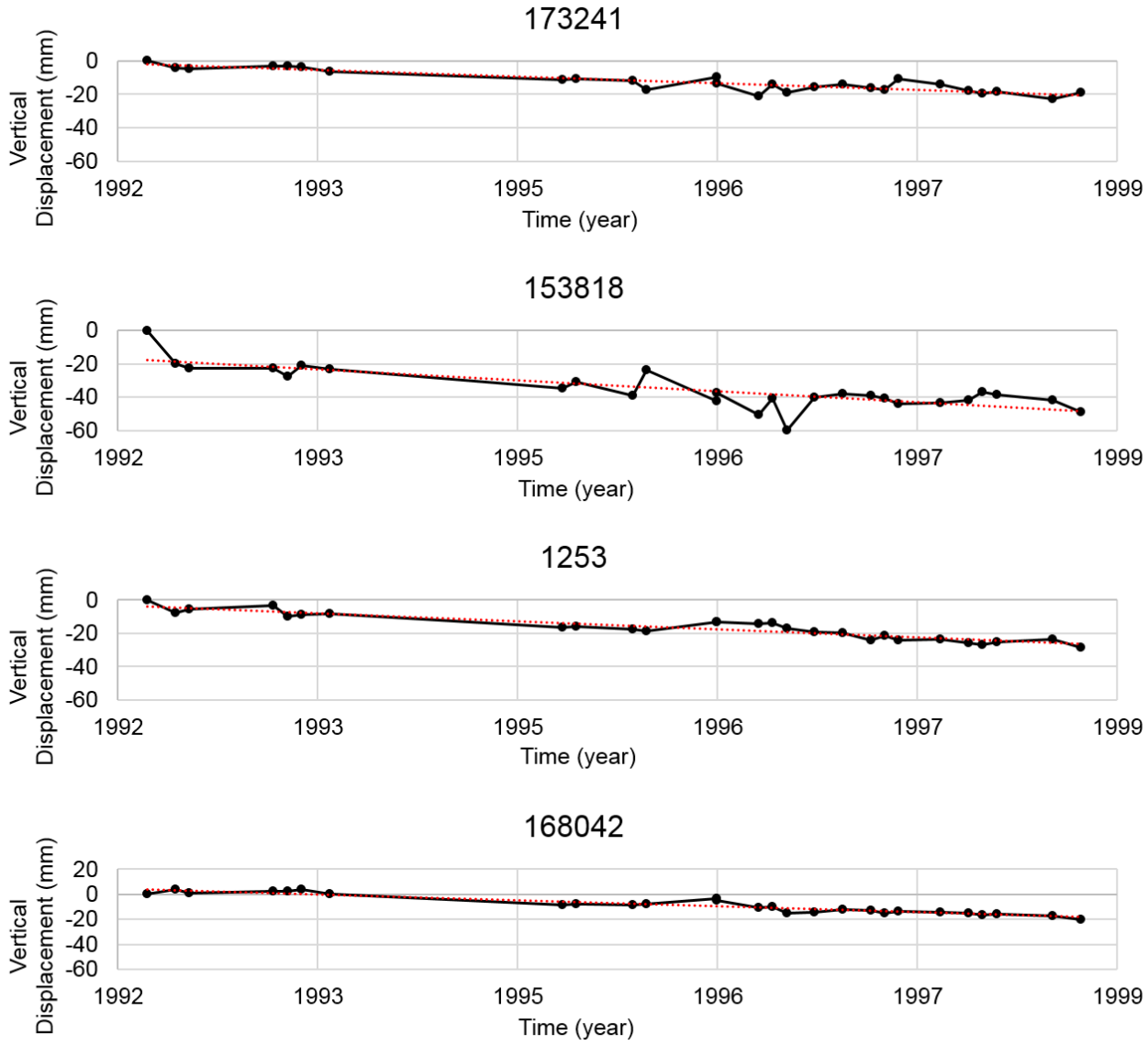

Figure 8. Vertical displacement time series of the points selected in the main areas of Norfolk affected by subsidence.

6. Conclusions

Global SLR is the main source of the increased flooding hazard along the low-lying coastal communities, such as the Atlantic regions of U.S. In these areas, flooding hazard can also be enhanced by relative SLR accelerations given by land subsidence. In this work, we assessed the contribution of land subsidence to the increased flooding hazard in two cities highly vulnerable to flooding: Miami Beach and Norfolk, Virginia. Two stacks of ERS-1/2 SAR images are processed using the PS and SBAS techniques. The results reported as velocity maps projected to the vertical direction, show that localized subsidence affected the city of Miami Beach in particular along the western coastal area, where the city was built over reclaimed land 80-90 years ago. The subsidence rates are in the range of -1.6 mm/yr - -3 mm/yr, from which it is possible to estimate through a linear consolidation model the total displacement since the city was built in around 18-20 cm. The results obtained over Norfolk, Virginia give measure of the movement relative to a reference point located outside the city limits

that is affected by the regional subsidence that occurs in the entire Chesapeake Bay area. For this reason, only the subsidence referred to that point can be calculated. The vertical velocity map shows that most of the city lies over a relatively stable territory: only few critical areas, such as part of the Hampton Road Beltway, are affected by subsidence up to -4 mm/yr. In this case, the presence of localized subsidence must be considered by the Authorities for the plan of the most suitable escape routes in case of hurricane or storm alert and for a proper management of the flooding risk in the area.

This study shows the importance of performing analyses addressed to calculate the localized subsidence that may affect residential areas and critical infrastructures such as highways and bridges; this is crucial in particular in areas highly vulnerable to flooding. The information provided by the application of DInSAR techniques for the monitoring of the territory, can be used to point out the areas more vulnerable to flooding and to produce more detailed flood hazard susceptibility maps. Continuous monitoring activities carried out with cost-effective technical solutions such as satellite interferometry, are necessary to be able to adopt more efficient mitigation measures to reduce the vulnerability of people and goods exposed to flood risk.

Future work will consist in the extension of the monitoring activity with the Sentinel-1A and 1B images once available over the U.S. This will allow us to determine the evolution over time of the subsidence trends and quantify the contribution of the subsidence on the actual flooding frequency in the studied areas.

References

Atkinson, L.P., T. Ezer, and E. Smith. 2013. "Sea level rise and flooding risk in Virginia". *Sea Grant Law and Policy Journal* 5 (2): 3-14.

Berardino, P., G. Fornaro, R. Lanari, and E. Sansosti. 2002. "A new algorithm for surface deformation monitoring based on small baseline differential interferograms". *IEEE Transactions on Geoscience and Remote Sensing* 40: 2375–2383.

Boon, J.D., J.M. Brubaker, D.R. Forrest. 2010. "Chesapeake Bay Land Subsidence and Sea Level Change". Virginia Institute of Marine Science Special Report No. 425 in *Applied Marine Science and Ocean Engineering*.

Chung, S.G., N.K. Lee, and S.R. Kim. 2009. "Hyperbolic Method for Prediction of Prefabricated Vertical Drains Performance". *Journal of Geotechnical and Geoenvironmental Engineering* 135 (10).

Eggleston, J. and J. Pope, 2013. "Land subsidence and relative sea-level rise in the southern Chesapeake Bay region". *U.S. Geological Survey Circular* 1392. 30 pp. doi: 10.3133/cir1392.

Engelhart, S.E. and B.P. Horton. 2012. "Holocene sea level database for the Atlantic Coast of the United States". *Quaternary Science Reviews* 54: 12–25.

Ezer, T. and L.P. Atkinson. 2016. "Sea Level Rise in Virginia – Causes, Effects and Response". *Virginia Journal of Science*.

Ferretti, A., Prati, C., and Rocca, F. 2001. "Permanent scatteres in SAR interferometry" IEEE *Transactions on Geoscience and Remote Sensing* 39 (1): 8–20.

Hay, C.C., E. Morrow, R.E. Kopp, J.X. Mitrovica. 2015. "Probabilistic reanalysis of twentieth-century sea-level rise". *Nature* 517 (7535): 481–484.

Kim, S.-W., S. Wdowinski, T.H. Dixon, F. Amelung, J.W. Kim, and J.-S. Won. 2010. “Measurements and predictions of subsidence induced by soil consolidation using persistent scatterer InSAR and a hyperbolic model”. *Geophysical Research Letters* 37. doi: 10.1029/2009GL041644.

McFarlane, B.J. 2012 “Climate change in Hampton Roads - Phase III - Sea level rise in Hampton Roads, Virginia”. Hampton Roads Planning District Commission report PEP12–06, July, 102 p. plus maps, accessed on September 22, 2016, at http://www.hrpdcva.gov/uploads/docs/HRPDC_ClimateChangeReport2012_Full_Reduced.pdf.

Melillo, J. M., T.C. Richmond, and G.W. Yohe, Eds. 2014. “Climate Change Impacts in the United States: The Third National Climate Assessment”. U.S. Global Change Research Program, 841 pp. doi: 10.7930/J0Z31WJ2.

Ouchi, K., 2013. “Recent Trend and Advance of Synthetic Aperture Radar with Selected Topics”. *Remote Sensing* 5: 716-807; doi: 10.3390/rs5020716.

Powars, D.S. and T.S. Bruce. 1999. “The effects of the Chesapeake Bay impact crater on the geological framework and correlation of hydrogeologic units of the lower York-James Peninsula, Virginia”. *U.S. Geological Survey Professional Paper* 1612. 82 pp.

Scott, T.W., D.J.P. Swift, G. R. Whittecar, G. A. Brook. 2010. “Glacioisostatic Influences on Virginia’s Late Pleistocene Coastal Plain Deposits”. *Geomorphology* 116 (1-2): 175-188.

Sella, G.F., S. Stein, T.H. Dixon, M. Craymer, T.S. James, S. Mazzotti, and R.K. Dokka. 2007. “Observation of glacial isostatic adjustment in “stable” North America with GPS”. *Geophysical Research Letters* 34. doi: 10.1029/2006GL027081.

Shanker, P., F. Casu, H. A. Zebker, and R. Lanari. 2011. “Comparison of Persistent Scatterers and Small Baseline Time-Series InSAR Results: A Case Study of the San Francisco Bay Area”. *IEEE Geosciences and Remote Sensing Letters* 8 (4).

Strauss, B.H., R. Ziemlinski, J.L. Weiss, J.T. Overpeck. 2012. “Tidally adjusted estimates of topographic vulnerability to sea level rise and flooding for the contiguous United States”. *Environmental Research Letters* 7.

Tan T.-S., T. Inoue, and S.-L. Lee. 1991. “Hyperbolic method for consolidation analysis”. *Journal of Geotechnical Engineering* 117 (11).

Wdowinski, S., Bray, R., Kirtman, B.P., and Wu, Z. 2016. “Increasing flooding hazard in coastal communities due to rising sea level: Case study of Miami Beach, Florida”. *Ocean & Coastal Management* 126. 1-8.

Zervas, C. 2009. “Sea level variations of the United States 1854-2006”. NOAA Technical Report NOS CO-OPS 053, 78pp, NOAA/National Ocean Service, Silver Spring, MD.

CONCLUSIONS

This Thesis has dealt with the use of satellite-based Differential Synthetic Aperture Radar Interferometry (DInSAR) techniques for the monitoring of the Earth surface in different locations. In particular, we focused on the detection and monitoring of geo-hazards such as landslides, subsidence and ground displacement caused by karstic activity. The motivation to carry out this work is to further improve the knowledge of the applicability of DInSAR techniques; to show which are the benefits of the exploitation and integration of SAR images acquired by different sensors; the importance of an appropriate post-processing management of the obtained results; to highlight the necessity to continuously monitor the territory in order to reduce the risk related to geological disasters. Moreover, part of the work is aimed to test the applicability of the Sentinel-1 satellite. In this Chapter the main findings of each case study are briefly summarized.

In Chapter 1, we used 25 years of SAR data to monitor the anthropogenic land subsidence affecting the city of Ravenna (NE Italy) and its coastline. The exploitation of four different SAR datasets with the SBAS techniques, allowed us to update the knowledge of the subsidence occurring in the study area and to assess its relationship with the main controlling factors. The time series analysis carried out on several control points showed that the deformation trends are almost linear in the industrial area of Ravenna and along the coastline, where the maximum values of subsidence registered were respectively of -280 mm and -250 mm during the 1992-2016 period. From the exploitation of the 200 available SAR scenes, we generated more than 500 thousands data points that we analysed though two statistical approaches in order to fully exploit their informative content. The analyses revealed that the main driving factor of the subsidence along the coastline could be the exploitation of the methane-gas fields, while there is no evident relationship with the water extraction activities. Land-use changes must also be taken into account to explain the high rates of subsidence caused by the sediments compaction under the loading of the new buildings that was detected in many locations of the study area. A second statistical approach, based on a new methodology called "ground-motion areas detection method" was used to precisely delineate the extension of the areas most affected by subsidence thanks to the automated analysis of the time series patterns. In this work, we demonstrated the benefits of a long term monitoring activity performed using DInSAR techniques thanks to which it is possible to reconstruct and analyse the trends of displacements occurring over wide areas starting from the 1992 with the ERS-1 satellite until today with the Sentinel-1 mission. Furthermore, we highlighted the importance of performing an adequate post processing management of the obtained results in a proper environment (e.g. GIS) to be able to extract information that otherwise might be lost.

In Chapter 2, we tested the capabilities of the Sentinel-1A satellite in a territory of the Italian Pre-Alps (NE Italy) affected by localized landslides. The study area is characterized by dense vegetation cover and the lack of large urban centres, which limits the number of high coherent scatterers. Furthermore, the typical landslides occurring in the area, mainly earth flows and roto-translational slides, are characterized by very slow movements, in the order of few millimetres per year, and generally interest localized non-urbanized areas making difficult their detection with DInSAR

techniques. To cope with these problems, we applied the PS technique that works at full resolution and is more suitable to measure subtle deformation over isolated targets. The C-band (5.6 cm wavelength) and the short revisit time (12 days) of Sentinel-1A allowed us to obtain a large number of PS (around 6000) and to detect several mass movements. In addition to the 64 already known landslides, other new areas affected by movements were detected. The use of Sentinel-1A images acquired by both ascending and descending geometries was necessary to enhance PS coverage and to obtain information about the components of plano-altimetric change. Despite the great benefits provided by the DInSAR monitoring activity, it can only serve to provide complementary information about the landslides activity, supporting the planning of the field works and directing the geological surveys that are needed to precisely assess the presence and extension of active landslides. The continuous monitoring activity performed with Sentinel-1 data can be successfully implemented in early-warning systems to recognise precursory signs of slope failure and reduce the potential risk related to landslides activity.

In Chapter 3, the Lisan Peninsula located in the Jordanian Dead Sea area was monitored through the SBAS technique. We exploited five different SAR datasets acquired with X, C, and L-band, in order to retrieve the measure of the displacements occurring in the area. The produced velocity and displacement maps revealed the complexity of the karst dynamics of the peninsula: the entire coastline is affected by very high rates of subsidence that every year exposes at increasing pace new portion of land. A maximum subsidence rate of -200 mm/yr was registered by ALOS-PALSAR in the Wadi Araba delta, while in the same area Sentinel-1A measured a maximum rate of -185 mm/yr. The Lisan Peninsula is also characterized by uplift in particular in its norther tip as consequence of the rising of the underlying salt diapir. Differential movements with peculiar semi-circular shapes that correspond to the margins of the diapir subdome were detected in the southern section. We produced the cumulated displacement map of the last 25 years, combining the information provided by the five analysed datasets. The sections drawn over the map showed that: the subsidence rates drastically increased after 2000 when the water decline rate reached -1 m/yr; the salt diapir raised constantly over the entire monitored period with rates in the order of 2 mm/yr - 2.4 mm/yr. The reliability of the obtained results was confirmed by the good correspondence between the tectonic features reported in literature and the location and extension of the detected displacements. We demonstrated that using and integrating SAR datasets acquired with different radar bands leads to obtain complementary results. We also showed that DInSAR can be applied for geological and geomorphological monitoring activity over areas characterized by bad environmental conditions.

In Chapter 4, we demonstrated that the use of DInSAR to monitor territories highly vulnerable to floods can be very useful to correctly assess the flood hazard and plan the more suitable mitigation strategies. We focused the attention on two cities along the Atlantic coastline of U.S., Miami Beach and Norfolk (Virginia) that are highly vulnerable to flood hazard as consequence of the combined effect of global sea level rise and land subsidence. Considering the technical limits of the PS and SBAS approaches in relation with the different density and distribution of the scatterers between the study areas, we used the PS to monitor Miami Beach, while SBAS was used for Norfolk. Unfortunately, only ERS-1/2 archive data were available for both areas, since no other datasets, including Sentinel-1, provided a number of scenes sufficient to perform multi-temporal analyses. Despite the limited amount of available data, we were able to detect localized subsidence in both localities. The measured subsidence rates ranges from -1.6 mm/yr to -3.8 mm/yr in Miami Beach and

from -2 mm/yr to -4.8 mm/yr in Norfolk. These results are quite interesting because they depict how the localized subsidence, even if occurring with low rates, may further expose portions of the territory to increased flooding hazard. Hence, the investigation of ground settlement using DInSAR is recommended to improve the flooding hazard assessment. These considerations can be extended to any coastal community where the risk related to flooding is high.

APPENDIX

Sustainable development and anthropogenic induced geomorphic hazards in subsiding areas

Najib Abou Karaki [1], Simone Fiaschi [2] and Damien Closson [3]

[1] Applied and Environmental Geology Department, Faculty of Science, The University of Jordan, Amman, Jordan.
[2] Department of Geosciences, University of Padua, Padua, Italy.
[3] Eurosense, Wemmel, Belgium.

Abstract

In many areas of the world, subsidence related to the lowering of the water table is modifying the landscape and provoking costly environmental hazards. We consider the Dead Sea (the Earth's lowest lake) as a model. Its water level was 395 m bMSL in the 1960s. Due to water diversions in the catchment area, as of 2016, the level has dropped to about 430 m bMSL. Here, as in other parts of the Anthropocene world, from China, to Iran, to Turkey, to Canada and the United States, consequences of human interventions are rapidly modifying the environment. Aggressive geomorphic processes leading to accelerated degradations are taking place and affecting landforms and infrastructures. In Tectonic terms, the lake is a pull-apart basin resulting from the motion of the Dead Sea Transform fault. Since the 1960s, a slice of brine of about 35 km^3 has been lost. The water table is dropping more rapidly in the lake than in the coastal zone creating an ever-increasing head difference. Consequently, groundwater moves towards the sea to compensate for the imbalance, provoking the reactivation of the area's paleo-channels with subsidence, sinkholes, and landslides. Since the 1980s, industrial-touristic infrastructure has covered newly emerging lands in geomorphic hazards-prone areas of the coastal zone.

Time series analysis of high to very high resolution visible/radar satellite images acquired from the 1970s to present, revealed major landscape evolution. Such dynamic systems prevailing in recent decades permitted the study of human/environment interactions to help minimize their effects.
Major deformations of an industrial dike were analysed and quantified. The results underline the necessity in the Anthropocene of careful analysis of relevant data sources acquired before and during subsidence, particularly in karst topography zones and prior to the development of major human activities in economically appealing environments around the world.

1. Introduction

Human social life takes place in buildings and with infrastructures created by engineers. Historically, beside houses, prestigious military and religious edifices such as the Petra monuments in Jordan (Ortloff, 2014), the Great Pyramid of Giza in Egypt (Barsoum et al., 2006) or the Aleppo Castle in Syria (Khirfan, 2016) have constituted major engineering structures. Other ancient infrastructures also include roads, bridges and dams: e.g. the Pont du Gard in France (Bossy et al., 2000), or the Zhaozhou Bridge in China – the oldest and largest stone arch bridge in the world – (Dajun, 1994). Their safety was guaranteed by a very long trial and error process and by conservative empirical measures. Likewise, nowadays, in Japan – the country most exposed to powerful geo-hazards – residents' feeling of safety in megacities is based on the fact that a given number of threats has been correctly anticipated and tackled by scientists who provided satisfactory designs against most common probable natural or induced hazards.

Past and present structures have been built in a particular paradigm. This paradigm assumes that the materials constituting these edifices and the materials on which their foundations rest have a critical mechanical resistance, above which they break. Designers do their best to ensure that the forces induced in these materials once assembled within these structures are low enough to avoid breakage. The difficulties of the exercise are significant and numerous (Delage, 2003). Beside gravity, it is difficult to predict other mechanical forces that will affect structures. They come from a variety of natural or induced hazards. Computer-age developments in statistical analysis provide tools for predicting the forces to be faced by the structures more precisely, but they need a sufficiently rich database gathered by rigorous observations across a significant period of time. Furthermore, buildings and their safety are constructed to be used for limited, specific periods of time – generally one or a few human generations – assuming that the parameters controlling the stability issue remain practically unchanged.

Delta Works, the series of construction works in the Netherlands designed to protect land around the Rhine– Meuse–Scheldt delta, are widely considered a major infrastructure in the timeline of human history. However, Dutch designers have recently faced a real anthropogenic problem since the project's completion (van Koningsveld et al., 2008). In 1997, the last storm surge barrier was inaugurated. It was the latest work of the 40-year-old mega-project. The same year, Douglas (1997) published the article 'Global Sea Rise: A Redetermination'. Dutch planners never imagined that after the completion of their major infrastructure, it would become necessary to rethink the whole project because of sea level rise on a global scale. When one of the fundamental parameters is not adequately evaluated, the whole edifice can collapse. Another example of this principle is evident in Jakarta, the capital city of Indonesia, where an important part of the urbanized area is sinking due to the over-exploitation of the groundwater resources (Abidin et al., 2015a, b). Floods and subsidence cause costly damage year after year. One of the proposed solutions consists of the setting up of sea walls, reclaimed land, and retention ponds in front of the city. What will be the height chosen for those dikes? A value computed from data recorded in the past or one based on a forecasting model(s) for the next century? How can sustainable infrastructures be better built in an unstable environment? Are there successful strategies for ensuring more successful major projects in the Anthropocene (Crutzen and Stoermer, 2000)? This paper addresses these questions based on a natural laboratory experiment:

the development and protection of major infrastructures along the Dead Sea coast, where the lake level is now dropping at the rate of 1.2 m/yr.

In Jordan, kilometric dikes, top hotels and resorts are threatened by subsidence around the Dead Sea. During the last two decades, monitoring of the Dead Sea area has allowed us to study the actions of primary stakeholders. Our working hypothesis is that the outcomes of this experiment will shed light on key geomorphic hazards elements to help create more sustainable major engineering projects in the Anthropocene.

The results we present in this paper concern the geo-hazards that are currently affecting the Arab Potash Company (APC) 'dike18' and salt evaporation pond 'SP-0A'. A 3 km deteriorating segment of the 12 km long industrial dike is the focus of our analysis (Figure 1: rectangle; Figure 2). Furthermore, our investigations highlight the limits of the classical geotechnical approach to secure major infrastructures in extreme environmental conditions which are prevailing in the Dead Sea area in general and in many other parts of the world as well.

We emphasize the role played by remote sensing techniques (visible and radar) in monitoring geomorphologic environmental degradation. We also show that clear identification, interpretation and field verification of geomorphic features is the key to preserving major assets at risk.

2. Key Parameters of the Dead Sea Natural Laboratory

2.1. Base level drop

The Dead Sea's water drainage area covers 41,650 km^2 (EXACT, 1998). It occupies the bottom of a pull-apart basin and its coastal zone represents the lowest emerged place on Earth at 429.90 m below the Mean Sea Level (bMSL) as of March 2016 (www.water.gov.il). In the early 1960s, the shoreline elevation was 395 m bMSL. In 1976-1979, the lake was about 1,000 km^2, compartmented in two sub-basins: northern and southern, linked by the Lynch Strait, and separated by the Lisan Peninsula (Figures 1 and 2). Since that time, the Dead Sea's surface has shrunk by a third, predominantly in the shallower southern part.

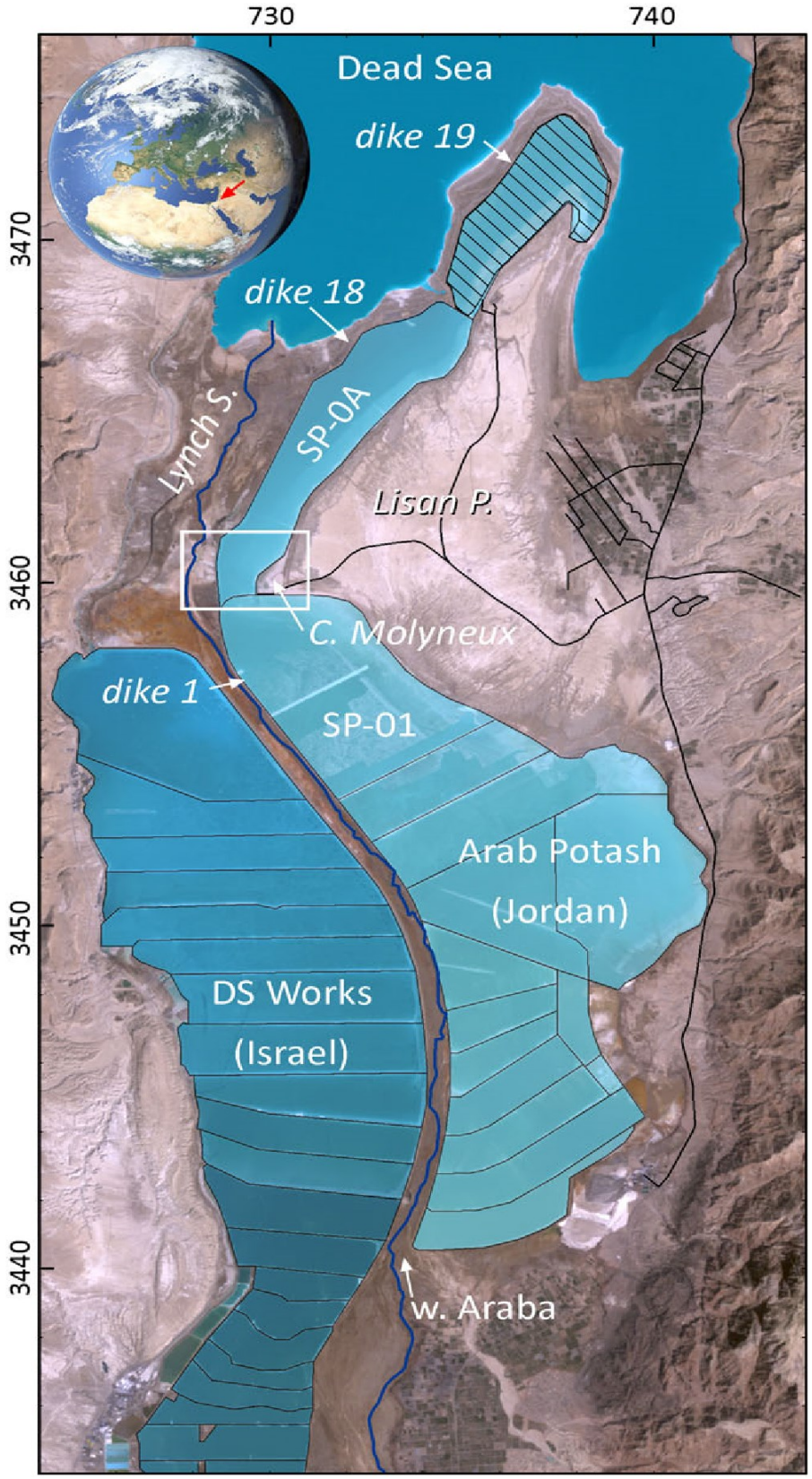

Figure 1. The Dead Sea is a hypersaline terminal lake located in the Middle East (inset). Its southern part is now exploited by Jordan and Israel. Mineral companies harvest salt on both sides of Wadi Araba (borderline). Their saltpans and dikes cover the southern lagoon. The hatched area corresponds to a saltpan destroyed on March 22, 2000 after the collapse of dike19 over 1650 m. The white rectangle around Cape Molyneux defines the area analysed in the results section.

2.2. Rapid geomorphologic developments

Concomitant to the drop in water level, secular environmental balances disappeared: the brine stratification vanished in 1978–1979 (Steinhorn et al., 1979); rivers' longitudinal profiles rejuvenated (Bowman et al., 2010; Storz-Peretz et al., 2010), bridges' basements were excavated and even collapsed; since the 1980s, subsidence, landslides (Figure 3) and thousands of sinkholes proliferated along the Dead Sea shore (Abou Karaki and Closson, 2012).

Figure 2. Cape Molyneux in 02-04-2007; view from the Western escarpment. The picture shows dike18' segment that was abandoned in February 2015 for safety reasons. A lens of fresh/brackish water is located below the Lisan peninsula. It is in equilibrium with Dead Sea water stocked in salt pans. The local base level is Wadi Araba. Water circulates below the ponds owing to a network of conduits located in the damaged zone of a fault mapped in the 1970s by Neev and Hall (1978). Resurgence underlines the connection between the Lisan and Wadi Araba.

2.3. Original young halo karsts system

There are several examples of major drying water bodies in the world other than the Dead Sea; the water level of Lake Urmia in Iran has been decreasing, provoking an increase in salinity, since 1995. This is also due to the diversion of rivers which used to discharge into the lake, there are now concerns that salt storms will affect the region all around (Hassanzadeh et al., 2011; Agha Kouchaka et al., 2015). In Asia, the Aral Sea began to decline rapidly in the 1990s after 30 years of gradual recession because Soviet authorities had diverted waters for agricultural purposes. The evaporation resulted in salt deposition. The leftover salt made the land unsuitable for agriculture. This salt can be carried by the wind causing salt storms that are ruining crops in the surrounding area and are causing diseases (Elpiner, 1999). There are concerns that the Dead Sea too will face harmful salt storms in the future (Abu-Qdais, 2008). However, by comparison with the Dead Sea ecological disaster, Aral Sea and Urmia Lake do not present sinkholes proliferation.

Figure 3. On August 11, 2012, a landslide destroyed the Holliday Inn front beach. A tractor was moved about two meters below the lake level. No one was present over the beach except the tractor driver. The day after, he records a video with his smartphone from which this capture was extracted.

Hence, the drastic water level lowering is not enough to explain numerous ground collapses. The fundamental differences are the karstic nature of the shore and the tectonic settings (Abou Karaki, 1987; Closson and Abou Karaki, 2009a).

In terms of sinkholes proliferation, the Dead Sea illustrates a karstic area affected by a sharp drop of the water table. Many karstic zones in the world feature similar issues. For example, in Tournaisis, the densely populated region of Belgium, dewatering operations in large quarries have lowered the piezometric heads and reactivated a paleo karst system covered by several decametres of Mesocenozoic deposits consisting of marls, sand and clay (Kaufmann and Quinif, 2002). Sinkholes destroyed buildings and threatened a high-speed railway, a motorway, and a waterway. In China, over the last 15 years, more than 10,000 sinkholes have appeared across the karst lands (Dereck Ford, 2011, personal communication). The water table decline is due to the over-pumping by industries. As an illustration, when new boreholes were sunk into limestone beneath an alluvial plain to supply the new town of Shuicheng, 1,200 sinkholes developed within less than 10 years (Waltham, 2009). These examples show that when the natural compensation mechanism becomes too slow with regard to the dynamics of the anthropogenic perturbation, the available energy of this unbalanced system is dissipated through mechanical and chemical erosions in the karstic drainage network. Progressively, the unstable conduits provoke geomorphic deformations and ground surface collapses.

2.4. Karstic nature of the Dead Sea shore

Lake Lisan, the Dead Sea′s ancestor, existed between 70,000 and 13,000 years B.P. (Haase-Schramm et al., 2004), and extended from 110km north of the present Dead Sea to 40 km to its south. During the Late Pleistocene, its water level was around 180 m bMSL (Abu Ghazleh, 2011). In southern Syria, the volcanic region of Jabal Arab-Druz erupted approximately 11,000-10,000 years ago. Salameh and Al Farajat (2007) observed that thick basalt flows reduced the catchments′ area from 157,000 km^2 to 41,650 km^2. They deduced that a new equilibrium state appeared in the hydrological budget of the lake. Its level stabilized around 400 m bMSL, creating the Dead Sea. Salty minerals soak coastal margins from 180 m bMSL downwards. The salinity of the surrounding groundwater increased with absolute prevalence of chloride (Salameh and Hammouri, 2008).

During the Holocene, the lake level fluctuated (Abu Ghazleh, 2011) creating favourable conditions for the development of a halo karsts system. The soluble rocks consist of alluvium and colluvium soaked with salt. In addition, from the 1990s onward, dozens of drilled boreholes revealed a salt layer, 6 m to 30 m thick, sandwiched between the Lisan (Pleistocene–Holocene) and Ze′elim (Holocene) Formations (Abelson et al., 2003; Yechieli et al., 2006). Radiocarbon dating gave an age range of 10,200-10,800 years, contemporary to the disappearance of Lake Lisan (Ezersky and Frumkin, 2013, and references therein).

During the Holocene, this salt layer was dissected by faults related to the tectonic setting. During the last 50years, such discontinuities have promoted underground drainage concentration and have helped to rebalance the perturbed hydrogeological system. Faulting allows greater subsurface water flow, and then mechanical and chemical erosions enlarge conduits over time, rapidly posing threats to infrastructures located above. Geophysical campaigns have shown that sinkhole clusters along the western coast are above the edge of the salt layer. Ezersky and Frumkin (2013) interpreted this co-occurrence as the position of a dissolution front moving progressively lake-wards. However, their conceptual model has to be put into perspective. From Corona pictures we found evidence of an active sinkholes zone from as early as May 1968 located next to the shore of the former southern lagoon (Figure 4: insets A-D). Even if this zone is found above the edge of the salt layer, its dynamics cannot be explained by a moving dissolution front since that part of the lake dried-up later in the 1970s, then was filled again artificially. Over the 1968 picture (Figure 4: inset B) the collapses′ dispersion suggests two parallel lineaments oriented SW–NE. The site of these sinkholes attests to the fact that (whatever the conditions) the Dead Sea shores are prone to dissolution and reactive to variations in the hydrogeological setting. This is a crucial point to keep in mind when dealing with problems related to the base level fluctuations there (drop or rise).

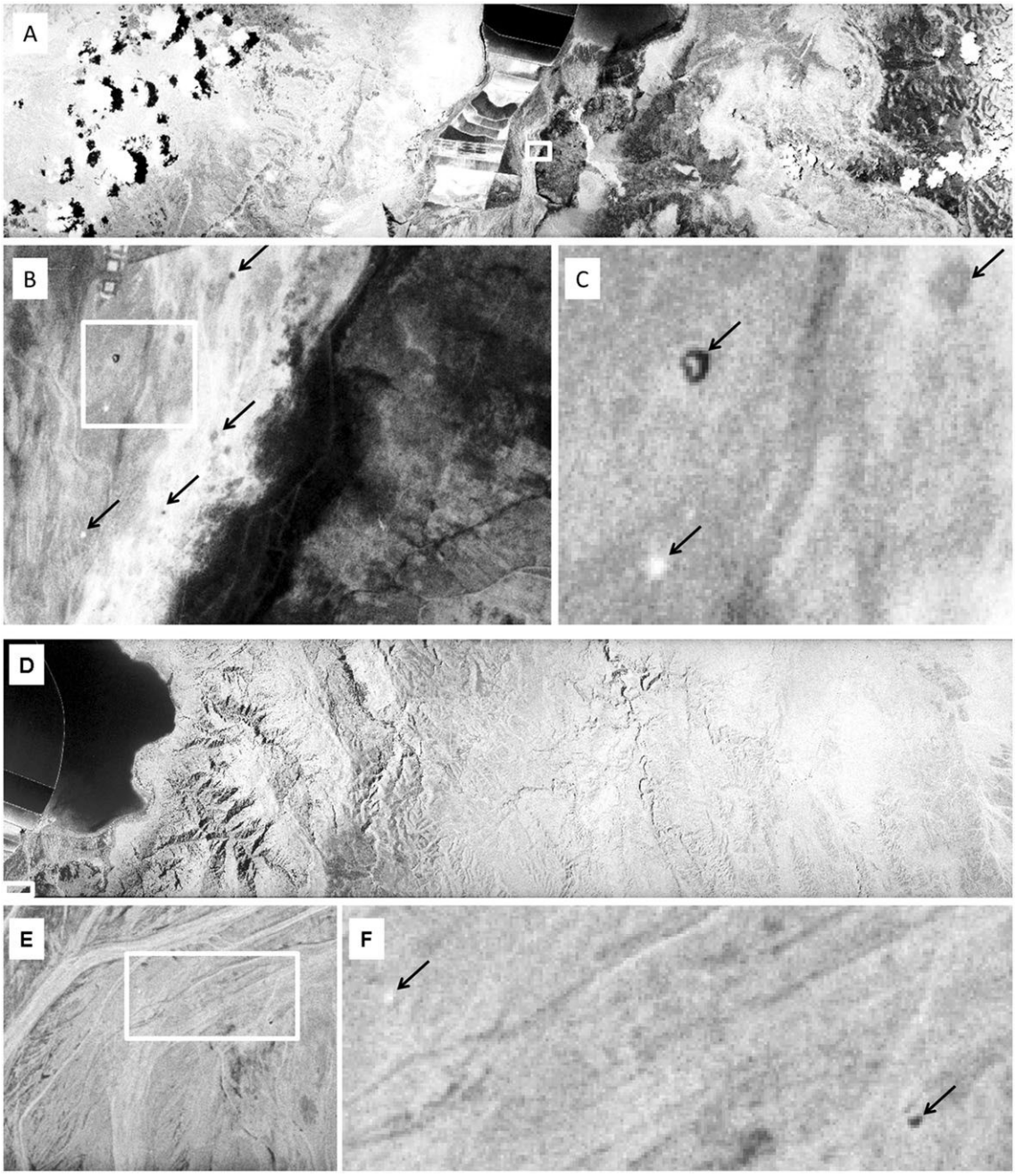

Figure 4. Corona pictures acquired in 1968–05-30 (A-B-C; ref: DS1103-2203DA178_b) and 1969–07-30 (D-E-F; ref: DS1107-1106DA011). A&D: Context, Dead Sea southern area; B&E: Zoom over the sinkholes' area; C&F: Individual sinkholes. This zone is still active in 2016.

2.5. Anthropogenic actions

The difference of 35 m between the Dead Sea level in the 1960s and the 2010s is due to two factors: water diversions upstream that are responsible for about 66% of the drop in water, and siphoning of the brine by mineral companies, which represent 33% (Tahal Group and GSI, 2010). In the early 1960s, with great geotechnical difficulties, the Israeli Dead Sea Works (DSW) developed a salt evaporation pond system over the western part of the 402 m bMSL southern basin (Closson and Abou Karaki, 2014a). Fifteen years later, APC finalized a similar infrastructure on the eastern Jordanian side (Figure 1: dike1 and saltpan "SP-01"). The profits of DSW and APC are proportional

to their ability to meet the market demand. The fertilizers trade has grown consistently during the last few decades in parallel with economic developments in China, India, and Brazil. DSW and APC capacities for production are linked to the size of their evaporation ponds. The two companies therefore aim to occupy emerging flat zones, left dry by the receding Dead Sea. They thus consider the continuous shrinking of the lake as providing them new opportunities: in practical terms, the emergence of new empty spaces means they can create new production units. This iterative process started in the 1960s but stopped on 22 March 2000 (Closson et al., 2003) when the 12 km earthen dike19 collapsed and 55 million m^3 of brine went back to the Dead Sea (Figure 1: hatched area).

3. Material and Method

Dike18 slow destruction phenomenon was investigated as follows:

3.1. Photographic / satellites / maps data collection

Aerial photographs of the Lisan peninsula and the Lynch Strait at the scale of 1:25,000 (Figures 1 and 2) are available from the 1950s, prior to the process that initiated the lowering of the Dead Sea level (Closson, Lamoreaux, et al., 2007). From 1962 to 1973, Corona pictures were used (Figure 4). Digital versions of the pictures were created by scanning a 30 times enlarged photograph at 300 pixels/inch (image and description courtesy of USGS). The 'pixel' size ranged from decametres to a few metres in the best cases. From 1973 to present, Landsat scenes pixel resolution improved (60m, then 30 m, and finally 15 m) and the number of images and spectral richness increased, allowing the mapping of soil moisture on newly emerged lands in this pure mineral environment (Closson and Abou Karaki, 2014b). Panchromatic SPOT-1 images were also used. Owing to their 10m resolution, they have provided crucial information on the karstic development in 1986 and 1992.

From 1992 onwards, C-band radar images of ERS-1/2 and ENVISAT satellites have been used to map the ground deformation fields at centimetre to millimetre scales with differential interferometry techniques (Closson et al., 2003). From 2007, L-band ALOS-PALSAR data were processed (Closson et al., 2010a) as well as the very high resolution radar images of COSMO-SkyMed in X-band (2011–2013). The latest complemented the information acquired in the visible window at nearly the same resolution or better (Closson and Abou Karaki, 2014b). In 2014, Sentinel-1A radar data have provided new inputs in the line of the previous ones (Closson et al., 2015).

In the 2000s, very high resolution optical infrared images were available allowing detailed monitoring of the landscape evolution. Those images supported several field campaigns (Closson et al., 2010b).

3.2. Images processing, geocoding, diachronic analysis in a common geographic framework

Information from radar images was elaborated using interferometric processing techniques. From 2000 to 2003, the software used was an in-house development carried out at the Space Centre of Liege, Belgium (Closson et al., 2003). From 2007 onwards, COS software were used such as the Radar Mapping Suite™ (Erdas Imagine) of and SARscape® (Sarmap). In 2015, SARPROZ™ was used

to process Sentinel-1A data (Closson et al., 2015). The SBAS service on G-POD (Casu et al., 2014) was successfully applied over the whole Dead Sea from a dataset of ENVISAT images (2003−2010). The results confirmed the processing carried out with SARscape®. Two techniques were applied: DInSAR combining 2, 3, and 4 images, and time series processing: PS and SBAS (Ferretti et al., 2001; Berardino et al., 2002). Table 1 summarizes and compares the two main techniques used.

Regarding the optical images (aerials and satellites), the most conspicuous work concerned the geo-referencing of the various files with great precision and accuracy, in order to compare them in a standard geographic space. The main difficulty was to position the images based on ground control points that have remained unchanged for more than 50 years. Additionally, as the area is uninhabited, only natural features could be considered. East of the Lynch strait, the bushes that grow along wadis were used, while to the west, the vegetation in sinkholes provided the necessary points (Closson et al., 2007). The bushes are present in all images because they are highly resistant to flash floods and extreme climatic and edaphic conditions. They appear clearly because of the contrast between the dark colours of their leaves over the white background surface. As they are numerous, they can be interconnected by straight lines and thus provide a stable geodetic triangulation-like network. These bushes allowed the positioning of dozens of ground control points several kilometres around the area of interest. ArcGIS software was used to for geometric corrections using spline functions.

Table 1. Interferometric techniques used to map the deformation fields.

	Differential InSAR	Time Series processing PS/SBAS
Requirements	A minimum of 2 images are necessary but 3 to 4 images can be combined if no external digital elevation model is available.	Generally, a minimum number of 20 images for PS and 8 images for SBAS are necessary.
Qualitative assessment	Relevant for a surveillance/probing system.	Very good for modelling and forecasting.
Quantitative assessment	The ground movement is indicated in fringes of colours, each fringe represents a change ranging from 1cm to 5cm (depending the frequency used X, C, and L).- Vertical movements of about 2cm to 3cm can be detected.	The ground movement is indicated in colour coded pixels.- Interpretation is more reliable as atmospheric effects can be minimized. The average vertical movement is about 1.5mm/yr.

Ground control points also exist in the saltpans owing to salt pillars growing from bottom to surface. These pillars are visible due to their appearance as white spots in dark water. Their small size allows for location with pixel precision. Further, they proved to be important markers in the analysis of underground water circulation. In several places inside saltpan ‘SP-0A’ (Figure 1), they lay next to sinkholes. Quality control was performed using GPS tracks recorded during field surveys.

Once properly geocoded, the images have been processed to find sinkholes, subsidence, landslides or other anomalies, such as soil moisture related to dike seepage. In this pure mineral environment, the area of interest presented two extreme cases: water (100% moisture) and Lisan peninsula surface (0% moisture). The digital numbers acquired over the dried-up Lynch Strait were classified in various categories based on these two extreme classes (Closson and Abou Karaki,

2014b). This allowed an efficient way to detect seepage at the surface of the Lynch Strait, especially from infrared channels.

3.3. Vectorization of the pertinent elements

Using analysis of photographic/satellites/maps, we aimed to understand how the landscape has evolved from one precise moment to another and to reconstruct that evolution. Also, one goal among others was to position the shoreline (base level) accurately. We focused on the phenomena of subsidence, collapses and tectonic settings. Seven field campaigns have been performed in the 2000s. Thousands of pictures have been taken and hundreds of them were also geo-located (Closson et al., 2007). Special care was directed to spots showing surface collapses proliferation in the study area. All elements (points, lines, and polygons, i.e. 'shapefiles') significant for the understanding of salt karst evolution were vectorised in view to produce maps.

4. Results

To quantify significant deformations of dike18, the monitoring of the ground instabilities occurring along the dike was carried out exploiting four different SAR datasets with the SBAS technique through the SARscape® software. The SAR datasets consist of: 10 C-band ERS-1/2 images covering the period 10/1997–12/2000; 10L-band ALOS-PALSAR, period 11/2007–02/2011; 20 X-band COSMO-SkyMed, period 12/2011–05/2013; 32 C-band Sentinel-1A, period 10/2014– 05/2016. The ALOS-PALSAR images were acquired in ascending geometry, while all the other datasets were collected in descending geometry. Among the available datasets, the proper sets have been chosen dropping the images acquired during the periods of building and major repair leading to strong coherence decrease. In particular, we dropped the ERS-1/2 images from 06/1992 to 02/1997 corresponding to dike 18 building period, and all the ERS-2 images after 12/2000 that were unusable because of satellite gyro system failure.

The processing chain of each dataset requires the selection of an adequate set of parameters to optimize the results. Considering the high phase decorrelation occurring in the areas over dike18 and the characteristics of each sensor, the computation have been performed only for the points with coherence, in a range from 0 (minimum) to 1 (maximum), greater or equal to: 0.35 for ERS-1/2; 0.35 for ALOS-PALSAR; 0.30 for COSMO-SkyMed; and 0.50 for Sentinel-1A. The vertical displacements and velocity maps obtained were used to extract the deformation along the 12-km-long dike18. The dike was divided into segments 500 m long, and the average value of all the pixels falling in a buffer of 40 m of each segment was calculated. The results are reported in Tables 2 and 3, where negative values, in red, represent subsidence while positive values, in blue, represent uplift. The sections with velocity in the range ±1.5 mm/yr are considered stable and coloured in green.

The sections in the table with missing data may correspond to areas with phase decorrelation due to either (1) constant dike repair work or (2) very high ground deformations not detectable by the sensor or (3) drastic change in the dielectric parameters of the ground due to brine seepage from the pond towards the base level (Wadi Araba).

The deformation rates of ERS-1/2 are much lower in comparison with the other datasets, probably because the movements are too fast to be detected by the sensor. In fact, the ERS-1/2 works in C-

band (5.6 cm wavelength) and its revisit time is 35 days. This can bring a complete loss of coherence in the areas with very fast movement or a partial registration of the displacement information. In comparison, even if COSMO-SkyMed and Sentinel-1A work with X-band (3.1 cm) and C-band (5.6 cm), they have shorter revisit time of 16 days and 12 days respectively, making them suitable to register higher displacements. Despite the very long acquisition interval (45 days), ALOS-PALSAR sensor uses a 23 cm L-band that can detect movements four times faster with respect to the C-band.

The results show three major areas affected by uplift during 1997–2000: from 0+000 to 5+500, from 8+000 to 10+000 and from 11+000 to 12+000. Segments from 6+000 to 8+000 and from 10+000 to 11+000 were affected by subsidence. In the period 2007–2016, most parts of the dike registered moderate to high subsidence. Very strong subsidence up to 207 mm/yr was detected from segments 6+000 to 8+500. These segments, in fact, are located in the areas most affected by vertical movements, as described in previous studies (Closson and Abou Karaki, 2014b). Moderate uplift was registered by COSMO-SkyMed (2011–2013) from 2+500 to 5+000. In the four monitored periods, the displacement rates are generally decreasing from the central part of the dike to its periphery, with the lowest values detected in the last segment, from 11+500 to 12+000.

Table 2. Cumulated vertical displacement and velocity on dike18 for the period 1997–2011. Chainage 0+000 (the zero reference point) along dike18 is located at the intersection between dike1 and dike18 (see Figure 7 and 8).

Dike 18 – Cumulated vertical displacement and velocity

Satellite		ERS-1/2		ALOS-PALSAR	
Period		10/1997-12/2000		11/2007-02/2011	
Chainage (m)		Displacement (mm)	Velocity (mm/yr)	Displacement (mm)	Velocity (mm/yr)
0+000	0+500	4.3	1.8	-84.9	-27.4
0+500	1+000	5.9	2.2	-53.1	-17
1+000	1+500	-	-	-	-
1+500	2+000	12.3	4.2	-182.1	-55.1
2+000	2+500	2.9	1.2	5	6.4
2+500	3+000	19.6	5.9	-28.3	-7.2
3+000	3+500	14	4	-98.7	-25.3
3+500	4+000	8.7	4	-84	-20.1
4+000	4+500	9.7	5.3	-51.1	-14.2
4+500	5+000	3.9	3.3	-2.3	0.03
5+000	5+500	19.2	6.4	-73.8	-16.1
5+500	6+000	-0.4	0.6	-150.2	-33.7
6+000	6+500	-12.1	-3.3	-266.2	-75.8
6+500	7+000	-26	-9.9	-420.9	-123.8
7+000	7+500	-15.6	-5.1	-639.5	-188.3
7+500	8+000	-7.3	-2.2	-503	-153
8+000	8+500	15	7.5	-431	-133.9
8+500	9+000	-	-	-128.2	-35.3
9+000	9+500	13.5	3.6	-23.7	-6.8
9+500	10+000	3.7	2.4	-8.4	0.9
10+000	10+500	-14	-5.2	-18	0.7

Legend
Subsidence
Uplift
Stable

10+500	11+000	-28.7	-7	-30.2	-8.6
11+000	11+500	44.8	14.6	-119.6	-34.2
11+500	12+000	10.6	3.5	-17.5	-7.8

Table 3. Cumulated vertical displacement and velocity on dike18 for the period 2011–2016. Chainage 0+000 (the zero reference point) along dike18 is located at the intersection between dike1 and dike18 (see Figure 7 and 8).

Satellite		**COSMO-SkyMed**		**Sentinel-1A**	
Period		**12/2011-05/2013**		**10/2014-05/2016**	
Chainage (m)		Displacement (mm)	Velocity (mm/yr)	Displacement (mm)	Velocity (mm/yr)
0+000	0+500	-33	-26.1	-66	-54.9
0+500	1+000	-9	-9.2	-119.1	-83.7
1+000	1+500	-17.6	-15.4	-110.5	-70.6
1+500	2+000	-69	-49.4	-107.6	-69.4
2+000	2+500	-29.5	-21.5	-69.3	-42.6
2+500	3+000	4.5	4.6	-45.6	-26.2
3+000	3+500	9.3	7.6	-42	-22.5
3+500	4+000	7.8	7.7	-52.5	-31.2
4+000	4+500	0.6	1.7	-52	-29.8
4+500	5+000	3.3	2.9	-36.8	-17.6
5+000	5+500	-58.4	-43.8	-115.1	-64
5+500	6+000	-97	-73.5	-179.5	-99.4
6+000	6+500	-97.7	-72.7	-245.5	-149.5
6+500	7+000	-131.7	-96.5	-267.2	-167
7+000	7+500	-211.8	-152.8	-346	-207.4
7+500	8+000	-178	-129.9	-195.2	-117.2
8+000	8+500	-164.7	-125.5	-165	-96.8
8+500	9+000	-113.2	-86.4	-115.7	-63.9
9+000	9+500	-66.1	-51.1	-112.9	-61.2
9+500	10+000	-41.9	-35.2	-108.2	-63.8
10+000	10+500	-35.7	-30.3	-79.1	-47.6
10+500	11+000	-5.6	-5.2	-40.7	-21.6
11+000	11+500	-3.3	-3.5	-42.2	-20
11+500	12+000	12.8	8	-10.4	-6.1

Legend
Subsidence
Uplift
Stable

The overall results concerning dike18 allow characterizing the development of a halo karst system below the southern part of saltpan SP-0A in five major phases:

4.1. 1953–1979: drying up of the Lynch strait and early stage of a fault induced karst system development in the southern part

The main landscape geomorphic elements around Cape Molyneux before the drying up of the Lynch Strait and the Southern lagoon are summarized in Figure 5. This was the case prior to APC

dike system completion (1979–1982). The shoreline position is derived from 1:25,000 aerial photographs taken in September 1953. At that time, the lake level was 393 m bMSL.

During the past millennia, a mature karst network developed in the sub-horizontal salty marl layers of the Lisan Formation over the peninsula. The latest has been divided into two members (Lower and Upper) according to diatomite zone (Begin et al., 1974). The lower laminated member is composed mainly of very fine varved laminae. The upper white cliff member (Abed, 1985), has higher detrital sediments than the laminated member and contains some centimetres-thick beds of gypsum and aragonite in the southern part. The lithological boundary represented in Figure 5 was mapped by Bartov et al. (2006). The Lisan is a plain (Figure 2) with isolated hills, punctuated by SE–NW elongated depressions. The latest are points of infiltration – recharge zone – in which Tamarix shrubs grow. This halophytic vegetation attests that unsaturated water with respect to salt is present at shallow depth although rainfall is only 70 mm/yr. Based on observations done elsewhere in the peninsula and discussions with APC engineers, recharge water also originates from the adjacent area of Ghor Mazra′a owing to a dense network of faults connecting the peninsula to the eastern rich aquifers fed by ~200/300 mm/yr rainfall over the Moab Plateau (about 10-15 km eastwards). The karst system′s porosity is characterized by fractures, bedding plane, and solutionally-enlarged voids such as channels and conduits developed from initial discontinuities (Rosendahl et al., 1998). It allows for rapid water flow.

Neev and Hall (1978) identified a transversal faulted zone, oriented S60°E, across the southern Dead Sea basin. It connected the eastern and western boundary fault systems, and affected the southern part of Lisan peninsula and the Lynch Strait. Faults and fault scarps bound Cape Molyneux. Erosional escarpments formed a 20–40 m step. In the southern part, one exposed fault strikes S67°E (Figure 5). Its trace is underlined by series of groundwater seepage and gullies. Brackish water is seeping and flowing downhill carving fretted valleys. The southern beach area displays structurally defined sag-ponds while the western coast is narrow and shows cave entrances (discharge zone), metres-wide in height, and decametres-wide in length (Closson, Lamoreaux, et al., 2007).

The energy dissipated in the karst system derives from three main sources of imbalance: the Dead Sea base level fluctuations, the uplift/subsidence related to the activity of the Lisan salt diapir, and the vertical displacements contributing to the formation of the pull-apart structure, with the type of extensional component evidenced in the focal mechanism of the 1979 earthquake calculated by Arieh et al. (1982). The availability of unsaturated (aggressive) water is demonstrated by the growth of Tamarix shrubs.

Under the Lisan peninsula, fissured Lisan marls are in contact with the sea. A lens-shaped body of brackish groundwater is buoyed by the denser Dead Sea. This brackish water literally floats on, and is in a state of balance with, the hypersaline water (Closson, Lamoreaux, et al., 2007). In the 1950s and 1960s, the Dead Sea water receded slowly. By the principle of ‘communicating vessels’, the lens-shaped body of brackish water uniformly followed the lowering movement.

When the recession of Dead Sea water accelerated in the 1970s, only the most fissured places like the damaged zones associated with the major transversal fault (Neev and Hall, 1978) allowed a faster underground flow. Consequently, chemical and mechanical erosions occurred along the exposed faults and fractures crossing the Lynch Strait. This period corresponds to the early stage of a karst system development or to its reactivation since the Dead Sea level fluctuated in the past (Klein and Flohn, 1987 and references therein). Retrospectively, after four decades of observations, a large

number of sinkholes and subsidence co-occurred with faults (Abelson et al., 2003; Closson, 2005; Yechieli et al., 2006; Closson and Abou Karaki, 2009a).

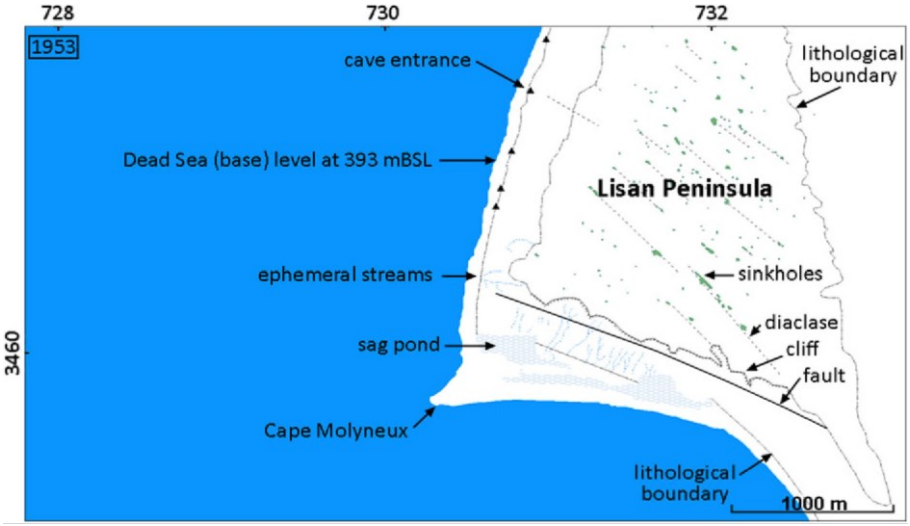

Figure 5. Cape Molyneux in the 1950s, 8 m of brine covered the shallow Lynch Strait. This landscape represents a secular equilibrium between a karst system and its environment.

4.2. 1979–1998: switch between the Dead Sea and the Wadi Araba base levels

From 1953 to 1970, the Dead Sea water level dropped slowly (3 m in 17 years) but at an accelerating pace. The shoreline moved southwards and westwards. Corona pictures have shown that Tamarix shrubs had time to develop over the newly emerged lands (Figure 6). This vegetation evidenced the circulation of unsaturated water below the wave-cut platform and
migration of the discharge zones lakeward (Figure 6: seepage area). Structurally defined sag ponds also appeared over the emerged platform (Figure 6: linear swamps).

Until the 1970s, Wadi Araba poured into the southern Dead Sea lagoon. During the building of the saltpan systems between the 1960s and the early 1980s, riparian states agreed to channel Wadi Araba across the shallow southern basin, along the borderline, up to the Lynch Strait and the northern Dead Sea basin (Figure 1). As a consequence, the longitudinal profile of Wadi Araba was controlled by the dropping Dead Sea level in the northern basin. Since the 1980s, therefore, the river has been continuously entrenching in the soft Lisan salty marls. The sediments are transported and deposited in a delta formed in the northern part of the Lynch Strait.

In 1982, after completion of an APC solar evaporation system in the southern sector of the Dead Sea, the very first sinkholes were observed in different places around the Lisan Peninsula.

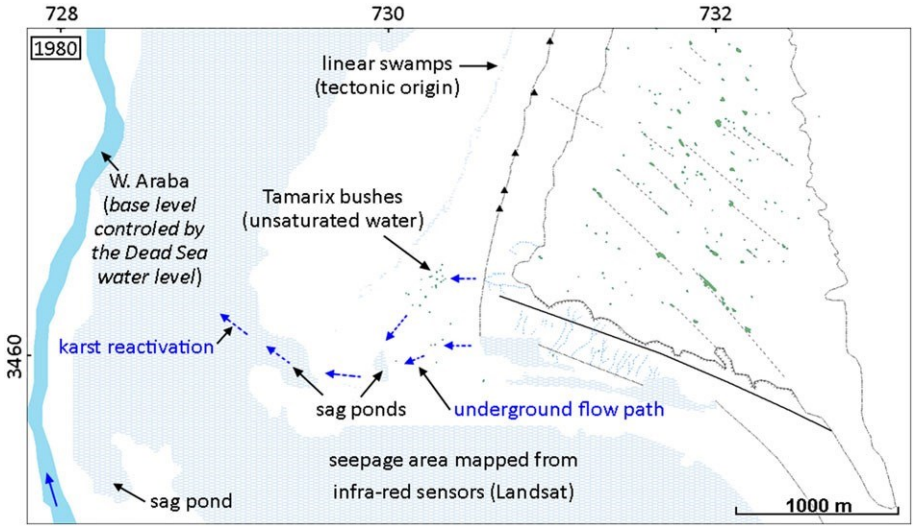

Figure 6. Emergence of the Lynch Strait and the Southern Dead Sea lagoon at the end of the 1970s. Wadi Araba becomes the new local base level.

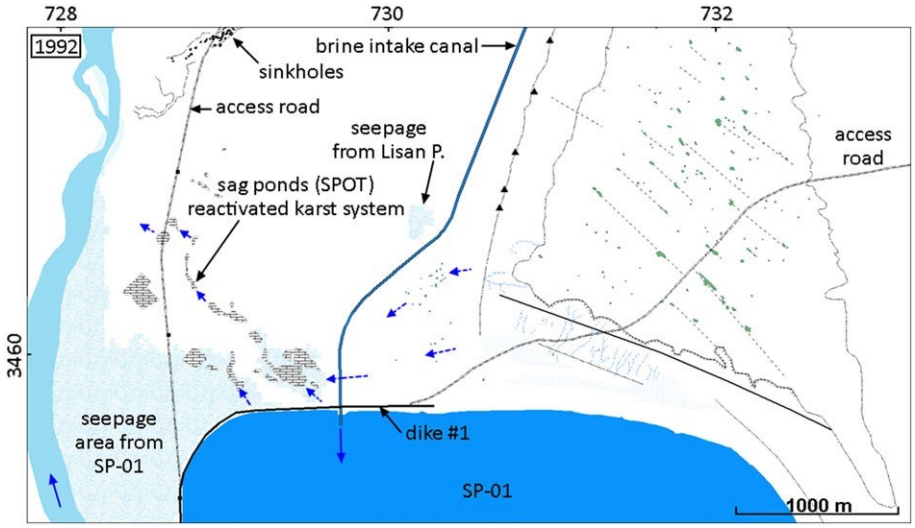

Figure 7. Development of a young and dynamic salt karst system across the new emerged lands. (Situation: early 1990s).

4.3. 1998–2001: saltpan SP-0A operational in the Lynch Strait

In the early 1980s, APC built up saltpan SP-01 next to the southern Lisan Peninsula (Figure 7). The brine elevation was 395 m bMSL (equal to the 1960s Dead Sea elevation). From that moment, a brackish water lens was re-established below the southern part of the Lisan peninsula at an elevation of 395 m bMSL. On its western side, the lens was around 5 m above Wadi Araba (400 m bMSL). The water in the lens moved directly towards Wadi Araba, crossing the path of the future dike18 (Figure 7: access road).

In the southern part of the Lynch Strait, the underground water flow was more rapid in damaged fault zones. Mechanical erosion of the conduits took place, leading to a young, dynamic, and reactivated halo karst system characterized by subsidence and sinkholes at the surface (Figure 7: sag ponds). Moreover, saltpan SP-01 (encompassed by earthen dike1) was built over porous (fractured) sediments. A significant part of the Dead Sea brine that was supposed to be stored in that reservoir

seeped into the subsurface to reach Wadi Araba a few hundred metres away, next to dike1 (Figure 7: Seepage area). The re-activated halo karst system was also used by the brine seeping from reservoir SP-01.

It is obvious from a panchromatic SPOT-1 image that this halo karst system was no longer at its initial stage of development in 1992. It had reached an intermediate stage where individual sinks had enlarged and merged with those in adjacent areas to form solution valleys (Figure 7: sag ponds).

Further, a flash flood event occurred during the winter of 1992. Ancient subsurface flow paths were suddenly reactivated. More than 70 sinkholes appeared across the access road that would have turned into dike18 (Figure 7: sinkholes). APC modified the design of the initially projected 12 km long dike (dike18, saltpan SP-0A, Figure 1), in order to bypass a 1.6 km long lineament of ground collapses and subsidence. As demonstrated by Figure 4 examples, the Dead Sea shores are very reactive to variations in the hydrogeological setting and are prone to dissolution.

From January 1996 to December 1997, during SP-0A construction phase, several additional incidents occurred (Tabbal and Mansour, 2009): vertical settlement of around 2–3 m in very soft clays, artesian conditions associated with sand and salt layers, and the development of sinkholes. The 12 km long dike was built to create a 95 Mm^3 pond at a cost of $32 M over a ground composed of soft to very soft silt-clay and massive salt rock (Lisan marls).

In 1997, a leak was discovered. Technical studies were conducted in collaboration with local and international experts, including Sir Alexander Gibb & Partners, who designed the dam. The reports indicated that the problem could be due to a sinkhole formed back in 1996, or to the development of seepage processes under the dam that caused internal erosion, as a consequence of an artesian water basin with a high water level (Atlas Investment Group, 2003).

In early 1998, during impounding operation, a landfill jetty 300 m long, 30 m to 60 m wide, was rapidly built from dike18 towards the basin centre due to seepage flow through a large channel below the dike. Since that time, this zone has been very active (Closson, Lamoreaux, et al., 2007) and it remains so in October 2015.

In 2001, dike18 was seriously damaged. Saltpan SP-0A was emptied. The production unit went back into service 5 years later.

4.4. 2002–2006: dike18 repair

Once saltpan SP-0A was emptied, the water lens below the Lisan (395 m bMSL) moved down to reach the elevation of Wadi Araba (~405 m bMSL). The fault-controlled halo karst system continued its development owing to that water lens and also to the brine seeping from SP-01 reservoir. Aerial and satellite images attest that the karstic activity continued (Closson and Abou Karaki, 2014b), e.g. salt deposits were detected over saltpan SP-0A bottom from artesian springs.

4.5. 2007–2015: post-repair damages

Field campaigns carried out between 2004 and 2009 have shown that, although repair works improved the safety coefficient, they failed to stop the problems. Many cracks and backfilled sinkholes were continuously located (Closson and Abou Karaki, 2009b).

By July 2008, a 400 m long dike segment was enlarged to improve safety conditions, tripling its width since 1997. In early 2011, APC launched a bid to fill underground cavities with cement on a 150 m dike segment, to protect a deteriorating part of dike18. The works included drilling approximately 40 boreholes to an average depth of 40 m through the dike body and foundations. Subsurface cavities and boreholes were filled with a grout mixture.

In December 2012, we identified a circular structure within SP-0A from a Worldview-2 image acquired on 2 April 2011 (Figure 8: circle around artesian spring). The structure was the biggest ever identified in the area (~300 m in diameter). A map of its deformation field was computed with COSMO-SkyMed images (Closson and Abou Karaki, 2014b). This circular feature was previously unknown and proved after further analysis to be associated with other circular features identified as sinkholes dating back to the mid-2000s. This 'finding' raised lots of questions regarding the origin of the underlying cavity, the capabilities of sinkhole prediction models developed in the area, as well as the strategies, approaches, and methods used by engineers and geophysicists to deal with such features. Analysis of satellite images revealed that this depression appeared after September 2006. Evidence of underground water circulation there dates back to the mid-1980s. Processing of satellite radar data has revealed that the overall diameter of the subsidence area is around 600 m across, threatening the stability of a more than 1km long section of dike18, which holds some 95 Mm^3 of Dead Sea brine.

In April 2013, a tender was launched to raise the height of dike18 on a 6450 m long segment and to perform risk control works. In February 2015, the SP-0A production unit was finally cut off from the first 3 km of dike18 in order to avoid its complete destruction (Figure 8: new dike). Four factors were identified that justifies this costly decision: (1) underground water circulating below the pond, from the Lisan Peninsula to the Dead Sea and Wadi Araba; (2) Dead Sea brine seeping from SP-0A and from a juxtaposed saltpan; (3) underground water circulation below the Lynch Strait owing to the supply of Wadi Araba; (4) natural settlement of the recently emerged coastal zones.

Nevertheless, the route of the new dike was poorly thought out. An important part of the karst system was by-passed (Figure 8: salt pillar). The new dike presents clear signs of weakness in areas affected by subsidence detected in 2011.

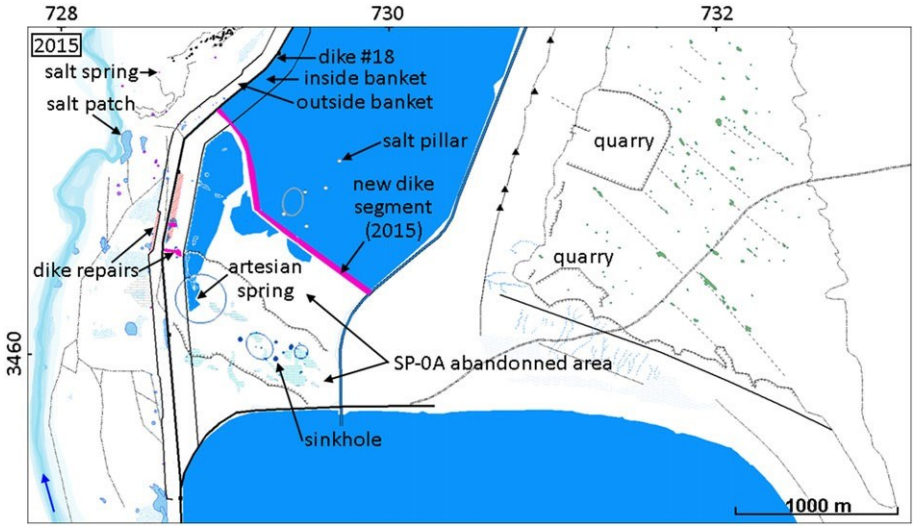

Figure 8. Mature halo karst system and amputation of 3 km of dike18.

5. Discussion

In the Anthropocene, it is becoming more and more obvious that the human intellectual and technical capacities to introduce profound alterations to the environment are increasing more rapidly than the human capacity to understand all the consequences and future effects of these actions. Our study indicates that the questionable approach of neglecting the dynamic nature of environmental parameters is costly. Since its construction in 1998, SP-0A (Figure 1) has been out of service for 25% of its lifetime. Repairs aiming to adapt SP-0A to problems (not solving them) totalling US $16 M represent an extra expenditure of half the original cost of the project. Furthermore, early in 2015, 15% of the saltpan area was amputated. All this was predictable and avoidable.

The idea of an expansion scheme in the Dead Sea area dates back to the 1980s. At that time, the Dead Sea sinkhole problem was spatially very limited and generally unknown to the public. In the early 1990s, during the design phase of dike18, one of the major elements of the industrial development in the area, dozens of sinkholes occurred across the trace of the future dike (Figure 7). In 1993, top world consultants were contacted and provided advice, but their warnings did not stop the project. APC engineers found technical solutions to build up a lucrative dike system in the southern Dead Sea basin. Even so, these projects did not benefit from careful and effective ideas based on sound investigations and realistic models regarding how the coastal environment of the Dead Sea would behave with a lower lake level.

It is clear that if the lake level and water table changes had been taken into account during the feasibility studies and design phase, the lifespan of major infrastructures such as dikes, bridges, and hotels would be drastically improved. For decades, scientists have developed concepts and robust methods to predict the consequences of lowering a base level and the associated groundwater table. It is known that lowering the groundwater table and displacing the fresh/brackish water interface will induce rapid karstification where optimal geological conditions for the development of the phenomena exist. See Bakalowicz (2015) for a recent synthesis study covering the Mediterranean area.

Investigations regarding responsibility for the setbacks such as the amputation of dike18 (Figure 8), or the earlier collapse of dike19 and the front beach of a five-star hotel (Closson et al., 2003; Abou Karaki and Closson, 2012), have highlighted some weaknesses inherent in the technical decision-making process and the general framework in which these types of projects originate, were designed and realized.

There are four categories of stakeholders in major projects including those of the Dead Sea: (1) fund providers; (2) engineers, architects, and planners; (3) companies chosen to build up the infrastructures; and (4) security engineers. They all have in common a desire to contribute to the building of successful and lucrative infrastructures. The economic concept of sustainability is understood as the time needed to achieve a return on investment, and the way to preserve employment.

Fund providers are coming from diverse perspectives and want a rapid return on their investments. They have profits in mind and are determined to achieve their goals. Environmental constraints are secondary issues for most of them. By way of an illustration, in 2004, investors presented a project for a harbour and boat cruises along the Dead Sea coast, in spite of the fact that the lake level was receding at a rate projected to exceed 1m/yr.

Engineers, architects, and planners have generally established their offices outside the project area. They are working on a range of global projects and are in charge of project design. Their knowledge of the environmental setting of any particular project is generally poor, or at best based on a limited dataset centred over the parcels they have to valorise. They clearly tend to minimize geomorphologic constraints. For example, a US-based architect's office was in charge of the "Detailed Master Plan" for the "Jordan Dead Sea Development Zone". They proposed to transform the Sweimeh area, in the northern section of the Dead Sea, into a kind of Californian Riviera. In their virtual landscapes, the rivers are in a state of equilibrium, while in reality, the rivers are entrenching, creating steep canyons with very unstable slopes. The architectural firm also positioned future resorts over active landslides. The real environment, and in this case geomorphologic consequences, are neglected or reshaped without taking into account the dynamic nature of ongoing deformations.

Companies qualified to construct infrastructures are a mixture of local and international enterprises. In general, local workers are more informed about the environmental issues in their areas of work because staff and engineers spend months at a time in the field. However, their objectives consist of the realization of the project, not of planning or questioning it. As an example; during the building phase of the Dead Sea Holiday Inn Resort, the beachfront suffered sinkholes and landslides. The project was nevertheless completed as it was initially designed, without adequate adaptations. In August 2012 the beachfront was destroyed again by a hectometre-size landslide. A tractor shifted several metres below the lake level (Abou Karaki and Closson, 2012). This is similar to the case of the APC's dike18 in which the access road was destroyed by sinkholes in that neither project was adequately questioned (Figure 7).

Security engineers in charge of preserving the projects once they are completed are locals who are fully aware of the Dead Sea's environmental degradation, although they lack a synoptic view and a sound understanding of the underlying mechanism. Their jobs consist of finding solutions to preserve assets at risk. Their methods and approaches to solving these problems are hardly sustainable, and usually involve quick and dirty repairs. Depending on their background and experience, they may or may not be open minded and ready to adapt their work to new ideas and techniques. In the case of APC, the Board of Directors and the Head of Security were aware of the results from and effectiveness of radar interferometry techniques and the benefits they could get in the frame of a well-adapted monitoring as far back as the year 2000 (Closson et al., 2003). However, it took more than a decade before the company began using radar remote sensing techniques. Present-day security engineers admitted that it was the only technique able to provide relevant and confident inputs in the management of the sinkholes' threat.

Dike19 collapse on 22 March 2000 represented a turning point in the study of hazards associated with the dropping of the water level in the Dead Sea because we succeeded in detecting precursory deformations several years before the destruction of the dike (Closson et al., 2003). From the early 2000s, and on, we have been continuously monitoring the Dead Sea area with regular field surveys complemented by visible and radar images processing and interpretations. Up to now, in the expression 'early warning system', the word 'early' must be understood as early enough to avoid a disaster by taking timely effective preventive measures and remedies for the case of already existing projects, or designing new ones in an appropriate conservative manner to ensure the sustainability of the infrastructures despite the environmental accurately forecasted alterations, including in worst case scenarios. This approach has proven to be efficient and successful. For example, in May 2008, based

on a model of sinkholes propagation in Ghor Al Haditha (Closson and Abou Karaki, 2009a), we warned the Numeira Dead Sea Salt and Mud Factory employees about a strong sinkholes threat. One year later the factory was moved to a safer area some 30km southwards, and the factory was totally destroyed. In December 2012, we informed APC of an important threat for dike18. Our prediction was correct and in February 2015, 25% of the 12 km dike18 was amputated as a preventive remedial measure. In August 2015, a new warning was sent to APC because the dike built to isolate the most dangerous part of dike18 is itself threatened in two places. Indeed, the route chosen for the amputation did not take into account another sinkhole site detected over images acquired in April 2011. This was a success in the sense that dike18 did not collapse in a catastrophic way as dike19 did, but it clearly shows the limitations of engineering at an exclusively local scale to solve an issue with a wider regional scale component.

Evidence of embryonic cracks and failures are difficult to detect remotely in densely urbanized areas, even with the best available resolution images. This is the particular problem of hotels of the northern Dead Sea. Such cases necessitate additional and more detailed field inspections because lives hang much more in the balance in these areas. At the Dead Sea, the collapse of buildings or hotels in sinkhole areas must be expected because such catastrophes happen worldwide, if subsidence and surface conditions are mature enough. One such recent incidents was in Florida, at the Summer Bay Resort in Clermont where dozens of guests were quickly evacuated after a sinkhole opened, destroying the hotel close to Disney World on 12 August 2013. Guests reported cracking sounds and windows breaking shortly before the building collapsed.

Based on previous results, we are growing more confident in the future success of the early warning system approach. The certainty of progress in space techniques is also enhancing our optimism concerning the future capabilities of detection. Owing to the Copernicus program (Sentinel-1A and B data are free of charge, with a revisit period of 12 days, and then 6 days when satellite B will be fully operational); the detection possibilities of ground deformations will increase in future years. This will allow for geo-hazard forecasts to increase in frequency and improve in accuracy so as to be dealt with more effectively.

Regarding the strategies that might increase the success of engineering projects, scientists working on karst can provide critical input. In recent years, important studies aimed at evaluating the impact of human activities on the karst environment have been carried out. For instance, the Karst Disturbance Index (KDI), proposed by van Beynen and Townsend (2005), and later modified by North et al. (2009), measures the disturbance induced by humans on karst, taking into account five categories (geomorphology, atmosphere, hydrology, biota and cultural factors), with each category described by several attributes. The KDI approach makes results readily understandable for policy-makers and the wider public. Another approach was the Karst Sustainability Index (KSI; van Beynen et al., 2012) that takes into account 25 indicators related to the environment, economy, and society. It was created as a standardized metric for sustainable development practices in karst settings, aimed at comparing sustainability practices temporally and spatially to highlight those specific areas where remedial policies or actions are needed.

6. Conclusions

The expansion scheme around the Dead Sea including the building of industrial dikes and touristic resorts is an economic necessity. However, the effects of the reduction in water level on the landscape and its stability cannot be ignored in the future if we are to guarantee a reasonably acceptable level of development sustainability in either the Dead Sea area, or in similar worldwide economically promising and environmentally sensitive areas.

The main obstacle to this sustainability is the lack of a synoptic view of ongoing geomorphologic alterations and environmental threats. A wide vision is mandatory to precisely position any project in a broader context, and to understand how it will interact with other components of the environmental system.

In Sweimeh on the northern Dead Sea coast where Dead Sea hotels are located, there are now many indications that the coast is unstable. Landslides are becoming more frequent and more severe. Costly damage recorded in the last two decades underlines the economic need for designers to think differently about the safety and sustainability of the infrastructures they design. Without adaptation and innovative preventive planning, common techniques taught in universities are insufficient in the Dead Sea and similar dynamic environments, even though they are successfully applied in many places worldwide. Among other things, cost-effective monitoring and early warning systems based on detecting the precursory deformations signalling future collapses should be set up to mitigate the consequences of major accidents, or even to prevent them altogether with suitable and effective early measures.

Results of adopting a systematic monitoring of the area with these techniques can be the basis of an effective early warning system capable of detecting potential threats early enough to take action, preserve expensive investments, and avoid disastrous consequences.

For a given project, the principle "observe-plan-do-check-adjust" should be applied each time a new stakeholder is involved.

Based on the habits of the new generation of stakeholders, each project should ideally have traceability for the common good and to enable stakeholders to learn from failures. In the Anthropocene more than ever, every project should have a platform where different stakeholders can communicate in complete transparency and share relevant information.

The implementation of indices like KDI and KSI, specifically developed for karst, may represent an important step in accurately defining the problems related to this fragile environment and developing proper land use planning and management techniques.

Acknowledgments

Thanks are due to anonymous reviewers, the review process has greatly improved this paper, and to H.E. Eng. Jamal Sarayreh, Chairman of the Arab Potash Company, to Eng. Brent Heiman President and CEO of APC, Dr. Dureid Mahasneh, for their support, also to Monique Morin and Simone Popperl for critically reading the manuscript. This work was done during a sabbatical leave of Najib Abou Karaki supported by the University of Jordan.

References

Abed, A. 1985. “Paleoclimates of the upper Pleistocene in the Jordan Rift”. In Studies in the History and Archaeology of Jordan. Department of the Antiquities of Jordan: Amman, Jordan II, 81–93.

Abelson, M., G. Baer, V. Shtivelman, D. Wachs, E. Raz, O. Crouvi, I. Kurzon, and Y. Yechieli. 2003. “Collapse-sinkholes and radar interferometry reveal neotectonics concealed within the Dead Sea basin”. *Geophysical Research Letters* 30. doi:10.1029/2003GL017103.1545, 52-1–52-4.

Abidin, H.Z., H. Andreas, I. Gumilar, and I.R.R. Wibowo. 2015a. “On correlation between urban development, land subsidence and flooding phenomena in Jakarta”. Proceedings of the IAHS 370: 15-20. doi:10.5194/piahs-370-15-2015 http://www.proc-iahs.net/370/15/ 2015/piahs-370-15-2015.pdf

Abidin, H.Z., H. Andreas, I. Gumilar, and J. Brinkman. 2015b. “Study on the risk and impacts of land subsidence in Jakarta”. Proceedings of the IAHS 372: 115–120 doi:10.5194/piahs-372-115-2015 http://www.prociahs.net/372/115/2015/piahs-372-115-2015.pdf

Abou Karaki, N. 1987. « Synthèse et carte sismotectonique des pays de la bordure orientale de la Mediterranée : Sismicité du system de failles du Jourdain - Mer Morte ». PhD Thesis, Université Louis Pasteur de Strasbourg, Institut de Physique du Globe (in French).

Abou Karaki, N., and D.Closson. 2012. Field Guide. EAGE Workshop on the Dead Sea sinkholes: Amman, Jordan. 23–25 September 2012. Available at: http://www.eage.org/images/cms/files/Conferences/Field%20Guide%20- %20color%20- %20min%20size.pdf (last visit 2015-09-18).

Abu Ghazleh, S. 2011. “Lake Lisan and the Dead Sea: their level changes and the geomorphology of their terraces”. Dissertation, Technische Universität Darmstadt.

Abu-Qdais. 2008. “Environmental impacts of the mega desalination project: the Red-Dead Sea conveyor”. *Desalination* 220: 16-23. doi:10.1016/j.desal.2007.01.019.

Agha Kouchaka, A., H. Norouzib, K. Madanic, A. Mirchid, M. Azarderakhshe, A. Nazemif, N. Asrollahia, A. Farahmanda, A. Mehrana, and E. Hasanzadehf. 2015. “Aral Sea syndrome desiccates Lake Urmia: call for action”. *Journal of Great Lakes Research* 41 (1): 307-311. doi:10.1016/j.jglr.2014.12.007.

Arieh, E., Y. Rotstein, and U. Peled. 1982. “The Dead Sea Earthquake of 23 April 1979”. *Bulletin of the Seismological Society of America* 72: 1627-1634.

Atlas Investment Group. 2003. Jordan - Equity Research - Arab Potash Co. - Dead Sea Harvest. October 18, 2003.

Bakalowicz, M. 2015. “Karst and karst groundwater resources in the Mediterranean”. *Environment Earth Science* 74: 5-14. doi:10.1007/ s12665-015-4239.

Barsoum, M.W., A. Ganguly, and G. Gug. 2006. “Microstructural evidence of reconstituted limestone blocks in the great pyramids of Egypt”. *Journal of the American Ceramic Society* 89 (12): 3788-3796. doi:10.1111/ j.1551-2916.2006.01308.x.

Bartov, Y., A. Amotz, E. Yehouda, and S. Mordechai. 2006. “Late quaternary faulting and subsidence in the central Dead Sea basin”. *Israeli Journal of Earth Sciences* 55: 17-31. doi:10.1560/K74U-07721642-6282.

Begin, Z.B., A. Ehrlich, and Y. Nathan. 1974. “Lake Lisan, the Pleistocene precursor of the Dead Sea”. *Geological Survey of Israel Bulletin* 63: 1-30.

Berardino, P., G. Fornaro, R. Lanari, and E. Sansosti. 2002. "A new algorithm for surface deformation monitoring based on small baseline differential SAR interferograms". *IEEE Transactions on Geoscience and remote Sensing* 40 (11): 2375-2383. doi:10.1109/TGRS.2002.803792.

Bossy, G., G. Fabre, Y. Glard, and C. Joseph. 2000. "The hydraulic engineering of the ancient aqueduct of Nimes and the Pont du Gard (Languedoc, France)". *Comptes Rendus de l'Académie des sciences - Series IIA Earth and Planetary Science* 330 (11): 769-775. doi:10.1016/ S1251-8050(00)00222-6.

Bowman, D., T. Svoray, S. Devora, I. Shapira, and J.B. Laronne. 2010. "Extreme rates of channel incision and shape evolution in response to a continuous, rapid base-level fall, the Dead Sea, Israel". *Geomorphology* 114 (3): 227-232. doi:10.1016/j.geomorph.2009.07.004.

Casu, F., S. Elefante, P. Imperatore, I. Zinno, M. Manunta, C. De Luca, and R. Lanari. 2014. "SBAS-DInSAR Parallel Processing for Deformation TimeSeries Computation". *IEEE Journal of Selected Topics in Applied Earth Observations and Remote Sensing* 7 (8): 3285-3296. doi:10.1109/ JSTARS.2014.2322671.

Closson, D. 2005. "Structural control of sinkholes and subsidence hazards along the Jordanian Dead Sea coast". *Environmental Geology* 47 (2): 290-301. doi:10.1007/s00254-004-1155-4.

Closson, D, and N. Abou Karaki. 2009a. "Salt karst and tectonics: sinkholes development along tension cracks between parallel strike-slip faults, Dead Sea, Jordan". *Earth Surface Processes and landforms* 34 (10): 1408-1421. doi:10.1002/esp.1829.

Closson, D, and N. Abou Karaki. 2009b. "Human-induced geological hazards along the Dead Sea coast". *Environmental Geology* 58: 371-380. doi:10.1007/s00254-008-1400-3.

Closson, D, and N. Abou Karaki. 2014a. "Earthen dike leakage at the Dead Sea". In Engineering Geology for Society and Territory – Volume 5. Lollino G, Manconi A, Guzzetti F, Culshaw M, Bobrowsky P, Luino F (eds). Springer International Publishing, Switzerland; 461-464. doi: 10.1007/978-3-319-09048-1_92.

Closson, D, and N. Abou Karaki. 2014b. "Dikes stability monitoring versus sinkholes and subsidence, Dead Sea region, Jordan". In Land Applications of Radar Remote Sensing. Holecz F, Pasquali P, Milisavljević N, Closson D (eds). Intech. ISBN 978-953-51-1589-2

Closson, D., P.E. Lamoreaux, N. Abou Karaki, and H. Al-Fugha. 2007. "Karst system developed in salt layers of the Lisan Peninsula, Dead Sea, Jordan". *Environmental Geology* 52 (1): 155-172. doi:10.1007/ s00254-006-0469-9.

Closson, D., N. Abou Karaki, H. Hansen, D. Derauw, C. Barbier, and A. Ozer. 2003. "Space-borne radar interferometric mapping of precursory deformations of a dike collapse, Dead Sea area, Jordan". *International Journal of Remote Sensing* 24 (4): 843-849. doi:10.1080/ 01431160210147388.

Closson, D., N. Abou Karaki, N. Milisavljević, F. Hallot, and M. Acheroy. 2010a. "Salt-dissolution-induced subsidence in the Dead Sea area detected by applying interferometric techniques to ALOS Palsar Synthetic Aperture Radar images". *Geodinamica Acta* 23 (1-3): 65-78. doi:10.3166/ga.23.65-78.

Closson, D., N. Abou Karaki, and F. Hallot. 2010b. "Landslides along the Jordanian Dead Sea coast triggered by the lake level lowering". *Environmental Earth Sciences* 59: 1417-1430. doi:10.1007/ s12665-009-0128-z.

Closson, D., N. Abou Karaki, D. Peressin, and Q. Yuxiao. 2015. “Dead Sea salt karst dynamics revealed by multi-temporal radar interferometric techniques”. *Proceedings of Asia Oceania Geosciences Society* annual meeting. Singapore, 2-7 August.

Crutzen, P.J., and E.F. Stoermer. 2000. The ‘Anthropocene’. In Global Change Newsletter, Vol. 41. International Geosphere-Bioshere Program (IGBP): Stockholm; 17-18.

Dajun, D. 1994. “Ancient and modern chinese bridges”. *Structural Engineering International* 4 (1): 41-43. doi:10.2749/ 101686694780602222.3.

Delage, P. 2003. “Risk in civil engineering: from natural to man-made hazards”. *Proceedings of Risk issues in contemporary science and engineering*, France-Stanford Conference, Stanford, 4–6 April 2003. http://stanford.edu/dept/france-stanford/Conferences/Risk/Delage.pdf.

Douglas, B.C. 1997. “Global sea rise: a redetermination”. *Surveys in Geophysics* 18: 279-292. doi:10.1023/A:1006544227856.

Elpiner, L.I. 1999. “Public health in the Aral Sea coastal region and the dynamics of changes in the ecological situation”. In Creeping Environmental Problems and Sustainable Development in the Aral Sea, Glantz MH (ed). Cambridge University Press: Cambridge; 128-156.

EXACT. 1998. “Overview of Middle East water resources - water resources of Palestinian, Jordanian, and Israeli interest”. Compiled by the US Geological Survey for the Executive Action Team, Middle East Water Data Banks Project (EXACT). ISBN 0–607–91785-7.

Ezersky, M., and A. Frumkin. 2013. “Fault-dissolution front relations and the Dead Sea sinkhole problem”. *Geomorphology* 201: 35-44. doi:10.1016/j.geomorph.2013.06.002.

Ferretti, A., C. Prati, and F. Rocca. 2001. “Permanent scatterers in SAR interferometry”. *IEEE Transactions on Geoscience and Remote Sensing* 39 (1): 8-20. doi:10.1109/36.898661.

Haase-Schramm, A., S.L. Goldstein, and M. Stein. 2004. “U-Th dating of Lake Lisan (late Pleistocene Dead Sea) aragonite and implications for glacial East Mediterranean climate change”. *Geochimica et Cosmochimica Acta* 68 (5): 985-1005. doi:10.1016/j. gca.2003.07.016.

Hassanzadeh, E., M. Zarghami, and Y. Hassanzadeh. 2011. “Determining the main factors in declining the Urmia lake level by using system dynamics modelling”. *Water Resources Management* 26 (1): 129-145. doi:10.1007/s11269-011-9909-8.

Kaufmann, O., and Y. Quinif. 2002. “Geohazard map of covercollapse sinkholes in the Tournaisis area, southern Belgium”. *Engineering Geology* 65 (2-3): 117-124. doi:10.1016/S00137952(01)00118-1.

Khirfan, L. 2016. World Heritage, Urban Design and Tourism: Three Cities in the Middle East. Routledge. ISBN 1134784791, 9781134784790.

Klein, C., H. Flohn. 1987. “Contributions to the knowledge of the fluctuations of the Dead Sea”. *Theoretical and Applied Climatology* 38: 151-156.

Neev, D., and J.K. Hall. 1978. The Dead Sea geophysical survey 19 July–1 August 1974: Final report No 2 Seismic Results and Interpretation. Geological Survey of Israel, Marine Geology Division, Report No MG/1/78, Jerusalem.

North, L.A., P.E. van Beynen, and M. Parise. 2009. “Interregional comparison of karst disturbance: West-central Florida and southeast Italy”. *Journal of Environmental Management* 9 (5): 1770-1781. doi:10.1016/j. jenvman.2008.11.018.

Ortloff, C.R. 2014. “Water engineering at Petra (Jordan): recreating the decision process underlying hydraulic engineering of the Wadi Mataha pipeline system”. *Journal of Archaeological Science* 44: 91-97. doi:10.1016/j.jas.2014.01.015.

Rosendahl, W., V. Wrede, and G. Rosendahl. 1998. “Höhlen in den LisanSchichten Jordaniens”. In *Natur und Mensch.* Jahresmitteilung der Naturhistorischen Gesellschaft Nürnberg 45-56.

Salameh, E., and M. Al Farajat. 2007. “The role of volcanic eruptions in blocking the drainage leading to the Dead Sea formation”. *Environmental Geology* 52: 519-527. doi:10.1007/s00254-0060484-x.

Salameh, E., and R. Hammouri. 2008. “Sources of groundwater salinity along the flow path, Disi–Dead Sea/Jordan”. *Environmental Geology* 55 (5): 1039-1053. doi:10.1007/s00254-007-1053-7.

Steinhorn I., G. Assaf, J.R. Gat, A. Nishry, A. Nissenbaum, M. Stiller, M. Beyth, D. Neev, R. Garber, G.M. Friedman, and W. Weiss. 1979. “The Dead Sea: deepening of the mixolimnion signifies the overture to overturn of the water column”. *Science* 206: 55-57.

Storz-Peretz, Y., D. Bowman, J.B. Laronne, and T. Svoray. 2010. “Rapid incision of a small, coarse and steep fan-delta in response to base-level fall: the case of Nahal Qedem, the Dead Sea, Israel”. *Earth Surface Processes and Landforms* 36 (4): 467-480. doi:10.1002/esp.2066.

Tabbal, M.A., and Z. Mansour. 2009. “Extensive geotechnical instrumentation program to control dike raising constructed on soft clay”. *Jurnal Ilmiah Semesta Teknika* 12 (2): 147-156.

Tahal Group, Geological Survey of Israel and Co. 2010. Dead Sea study: best available data reports (Revised). IL-201280-R10-054A. Red Sea – Dead Sea Water Convoyance Study Program.

van Beynen, P.E., and K.M. Townsend. 2005. “A disturbance index for karst environments”. *Environmental Management* 36 (1): 101-116. doi:10.1007/s00267-004-0265-9

van Beynen, P.E., R. Brinkmann, and K. van Beynen. 2012. “A sustainability index for karst environments”. *Journal of Cave and Karst Studies* 74 (2): 221-234. doi:10.4311/2011SS0217.

van Koningsveld, M., J.P.M. Mulder, M.J.F. Stive, L. van Der Valk, and A.W. van Der Weck. 2008. “Living with sea level rise and climate change: a case study of the Netherlands”. *Journal of Coastal Research* 24 (2): 367-379. doi:10.2112/07A-0010.1.

Waltham, T. 2009. “Sinkhole geohazards”. *Geology Today* 25 (3): 112-116. doi:10.1111/j.1365-2451.2009.00718.x.

Yechieli, Y., M. Abelson, A. Bein, O. Crouvi, and V. Shtivelman. 2006. “Sinkhole ‘swarms’ along the Dead Sea coast: reflection of disturbance of lake and adjacent groundwater systems”. *Geological Society of America Bulletin* 118: 1075-1087. doi:10.1130/B25880.1.